Advances in Electroporation-Mediated Delivery of Macromolecules

By

Erik J. Aiken

A dissertation submitted in partial fulfillment of

the requirements for the degree of

Doctor of Philosophy

(Electrical Engineering)

at the

UNIVERSITY OF WISCONSIN-MADISON

2018

Date of final oral examination: 5/21/2018

The dissertation is approved by the following members of the Final Oral Committee:

John H. Booske, Professor, Department of Electrical and Computer Engineering
Susan C. Hagness, Professor, Department of Electrical and Computer Engineering
Hongrui Jiang, Professor, Department of Electrical and Computer Engineering
Christopher L. Brace, Associate Professor, Department of Radiology

Abstract

Electroporation is a dynamic phenomenon in which pores form in a cell's extracellular membrane due to an externally applied pulsed electric field (PEF) of sufficient duration and intensity. These pores allow normally membrane impermeable substances, such as ions and molecules, to pass into the cell. Pores opened in this manner can close after a short duration of time, on the order of seconds to minutes, or remain open until they cause cell death depending on the PEF parameters among other factors. The former case is known as Reversible Electroporation (RE) and the latter is known as Irreversible Electroporation (IRE). Both RE and IRE have important clinical applications. RE is a promising technique for delivering macromolecules such as proteins, DNA, RNA [1]–[3], antibodies [4], and nanoparticles [5], [6] into the cytoplasm. IRE shows promise as a non-thermal technique for ablating unwanted tissue [7].

The primary motivation for this PhD research was to improve electroporation-based treatments, and specifically to address gaps in electroporation-based healthcare applications, such as minimally invasive techniques for gene therapy. We identified several shortcomings in the current published literature for clinical electroporation devices. Specifically, a lack of devices for difficult to reach tissues or physically confined spaces. For example, most clinical electroporation devices rely on invasive entry to access the site. Few devices have been developed for endoscopic, laparoscopic, and other catheter-based applications. We developed and tested a device to reversibly electroporate liver hepatocytes that could be used to deliver gene therapy treatments in porcine liver and has potential to be further extended to human treatment.

Acknowledgements

This research was supported by the Duane H. and Dorothy M. Bluemke professorship and the Philip Dunham Reed professorship.

I would first like to thank my advisers, Dr. Susan Hagness and Dr. John Booske for their support and mentorship. I have enjoyed and appreciated the opportunity to work in their lab. Your attention to detail has forever improved my research, writing, and presentation abilities. I also would like to thank my committee members, Dr. Hongrui Jiang and Dr. Christopher Brace for their support, input, and feedback. Also thank you to Dr. Daniel van der Weide, for serving on my preliminary committee and for his feedback and suggestions.

Thank you to our collaborators with the Department of Surgery, Dr. Hans Sollinger, Dr. Tausif Alam, and Dr. Paul Laeseke. Their collaboration has greatly improved this project. I also need to thank my fellow graduate students and officemates, Tyler Roewe, Konstantinos Mavrakakis, and Patrick Forbes for their help with MATLAB and CST Studio. Thanks to all my fellow graduate students in the UWCEM group, especially Owen Mays, Hung Luyen, James Sawicki, Luz María Neira, and Yahya Mohtashami for their help, feedback, and support. Finally, thank you to the undergraduate students, Da Cao, Brian Kilberg, Mitchel Beres, Matthew Jensen, Siyuan (Richard) Yu, Emily Anaya, and Ashley Zagaros who worked in the lab with me and assisted with many experiments during my time here.

To Sarah Mason, Suzanne Smith, and the entire team at the Wisconsin Collaboratory for Enhanced Learning (WisCEL), I thank you for everything you have done in aiding me professionally as I have pursued my degree.

I owe a special thanks to my parents, Gregg and Kay, who have been an enormous source of knowledge, inspiration, and support throughout my life. I could have never done this without your unwavering support and belief in me. I would also like to thank my brother, Ross, for all of our

technical discussions and suggestions with coding, and my sister, Laura, for being a constant source of support and aid.

Lastly, a special thanks to my wife, Vera Cardoso Ferreira Aiken, for her help with statistics and proofreading throughout my degree, and for her unwavering and enthusiastic support of both this project and me.

Table of Contents

Chapter 1: **Introduction**

Electroporation is a dynamic phenomenon in which pores form in a cell's extracellular membrane due to an externally applied pulsed electric field (PEF) of sufficient duration (typically ns to ms) and intensity (on the order of V/cm to kV/cm). These pores allow normally membrane impermeable objects, i.e. molecules, to pass into the cell. Pores opened in this manner can close after a short duration of time, or remain open until the cell dies, depending on a variety of parameters. The former case is known as Reversible Electroporation (RE) and the latter is known as Irreversible Electroporation (IRE). Both RE and IRE have important clinical applications. RE is a promising technique for delivering macromolecules such as proteins, DNA, RNA [1]–[3], antibodies [4], and nanoparticles [5], [6] into the cytoplasm. RE has been shown to be more reproducible, efficient, and predictable than other macromolecule delivery methods such as viral or chemical manipulation of membranes. IRE shows promise as a non-thermal technique for ablating unwanted tissue [7].

The focus of this dissertation was to improve electroporation techniques and methods to overcome challenges in efficiency, thereby allowing electroporation to be a more successful clinical technique. We identified three primary aims to achieve this goal.

Early on, we identified the need to develop a more reliable, precise, and fast method for determining electroporation outcomes. Our existing method of tracking fluorescence of a single microscope frame of cells did not allow enough throughput to realistically analyze enough samples in a timely manner for any of our proposed studies. Specifically, the new method needed to be compatible with a single channel fluorescence microscope and had to be able to accurately differentiate between RE and IRE cells in a timely manner. Being able to do this quickly is important when searching for the best PEF parameter values for a given application, and therefore necessary to achieve the subsequent research for this dissertation. In a laboratory setting, one common technique for doing this is labeling cells with two membrane integrity indicators, one added to the sample prior to

electroporation, and one added after the transient pores have had time to close. Internalization or exclusion of these markers can indicate whether a cell was electroporated, and if it was, whether it was RE or IRE. We have developed a modified version of this method for the use in our lab. This is referred to as Aim 1 throughout this dissertation.

The next area we identified as a research goal was improving the likelihood of RE outcomes. Currently, for example, when using electroporation for DNA delivery, only approximately 20-60% of the treated cells are successfully transfected using current electroporation techniques [1], [8], [9]. Successfully and stably getting DNA into the cell has been identified as a major challenge in gene therapy [10], [11], meaning that improving RE rates will make electroporation more valuable clinically. Many factors influence whether a cell will be IRE, RE, or non-electroporated (NEP). In addition to the PEF intensity and duration, cell size, orientation, resting membrane potential, temperature, type, etc. can affect the electroporation outcome. For this research, we decided to look further into modifying the membrane potential as a method to improve RE. A previous study showed that the cell membrane could be primed for electroporation using cationic peptides, therefore reducing the PEF intensity required to achieve electroporation [12]. However, this study only focused on the effects on IRE since the peptides were toxic and thus not applicable for RE uses. We investigated this phenomenon using ionomycin, which at low concentrations appears to be non-toxic, to induce a change in the resting membrane potential and examined the effects on both RE and IRE. We refer to this as Aim 2 throughout this dissertation.

The third area we address in this dissertation is development of electroporation devices for *in vivo* use. We identified several shortcomings in the current published literature for clinical electroporation devices. Specifically, published research is lacking for minimally invasive techniques, especially in difficult to reach or physically confined spaces. For example, most clinical electroporation devices rely on line of sight to access the location, requiring multiple incisions near the target tissue. Only a few

devices have been developed for catheter, endoscopic, or laparoscopic applications [13]–[19]. We worked with colleagues at UW-Hospital to develop a minimally invasive clinical electroporation device for gene therapy. We refer to this as Aim 3 throughout this report.

In summary, in this dissertation, I present my findings related to these three specific aims, which improved electroporation treatments and addressed gaps in electroporation-based healthcare applications.

Aim 1. Develop an accurate and precise method for determining electroporation outcomes using two membrane integrity indicators to differentiate between RE and IRE.

Aim 2. Investigate the effects of modifying membrane potential on electroporation outcomes.

   a. Modify the membrane potential using ionomycin with the intent of enhancing RE outcomes.

   b. Repeat part (a) with a focus on enhancing IRE outcomes by using longer pulse durations.

Aim 3. Develop and evaluate a new PEF delivery device for electroporating and transfecting cells using minimally invasive methods in physically constrained tissue locations.

Chapter 2: **Background**

2.1 Cell Structure/Cell Membrane

All cells can be grouped into two groups, prokaryotes and eukaryotes. Prokaryotic cells are simpler, consisting of a single compartment enclosed by a plasma membrane, which is defined as the membrane that separates the internal portion of the cell (cytoplasm) from the exterior of the cell

(exoplasm). Eukaryotic cells have multiple compartments or enclosed structures within the plasma membrane. These structures are called organelles. The part of the cell enclosed by the plasma membrane is called the cytoplasm, and the liquid enclosed in the cell is called the cytosol [20], [21].

All cellular membranes are made of a phospholipid bilayer. Phospholipids are organic molecules consisting of a hydrophilic head, which faces outward and a hydrophobic tail, which faces inward. These phospholipid bilayers form a sealed compartment, which can enclose an entire cell or an organelle. In addition to phospholipids, cell membranes are also made up of proteins, which mediate transport of molecules through the membrane [20], [21]. A typical membrane thickness is on the order of 5 nm [22]. This thickness can be affected by heat since heat causes more movement of the phospholipids and other membrane molecules. This motion causes the membrane to shrink slightly in thickness [20].

The plasma membrane of a cell serves several functions. First, it protects the cell by isolating it from the surroundings, and attaches to the cytoskeleton, providing a cell with its basic shape [20], [21], [23]. Second, it controls which substances and molecules can pass into and out of the cell [20], [21], [23][20]. The plasma membrane is also involved in many other processes, such as signaling, adhesion, and ion conductivity [20], [21], [23].

2.2 Intracellular delivery of membrane impermeable macromolecules

Delivery of membrane impermeable macromolecules to a cell's cytoplasm is useful in a wide variety of applications, ranging from research to clinical treatments. Types of molecules that are membrane impermeable and desirable to be delivered into cells include DNA, drugs, peptides, enzymes, antibodies, and imaging agents [24], [25]. The ease with which a given molecule can pass

through a membrane is called permeability [25]. There are many techniques available for allowing membrane impermeable molecules to cross the plasma membrane.

The first category of methods for allowing molecules to cross a cell membrane is through a natural process called diffusion [26]. There are two types of diffusion, passive diffusion and facilitated diffusion. Passive diffusion is the simplest method of molecules passing through the plasma membrane [25]. A molecule naturally flows through the membrane barrier from a higher concentration to lower concentration [26]. During passive diffusion, a molecule is dissolved in the phospholipid bilayer, then passes across the bilayer to the other side of the membrane [26]. No other membrane structures, such as proteins, are involved in this process [26]. Small nonpolar molecules like oxygen (O_2) or carbon dioxide (CO_2), and small uncharged polar molecules such as water (H_2O) can diffuse through the phospholipid bilayer in this manner [26]. Larger uncharged molecules and charged molecules cannot diffuse through the membrane through passive diffusion [26]. Facilitated diffusion is similar to passive diffusion, in that it follows the concentration gradient and no external source of energy is required for molecules to pass through the membrane [26]. Unlike passive diffusion however, with facilitated diffusion, molecules are not dissolved in the plasma membrane. Instead, proteins mediate transport across the membrane [26]. This typically works for small, moderately polar molecules [25], [26].

The next category of molecules passing through a plasma membrane is called active transport, or transporter-mediated entry, in which energy is used to transport molecules across the cell membrane [25], [26]. Hydrolysis of ATP is the most common source of energy for this type of interaction [26]. An example of this is ion channels, such as the sodium/potassium pump, which transports three sodium ions out of the cell and two potassium ions into the cell for each ATP molecule used. This exchange of potassium and sodium ions results in the inner portion of the cell becoming more negatively charged than its exterior [25]. Another source of energy for active transport is existing ion

gradients. In the aforementioned sodium/potassium exchange, it creates a strong sodium gradient, which is used by cells to bring two sodium ions and one glucose molecule into the cell [26].

The next category is transport using a carrier such as certain peptides, toxins, and viruses. This type of transport happens when a molecular cargo (for example, DNA, RNA, quantum dots) is carried through the membrane. For example, some peptides, known as cell-penetrating peptides (CPP), have been reported to be able to cross a cell membrane, though the mechanism for this is still unclear [25], [27], [28]. CPPs have been used to transport drugs such as cancer inhibitors and viral inhibitors, and contrast agents such as green fluorescent protein (GFP) and quantum dots to cells [29]. In addition to CPPs, some plant and bacterial toxins are capable of forming their own pores and entering into cells [25], [30]–[33]. Lastly, viruses can enter the cell either directly through the plasma membrane or from binding to cellular receptors and triggering pathways into the cell [25], [34]–[39]. All viruses consist of two parts, the viral genome or genetic material (DNA/RNA) and a capsid which protects the viral genome and is involved with transport through the membrane [40]. Viruses can be stripped of their natural viral genome and replaced with a new genome, called a cassette, such as a therapeutic gene. The virus then transports the cassette through the membrane [41].

Additionally, several physical methods exist to transport molecules through cell membranes. Physical methods include direct injection and particle mediated insertion. Direct injection is considered the most straightforward physical delivery method [24]. In this method, a single cell's plasma membrane can be penetrated using a microneedle, where a small-diameter micropipette tip is placed directly in contact with the cell, creates a small tear in the membrane, then injects the molecules of interest into the cell [24]. While effective, this technique has limited use due to the slow delivery rate and low throughput [24]. Similarly, this can be done with a high-velocity, ultrafine stream of the macromolecule instead of a pipette [24], which is known as jet injection [24]. A more complicated physical delivery method is particle-mediated delivery. Particle-mediated delivery involves launching

the molecules at high speeds towards the target cells. These molecules penetrate the membrane due to their high velocity. One example of particle-mediated delivery is particle bombardment using the biolistic method, commonly referred to as the gene gun method. Particle bombardment is performed using heavy metal particles coated with the molecule of interest, which are then inserted into a solution near the cells, separated by a mesh [11], [24], [42]–[44]. This particle is then accelerated in the direction of the cells, and halted rapidly by the mesh [11], [24], [42]–[44]. The mesh catches the heavy metal particles and allows the macromolecules to pass through and into contact with the target cells with high velocity, penetrating the cell membrane [11], [24], [42]–[44]. This technique has been primarily used for plant cells, and some mammalian cells and tissues, but is limited in clinical applications by a low penetration depth on the order of 200-2000 μm [11], [24], [42]–[45].

The last category of methods for molecules passing into cells covered in this review is field-induced membrane poration. Field-induced membrane poration uses fields and waves, such as electric fields, and mechanical waves to disrupt the membrane and open pores in the membrane. Examples of methods which use field-induced membrane poration include sonoporation/mechanoporation, optoporation, and electroporation. Sonoporation, otherwise known as mechanoporation or ultrasound-mediated membrane poration is a relatively new technology [24]. The exact mechanisms of this method are not fully understood, but the prevailing theory is that periodic oscillation of gas bubbles induced by ultrasound waves creates shockwaves that induce reversible poration, or the opening of temporary pores in a cell's membrane [24], [46], [47]. The second form of field-induced membrane poration is laser-mediated membrane permeabilization, or optoporation [24], [48], [49]. This is sometimes also referred to as optoinjection, optical transfection, or laserfection [50]–[53]. This technique uses focused, ultrashort laser pulses to open transient pores in cell membranes [48], [49]. The last field-induced form of membrane poration covered here is electroporation. Electroporation

uses short duration, high intensity pulsed electric fields to open transient, reversible pores in a cell membrane, which allow normally membrane impermeable molecules to pass into the cell [54]–[57].

Each of these techniques has its own advantages and limitations. For example, viral vectors are one of the most common delivery methods for DNA, however, viral delivery may invoke an immune response from the host that limits its uses clinically [8]. Viral vectors also are limited in the size of DNA that can be carried [58]. On the other hand, most non-viral techniques are either inefficient or toxic. Electroporation is one technique that may be able to overcome many of the challenges presented with delivery of macromolecules. However, currently it is hindered by low efficiency. For example, with DNA delivery, only approximately 20-60% of the treated cells are successfully transfected using current electroporation techniques [1], [8], [9].

2.3 Electroporation Background

Electroporation, the technique of applying an electric field across a cell to induce pore formation, has been reported since the 1950s, when the first published observations of the phenomenon were recorded [22], [59]. In 1967, researchers discovered that pulsed high intensity electric fields could cause cell death due to irreversible damage to cell membranes [60]. By the early 1970s, studies showed this damage could be reversible when a sufficiently short duration pulse was applied [61]–[63]. It was also discovered that a sufficient voltage across the membrane could cause dielectric breakdown, which is defined as current flowing through something that is normally an insulator, like lightning for example [61], [62]. This was eventually given the name of reversible membrane breakdown [64]–[67], and the idea that pulsed electric field induced dielectric breakdown of the cell membrane resulted in pore formation was first proposed in 1977 [68]. The general idea is the electric fields cause a slight separation to occur between the lipids of the phospholipid bilayer, resulting in a hydrophobic pore. Exposure to water causes the hydrophobic tails of the phospholipids to turn inward and the

hydrophilic heads face outward, resulting in a pore [69]–[71]. These induced pores allow for membrane impermeable molecules to pass through the membrane [72].

Electroporation was first used to deliver small molecules through cell membranes in the early 1980s [72]. Shortly after, the term electroporation started being used to describe this phenomenon, around the same time it was first used *in vitro* to transfect DNA into mammalian cells [54], [73]. The first use of electroporation *in vivo* was performed in the late 1980s, as a method to improve chemotherapeutic drug uptake into solid rat tumors [74]. This later became referred to as electrochemotherapy (ECT) [54]. Since then, electroporation has been used in a wide variety of medical and laboratory research applications, such as cancer treatments, heart disease, gene delivery, and drug delivery [22], [75]–[78].

There are three known phases of the electroporation process. The first is pore formation, which happens in microseconds. The second is pore size expansion, which occurs for microseconds to milliseconds after the electric field pulse is complete. The third phase is pore resealing, which lasts a few minutes, and may not occur [1], [68], [69], [79]–[83]. If the membrane successfully reseals, the cell is considered reversibly electroporated (RE) [1], [68], [69], [79]–[83]. If the cell membrane never completely reseals the cell is considered irreversibly electroporated (IRE) [1], [68], [69], [79]–[83]. Molecular transport through the membrane due to electroporation has been observed during all three phases [84]–[87], while DNA transfection requires electrophoretic forces [4], [88]. Therefore, DNA delivery is more effective at longer pulse durations, since the longer pulse duration provides a larger window of time that the electrophoretic forces are assisting the gene through the plasma membrane [56], [88].

To further understand electroporation and predict results, it is helpful to understand the mathematical equations that describe pore formation. There are multiple proposed mathematical models to describe pore formation caused by electroporation. The most widely accepted model is the

transient aqueous pore model, which assumes hydrophilic pores are created in the cell membrane when exposed to a pulsed electric field of appropriate intensity and duration [89]. This model claims micro-pores are formed due to natural thermal fluctuation in the lipid bilayer. Externally applied pulsed electric fields cause ions inside the cell to relocate to the cell membrane, resulting in a large increase the transmembrane potential of the cell's external membrane. This field amplification at the membrane causes these micro-pores to rearrange and become larger, hydrophilic pores [1], [70], [90]. The equation describing the induced transmembrane potential in a spherical cell is:

$$U = -1.5 \times r \times E \times cos(\varphi) \quad (1)$$

where U is the induced transmembrane potential, r is the radius of the cell, E is the strength of the externally applied electric field, and φ is the angle between the electric field and a line from the midpoint of a cell to a selected point on the cell's surface. These values are shown in Figure 2-1. This is known as Schwan's equation [1], [70], [89]. The transmembrane potential threshold for electroporation typically occurs for U between 200 mV and 1V when using pulse durations on the order of microseconds to milliseconds, and is dependent on the specific pulse duration used [22], [90], [91]. Creation of pores in a manner such as this allows for normally membrane impermeable macromolecules to be delivered into a cell. Depending on the intensity of the electric field, the pulse duration, the cell shape and radius, and numerous other factors, a cell exposed to pulsed electric fields can be RE, IRE, or unaffected (non-electroporated, NEP). Due to the different possible outcomes, the electroporation parameters must be carefully considered and chosen for a specific application.

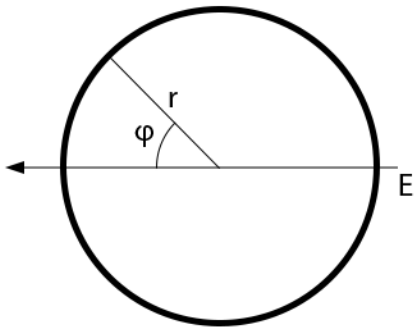

Figure 2-1. Diagram of cell depicting radius *r*, electric field *E*, and angle φ.

2.4 Electroporation Parameters

Electroporation outcomes are dependent on many parameters, including pulse duration, amplitude, number of pulses, frequency, pulse shape, orientation, and temperature [56], [92]–[100]. Changing these parameters can alter the outcome. For example, whether a cell is RE or IRE is largely dependent on electric field strength and pulse duration. The charge buildup across the membrane causes electroporation to occur due to ions and protons relocating to the external membrane of the cell in the presence of the electric field [22], [101], [102]. This means a minimum effective pulse duration is required to allow time for the charged particles to rearrange and build an electric potential difference across the plasma membrane. Pulse durations shorter than this threshold are not likely to affect the plasma membrane (though they can still affect internal organelle membranes) [4]. Since changing parameters can drastically alter results, it is important to have an in depth understanding of how each specific parameter can affect the outcome to predict the most likely outcome.

Weaver *et al.* assembled a rough summary of expected outcomes and applications based on field strength (0.1 kV/cm – 100 kV/cm) and pulse duration (on the order of ns to s), shown in Figure 2-2 [56]. However, as Weaver *et al* describe, there are still relatively unexplored regions, meaning more

experiments need to be done to determine expected results and the appropriate parameters for specific applications. The values of applied field strength and pulse duration for different applications reported in this summary are consistent with our own findings in the lab and other published literature [7], [11], [109], [110], [13], [22], [103]–[108]. For example, someone interested in performing electrochemotherapy (ECT), which uses RE to deliver a chemotherapeutic drug to tumor cells, would choose a pulse duration in the range of 0.1 – 1 ms and an applied field strength of approximately 1 kV/cm, depending on cell type and other laboratory settings. Someone interested in IRE ablation, or using IRE to destroy cells, would typically use a pulse duration in the range of 0.1 – 100 ms, and an applied electric field strength of around 2 kV/cm. While the end goal of both methods is to destroy tumors, the parameters and mechanisms used are different. With ECT, the primary mechanism of cell death is the chemotherapeutic drug, which has the advantage of sparing non-cancerous tissue in the nearby region [13], [103], [104], [111]. In contrast, with IRE ablation, the primary mode of cell death is rapid cell death resulting from the damage to the cell membrane [7], [12], [56], [112]. IRE can also cause delayed cell death (apoptosis) due to DNA or internal organelle damage at different pulse parameters, specifically high intensity, ns durations [56]. These ranges represent an approximation for the types of electroporation expected at the listed pulse durations and intensities, however as previously stated, electroporation is dependent on numerous other parameters [56], [92]–[100], and therefore these estimates should be verified for specific cases. Additionally, heterogeneity of the tissue can drastically change field strengths *in vivo* and should be considered for *in vivo* applications [113].

The majority of electroporation applications are done with either unipolar or bipolar square wave pulses, however other pulse shapes have been used [114]–[116]. Different pulse shapes can have an effect on molecule uptake for a variety of reasons, including altering the voltage threshold for electroporation and, in the case of unipolar versus monopolar, affecting how charged particles move through the membrane [115], [116]. Additionally, the orientation of the electrodes can impact results

depending on cell orientation in non-spherical cells [117]. For example, oblong cells will electroporate more like smaller cells if their longer direction is perpendicular to the electric field and will undergo electroporation more like larger cells if the longer direction is parallel to the electric field. To overcome this, some applications, (usually *in vivo*), use pulses from multiple angles/orientations [92], [95], [118], [119].

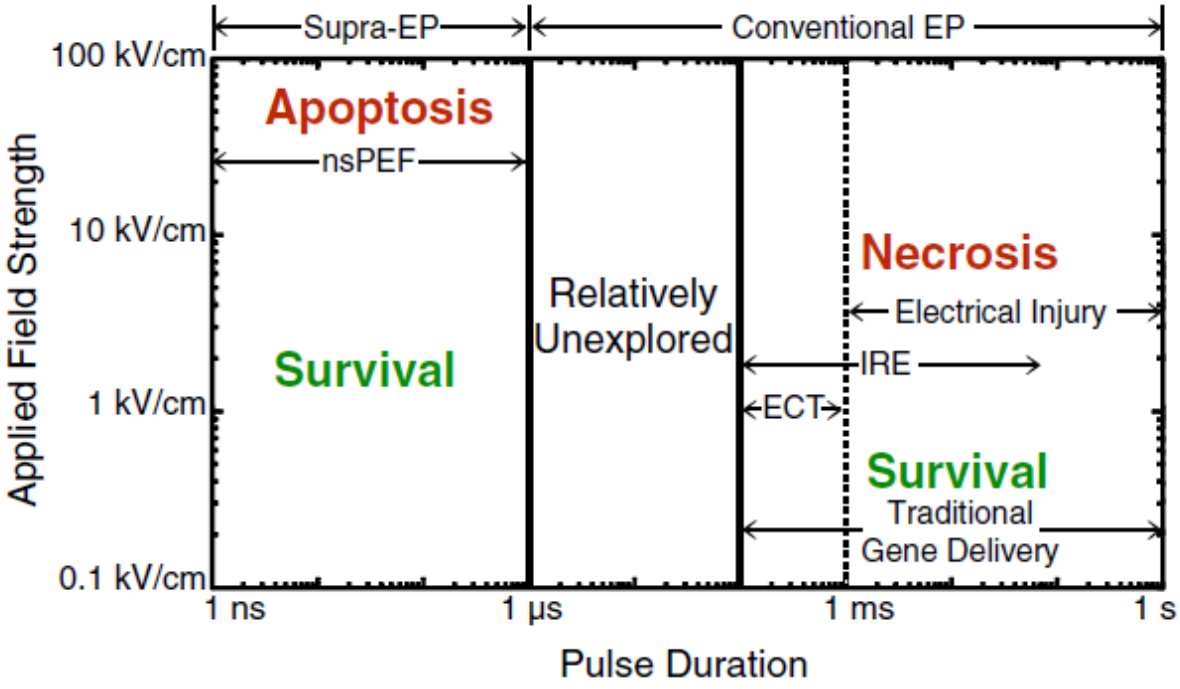

Figure 2-2. Pulse duration and applied field strength extracted from Weaver et al. 2012. Note that different applications use different pulse durations and applied field strengths. Figure reprinted with permission from Elsevier. Copyright 2012. Source: [56].

While general guidelines such as those presented above from Weaver et al. are useful in determining the approximate values to use for certain applications, it is difficult to predict precise optimal parameters. This is because the relationship between pulse parameters and RE/IRE outcomes has not yet been fully determined. Several studies have concluded that electroporation outcomes are not related to energy delivered [95], [96], but instead follow a complicated relationship between

multiple parameters and the extent of membrane electroporation. [100]. Multiple pulses and pulse frequency also both play rolls in electroporation outcomes. For a given pulse duration, a threshold electric field strength exists which is required for any electroporation to occur, below which little to no electroporation occurs. Also, previous research has indicated that longer pulse durations are more applicable for delivering large molecules since they open larger pores [57], [98], [120], and are widely used for delivering DNA since the electric field aids the DNA in passing through the membrane (unlike smaller macromolecules which enter through diffusion) [56]. It has been suggested that increasing the applied electric field opens more pores, while increasing duration opens larger pores or helps facilitate larger molecule transport through pores [121]. Other studies have had success transferring large molecules using microsecond pulses [122]. For electric field intensities above the threshold required for electroporation to occur, increasing the number of pulses can increase the amount of electroporation, while also affecting viability [92], [97], [123]. Additionally, there is a limit to the number of pulses that result in a meaningful increase in pore formation, where additional pulses do not generate many additional pores [92], [97]. This limit is around 16-20 pulses [92], [97].

2.5 Theoretical modeling of electroporation and membrane potential

As mentioned above, many different studies have modeled the effects of electroporation to predict outcomes. Most of those studies use one of two theoretical models to predict electroporation. The first is an electromechanical approach, which uses electrostatics and elasticity principles to predict pore formation [124]. The other views the effect of the applied pulsed electric field on the stochastic model of pore expansion [90]. This model assumes the applied electric field decreases the energy barrier for formation of pores because the polarization energy of water in the pores is lower than that of the lipid membrane [125]. Both models commonly ignore the effect of the cellular resting membrane potential because it is small when compared to the applied electric field [126]. When

included in models, studies typically examined the effects on the plasma membrane, and did not investigate the possible effect it could have on cell viability [22], [70], [77], [83]. Therefore, we decided to explore the effects of membrane potential in more detail.

2.6 Membrane potential and its effect on electroporation

As described by Schwan's equation (1), the dependence on the cosine of the angle of the electric field (φ) suggests that pores created due to electroporation occur near the cathode and anode. However, a study performed by Chock *et al* [126] demonstrated that pores form more easily near the anode, implying the cell's resting transmembrane potential affects pore formation, which is not directly accounted for in Schwan's equation. More specifically, this study showed that by gradually increasing the applied electric field strength, a fluorescent molecule would penetrate the plasma membrane near the anode at a lower field strength than the cathode. This implies that the resting potential of the cell affects electroporation [126]. This effect was more noticeable for lower applied electric field strengths and did not occur when using bipolar pulses. Additionally, other studies showed that while more electroporation happens close to the anode, larger pores open near the cathode, though fewer in number [4], suggesting that altering the membrane potential could potentially be useful for applications related to small molecule delivery into cells.

It was theorized by Kennedy *et al.* [12] that the plasma membrane could be primed for electroporation by artificially increasing the voltage across the membrane at localized points, therefore reducing the externally applied pulsed electric field intensity required for electroporation to occur. We speculated we could use this to improve RE outcomes, since decreasing the externally applied electric field intensity would reduce damage to internal organelles, therefore increasing cell viability. Reducing cell death while maintaining the same number of electroporated cells would then make it possible to

enhance RE. As previously mentioned, the mechanisms of cell death through electroporation are either apoptosis or necrosis [56], [127], [128]. The type of cell death is primarily dependent on pulse duration, with short duration pulses primarily causing apoptosis, and long duration pulses resulting in more necrosis [56], [127], [128]. High intensity pulsed electric fields affect not only the plasma membrane, but also intracellular structures, such as the nucleus, endoplasmic reticulum, and Golgi complex. At longer pulse durations, cell death is immediate due to significant membrane damage, but at shorter pulse durations, damage to internal structures can lead to apoptosis [127]. Therefore, decreasing the externally applied pulsed electric field intensity may help reduce damage to these organelles and structures, thereby reducing apoptosis, and improving RE at certain pulse durations/intensities. In addition to influencing RE, at higher pulsed electric field intensities, more membrane damage was expected, resulting in more immediate cell death (necrosis). Kennedy *et al.* [12] adjusted the plasma membrane potential at localized points using a cationic peptide to test the hypothesis that it would result in more rapid cell death. This cationic peptide co-localized to the plasma membrane, which locally increased the transmembrane voltage without affecting internal organelles. This work focused on an IRE ablation technique due to the high toxicity of the cationic peptides used, and did not explore the possibility of membrane potential affecting RE.

Non-toxic methods must be used for membrane potential manipulation to be tested for enhancing RE in clinical applications. One possible non-toxic method for altering the membrane potential could involve exploring the effects of ionomycin. The reasoning is that several studies have reported the drug ionomycin activates K(Ca) channels, which affects the membrane potential, E_m according to the Nernst Goldman Equation below [129], [130]:

$$E_m = \frac{R\,T}{F}\ln\left(\frac{\sum_i^N P_{M_i^+}[M_i^+]_{out} + \sum_j^M P_{A_j^-}[A_j^-]_{in}}{\sum_i^N P_{M_i^+}[M_i^+]_{in} + \sum_j^M P_{A_j^-}[A_j^-]_{out}}\right) \quad (2)$$

where E_m is the membrane potential in volts, R is the ideal gas constant in joules per kelvin per mole, T is temperature in kelvin, F is Faraday's constant in coulombs per mole, P_{ion} is the permeability for the specific ion (M_i^+or A_j^-) in meters per second, $[ion]_{out}$ is the extracellular concentration of that ion (M_i^+or A_j^-) in moles per cubic meter, and $[ion]_{in}$ is the extracellular concentration of that ion (M_i^+or A_j^-) in moles per cubic meter. When dealing with potassium, the equation for $E_m$can be approximated by:

$$E_m = \frac{R\,T}{z\,F}\ln\left(\frac{[Ion]_{out}}{[Ion]_{in}}\right) \quad (3)$$

where z is the charge of a single ion, which for potassium is 1.

2.7 Electrochemotherapy

One illustrative application of modifying membrane potential for RE applications is electrochemotherapy (ECT). ECT combines RE with a chemotherapeutic drug which normally will not cross the cell membrane. RE allows the chemotherapeutic drug to enter the target cells, while minimizing the dose to healthy cells. Under the correct electroporation conditions and drug concentrations, ECT can leave healthy tissue intact (even if it lies within the treatment zone), while specifically targeting cancerous tissue, can be particularly useful treating tumors in sensitive areas. [104]. The most commonly used drugs for ECT are bleomycin and cisplatin. Bleomycin is either injected intravenously (IV) or intratumorally (IT), while cisplatin is reported as only IT. If a non-toxic

method for increasing membrane potential shows an advantage in cell viability during electroporation, it could potentially improve ECT treatment methods by doing less damage to healthy tissue in the treatment region, which is particularly useful in certain types of tumors (e.g. brain).

2.8 Gene delivery

One exciting prospect for using RE both clinically and in research settings is gene delivery. Gene delivery occurs when a gene, the functional portion of a DNA sequence, is transferred into a target cell. Once inside the cell, the foreign gene enters the nucleus where it is incorporated to the DNA sequence of this cell [131]. When the altered sequence replicates, it will produce different functional or regulatory proteins, changing the function of the cell. This change can be used for many purposes, ranging from labeling cells in a culture, for example by producing fluorescent proteins, to treating many types of genetic diseases by stopping the production of harmful proteins or activating the production of proteins that are lacking [131], [132]. Many methods exist to aid in genes passing through a cell's plasma membrane, such as direct injection, viral delivery, plasmid liposome complexes, cationic lipids, and electroporation [11], [76], [110], [133]–[135]. These methods were discussed in more detail in Section 2.3.

Currently, viral methods are the most commonly used technique despite drawbacks such as immune response to the virus, homologous recombination (which occurs when nucleotide sequences are exchanged between two similar sets of DNA), and possible oncogenic (cancer generating) effects [11], [136], [137]. For example, adeno-associated viral (AAV) vectors, one of the most useful type of viral vectors for gene therapy, have been used in clinical trials to treat a wide variety of diseases and conditions such as hemophilia B [138]–[142], lipoprotein lipase deficiency (LPLD) [143], Parkinson's disease [10], among others [135], [144]. The primary challenges with AAV vectors are the immune

response to large doses and the associated cost [139], [145]. Electroporation has shown promise to overcome the challenges with viral gene delivery methods [133].

Electroporation is particularly of interest for gene therapy for localized treatments (e.g. liver, kidney) [133]. It has been used for gene delivery primarily in small animals. More recently it has been used in humans in a handful of clinical trials such as delivering genes that reprogram the immune system to target cancerous cells [109], [146]. As discussed in Section 2.4, thus far, researchers have primarily used three different sets of pulse characteristics for electroporation-aided gene delivery, depending on the experimental goals [4]. First, using short duration pulses, on the order of 100 μs, a marginal level of gene transfection can occur with low cell mortality [122]. One example applying this technique found 30-40% of electroporated rat liver cells expressed a genetic marker 48 hours after experimentation, with around 5% of those still expressing the marker after 21 days [122]. Secondly, longer duration pulses, on the order of 20-50 ms, have shown higher transfection rates [147]. Lastly, a few studies have used a mixture of high amplitude, short duration pulses followed by a single low amplitude, long duration pulse with significant increases (greater than three times uptake) in expression of certain gene types at specific pulse durations and electric field strengths (80 V/.cm, 83 ms and 800 V/cm 0.1 ms, in muscle tissue) [148]. Each of these pulse characteristics have advantages and disadvantages. For example, longer pulses result in higher transfection rates, but also results in more cell death in the treatment region. Therefore, in sensitive regions, it may be better to use short duration pulses since they result in lower cell mortality, but also have lower transfection rates. For gene transfection, long duration pulses, on the order of 10-50 ms, are the most commonly used [85], [103], [110], [120], [133], [147], [149]–[151].

One potential method for increasing gene therapy delivery is combining aspects of different techniques. For example, one study combined adenovirus delivery of Smad7 with electroporation, which improved transfection of the gene in kidneys over either method alone (for short-term

expression of the gene) [110]. Another study tested a combination of AAV with numerous small molecules and discovered 13 different compounds which enhanced transgene expression [152]. These studies indicate there may be many yet untested ways to improve gene delivery well beyond what is currently available.

2.9 Tissue ablation with IRE

Irreversible electroporation also has clinical uses. Specifically, it has been used to ablate unwanted tissue, such as destroying tumors in patients with cancer or to deal with heart arrhythmias by destroying arrhythmogenic substrate [153]–[155]. IRE is currently considered an emerging technology in the field of cancer treatment [156]. Sources suggest various parameters for the electric field strength and pulse duration to optimize IRE, but the general consensus is to use electric fields of approximately 2000+ V/cm and pulse durations of 100 or 800 μs [106], [107], [157], [158].

IRE is being researched as a tumor ablation method for several reasons. One advantage IRE has over thermal based ablation techniques is how it interacts with nerves and blood vessels. IRE is less damaging to nerve and blood vessel structures, due to the innate structural differences between the tissue being treated and the structure of the nerves and blood vessels [105]. Electroporation is a membrane treatment, thus non-cellular structures such as the extracellular matrix remain intact, resulting in less swelling and faster healing [105]. Additionally, since IRE is a non-thermal ablation technique, it is not affected by the heat sink effect thermal ablation techniques suffer from when treating tumors near blood vessels [105]. The heat sink effect in this case occurs because blood flowing through blood vessels conducts heat to/from the nearby tissue, reducing effectiveness of thermal techniques near the blood vessels [105].

IRE can efficiently kill unwanted cells and has the potential to be a viable treatment option for many kinds of therapies, including destroying tumors. However, many challenges exist with successful implementation of this technique in a clinical setting. Among those are the high cost of equipment and electrodes, the necessity to perform multiple puncture wounds for each treatment (especially for large treatment zones), the learning curve required to efficiently use the equipment, and safety/pain concerns. For example, the most significant safety concern is that if the pulses are not correctly applied, they can result in transient ventricular arrhythmia. This can be overcome with ECG-synchronized delivery. [159]–[161]. Each factor needs to be considered and overcome when designing and using an IRE approach in a clinical setting. It is yet to be determined whether the advantages, such as being able to treat tissue close to veins and arteries and leaving structural and nervous tissue intact are beneficial enough to outweigh the drawbacks of this procedure.

2.10 Electroporation Equipment – Laboratory Setup

This section describes the basic electroporation equipment we used to perform *in vitro* experiments and test field strengths *ex vivo* in our lab. A pulse generator is typically used to deliver the pulsed electric field used for electroporation. We used the BTX ECM 830 Square Wave Electroporation System as our pulse generator to generate pulsed electric fields for all experiments in this investigation (shown in Figure 2-3). For *in vitro* experiments, the pulse generator was connected to a safety stand which encloses cuvettes and prevents accidental electric field exposure to researchers (Figure 2-4). Cuvettes, which hold *in vitro* samples containing cells and surround the samples with parallel conductive plates (Figure 2-5), were used extensively in our experiments. We filled these cuvettes (2 mm gaps between plates) with cultured cells which were suspended in an electroporation medium, placed in the safety stand, and then electroporated. Results were monitored using fluorescence microscopy, bright field

microscopy, or a luminometer, depending on the experimental design. Fluorescence microscopy uses absorption and re-emission of light at a different wavelength to detect molecules. This can be used to identify cells which have internalized a fluorescent molecule by shining light into a sample at a specific wavelength (called excitation). The fluorescent molecule absorbs that light and emits light at a longer wavelength, which can be detected by a fluorescent microscope [162]. Bright field microscopy is the simplest type of microscopy, which shines (bright) light on a (dark) sample, and is useful for a wide variety of applications [163], [164]. A luminometer is another device used to detect low levels of light, usually produced from luminescence/phosphorescence, or light emitted without a heat source [165]–[167]. One common example of this is luminescence occurring in a firefly from luciferase activity [167].

Figure 2-3. BTX ECM 830 Square Wave Electroporation System [168].

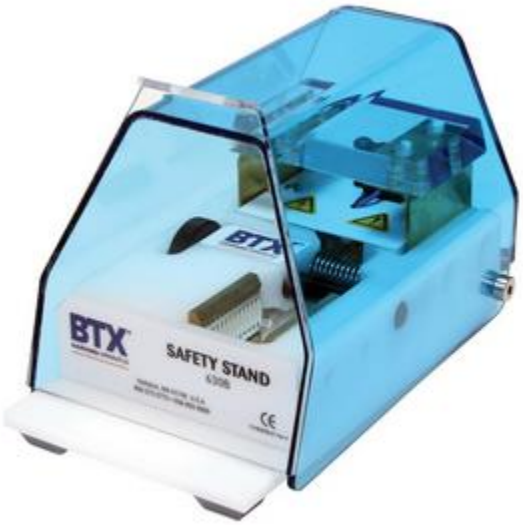

Figure 2-4. BTX Safety Stand [168].

Figure 2-5. Electroporation Cuvette [168].

2.11 Devices used for clinical electroporation delivery

Choosing the correct device for delivery of the electric fields is a vital step when using electroporation in vivo. The most common delivery method of pulsed electric fields for electroporation is using an electrode which is positioned at the targeted location (e.g. tumor location). Many different types of electrode designs have been used to deliver electroporation-based treatments both in *in vivo* animal studies and in the clinical setting. These electrode designs vary based on desired application and the tissue being treated. There are several classes of electrode design types: needle electrodes, plate electrodes, and endoscopic/catheter-based electrodes.

Among those, the most basic electrode design involves individually placing single needle electrodes in the desired location. This can be problematic because the distance between the tips can change if one of the electrodes is bumped, and it requires precise imaging to verify the electrodes are in the correct location and the correct distance apart. This distance is important because it directly impacts the electric field in the treatment region since electric field is dependent on distance. Precise positioning is important to achieve the desired electric field to be produced between the electrodes and reach the target location. This can be addressed by using a fixed array of needles. The needles in these arrays can be arranged in circular, linear, or other designs [112], [169]–[172]. Since the distance between the electrodes is known, the correct voltage can easily be chosen to yield the desired electric field strength for the procedure. If the treatment area is larger than the electrode, the electrode can be repositioned to treat the entire area. One downside of such procedure is it results in multiple entry points into the patient. For situations where it is important to have only one entry point (for example when treating brain tumors), an expandable array can be used [173]. This type of array has all the

probes packaged into a single tube, which is inserted into a single incision point. Once the tube is positioned at the treatment area, the electrodes extend outward from the tube and spread out, creating an array of needles [173].

The second class of electrodes is plate electrodes. Plate electrodes are most often used to electroporate the skin [4], [106], [111], [171]. These electrodes are either fixed in place or have a caliper design to clamp around the treatment area [4], [106], [111], [171]. Due to its design, these probes have limited practical applications and are not relevant to the proposed research presented here, and therefore are not discussed in detail in this background.

The third class of electrodes, endoscopic probes, are used to treat tissue located in cavities or hollow organs within the body. Several different designs for endoscopic probes have been developed. One common design involves two plate electrodes located at the end of the endoscope, and a vacuum system to draw tissue into the gap between the plates [174]. Current endoscopic probe designs are focused on larger dimension applications, such as colorectal and gastric tumors [174]. Another similar type of device is catheter-based electroporation instruments. A catheter is a flexible tube inserted through a small opening in the body and can be used to access structures such as veins, arteries, and the urinary tract. Existing electroporation catheters tend to be used in drug delivery or IRE applications into vein walls or tissue close to the device [15], [17], [175], [176]. One such use is the use of IRE to treat atrial fibrillation by destroying the electrically active tissue inside the pulmonary vein which causes atrial fibrillation [18]. Another is delivering genes to the spinal cord, which can potentially be used clinically to treat acute or chronic pain [16]. Additionally, vascular wall integrity is maintained when vessel walls are exposed to IRE, indicating that even for RE applications, small volumes IRE near the vessel walls is allowable [176], [177].

Most of the aforementioned electrode types require large or multiple incisions to reach tissues deep within the body, limiting the uses for *in vivo* applications such as gene delivery and tumor ablation

in such tissues. To address this, we designed a catheter type probe which can be used to treat tissues within the body with minimal incision. This device is described in detail in Chapter 6.

2.12 Statistical analysis used in this dissertation

Several different types of statistical analysis were used throughout this dissertation to fit the specific hypothesis being tested. We used the Student's T-test [178] to test the null hypothesis, that the means between two samples (e.g. treatment and control) were the same, versus the alternative hypothesis that they were different.

$$t = \frac{\bar{X}_1 - \bar{X}_2}{s_p\sqrt{2/n}} \qquad (3)$$

where

$$s_p = \sqrt{\frac{s_{X_1}^2 + s_{X_2}^2}{2}} \qquad (4)$$

s_p is the pooled standard deviation for $n = n_1 = n_2$, and $s_{X_1}^2$ and $s_{X_2}^2$ are the variances of sample one and sample 2 respectively. *t* values in conjunction with the respective degree of freedom for the specific test were used to estimate p-values (defined as the probability of getting a value more extreme or as extreme than the one observed, given the null hypothesis is true). Unless otherwise noted, we used a threshold for p-values of $p = 0.05$ for determining significance.

For situations where we wanted to predict and/or determine significance of a treatment effect on a continuous outcome variable, we used regression analysis. Regression analysis provides information on the change expected in the outcome variable by one unit change in the predictor [179]. In our specific context of design of experiments that explored a two-way completely randomized design we can understand results of the regression as the "effect" of treatments on the outcome. This research

focused on two: polynomial and spline regressions. This is because the relationship between predictors and outcome was, in all cases, complex and not expected to be linear. For non-linear relationships, polynomial regressions are better suited when relationships can be explained by low degree polynomials [180], as the biological interpretation of results becomes challenging as one departs towards higher order polynomials. At the same time, low degree polynomials have limits in the relationships they are able to depict, and high degree polynomials have a high cost and risk of overfitting data [180]. Spline regressions can overcome those issues and work well in certain situations that are not well modeled by polynomial regressions [180]–[184].

Polynomial regressions model the relationship between explanatory variables and the outcome variable using an n^{th} degree polynomial for each predictor. When modeling with polynomials, it is possible to underfit and overfit the model, therefore care must be taken when choosing the correct order for the polynomial to fit the data [63], [185]–[187]. Researchers should be able to justify the order of the polynomial used to model based on the underlying function they are trying to fit and expected complexity of the relationship. For example, in biology, there should be a biological reason for trends observed using the model [182]. In addition to a physical justification for the fitting, the Akaike Information Criterion (AIC) [63] and Bayesian Information Criterion (BIC) [185], [186] can be used to help determine the appropriate order by penalizing overfitting.

Spline regressions are similar to polynomial regressions, except they break the predictor variable into regions. Splines allow for better representation of highly non-linear data than polynomial regressions [180], [188]. The breakpoints that divide the separate regions are known as knots, which can be chosen by hand or through the use of pre-defined methods [183]. Spline regressions can allow different levels of smoothness by changing the order of derivative required at these knots [181]. In all analyses in this dissertation, we used cubic spline regressions, continuous for the first and second order derivatives, and selected knots to separate known regions. Cubic splines are commonly used to

model complex data, and continuous first and second order derivatives ensure the representation is smooth.

Chapter 3: **Cationic peptide exposure enhances pulsed-electric-field-mediated membrane disruption**

The preliminary research for this thesis started with finishing work related to a study performed by a previous graduate student, Steve Kennedy. This study investigated the use of cationic peptides to enhance electroporation [12]. In this study, a cationic peptide, polyarginine, was added in varying concentration to samples of HL-60 cells. These cells were electroporated with propidium iodide (PI) in the electroporation medium, which was used as a membrane integrity indicator. A variety of electric field strengths and pulse durations were tested. At field strengths of approximately 1-2 kV/cm and concentrations of >50 μg/ml of polyarginine, high levels of PI uptake were observed, while at these same levels in the absence of polyarginine, little PI uptake was detectable. Additionally, he concluded that PI entered primarily through the anode-facing side of the cells when exposed to the peptides. Cationic peptides localized to the membrane, and increased the membrane potential, making it easier to electroporate the cell at electric field intensities that normally do not cause such phenomena. This effect could be combined with cell targeting techniques to become a useful tool in destroying targeted cells. The focus of this paper was on destroying cells with IRE since the cationic peptides used were toxic and therefore not a good candidate for RE applications. This paper provided more evidence that adjusting the membrane potential prior to electroporation could improve electroporation effects and prompted us to want to explore the RE case in more depth with a non-toxic method for modifying the resting charge across the membrane.

My contributions to this research involved determining the relationship between propidium iodide fluorescence intensity and electroporation type (RE or IRE) by using a second membrane integrity indicator, trypan blue (TB). Addition of TB allowed us to determine whether there indeed was a relationship between electroporation type and fluorescence intensity, and if fluorescence intensity could be used to estimate the percentage of a sample that was IRE. Since TB addition partially interfered with the fluorescence brightness, we adjusted exposure times to allow for the same levels of brightness for RE cells. We observed a strong correlation between brightness and TB inclusion/exclusion. The baseline case (NEP cells) had low levels of light detected that were statistically lower from cells exhibiting RE and IRE signatures. RE cells typically internalized less than 200 million PI molecules per cell and had distinct levels of brightness from both NEP and IRE cells. Cells with fluorescence levels consistent with more than 200 million PI molecules entering a cell also internalized TB, indicating prolonged membrane disruption and likely cell death. These results are shown in Figure 3-1.

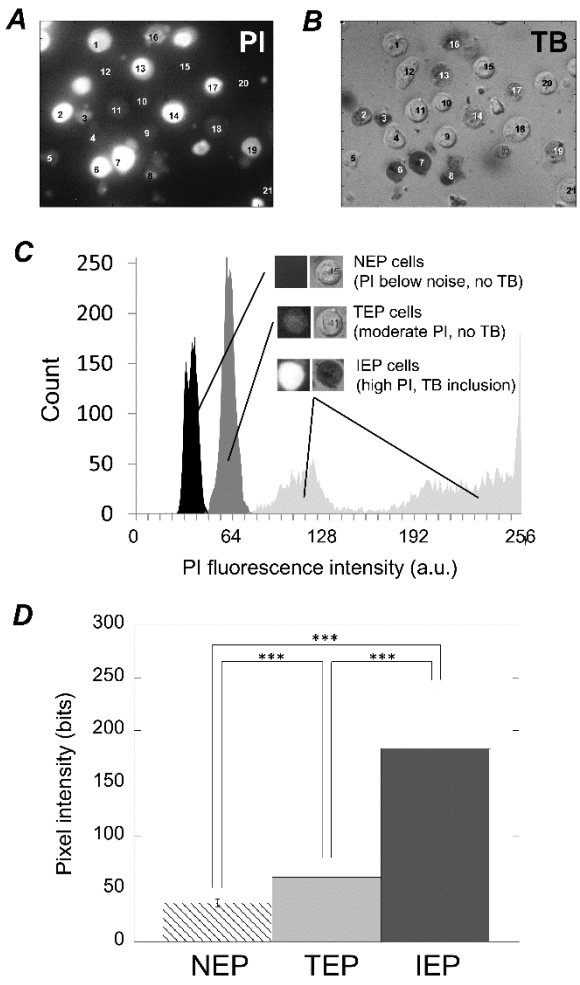

Figure 3-1 Relationship between Fluorescence intensity and electroporation type. From Kennedy *et al* [12]. A) PI fluorescence image, which was used to determine fluorescence levels of each cell. B) Bright field image used to determine each cell's location and whether TB entered the cell. C) Histogram of fluorescence intensities. The PI fluorescence was strongly related to the electroporation type determined by PI and TB method. D) Average fluorescence intensity of the different electroporation types.

This project provided background research necessary for achieving the second aim of improving RE outcomes by modifying membrane potential. Though this method proved there was a high correlation between fluorescence brightness and electroporation type, and was sufficient for this project, it also provided motivation to develop a higher throughput method for analyzing our samples.

Chapter 4: Analyzing Electroporation Outcomes with Fluorescence Microscopy

The purpose of this project was to improve our ability to detect electroporation compared to the propidium iodide uptake versus time analysis performed previously in our lab, and therefore satisfy Aim 1 of this thesis. The original protocols in our lab involved analyzing propidium iodide uptake over time. This provided valuable insight into certain aspects of electroporation, however most of the planned projects would require more samples than could be easily attained by analyzing one slide for 20-30 minutes. We developed a method that formed the basis for the rest of the *in vitro* electroporation research performed in this thesis.

4.1 Method for Analyzing Electroporation Outcomes with Fluorescence Microscopy

Erik J. Aiken, Brian G. Kilberg, Susan C. Hagness, John H. Booske

Abstract—Electroporation is a technique that uses pulsed electric fields to transiently or irreversibly open pores in cell membranes. Transient electroporation (TEP) offers a means for introducing normally membrane impermeable macromolecules such as DNA or drugs into a cell's cytoplasm, while irreversible electroporation (IRE) may be used to destroy diseased or unwanted cells. Identifying suitable pulse parameters (e.g. voltage, duration, and number) that achieve the desired effect requires the ability to differentiate between electroporation outcomes. Electroporation is often detected using fluorescent molecules as membrane integrity indicators. In this paper, we present a computer-based method to quantitatively analyze fluorescence microscopy images and distinguish between non-electroporated (NEP) and electroporated cells by comparing each cell's fluorescence

intensity to the local background luminescence. Discrimination between TEP and IRE is based on internalization or exclusion of a second membrane integrity marker. This procedure improves precision and accuracy over previous methods for analyzing fluorescence microscopy images to determine fluorescent marker uptake and electroporation outcome. In an example using propidium iodide as the electroporation indicator, the observer-to-observer variability in the determination of electroporation outcome was significantly reduced by replacing a purely visual inspection of fluorescence images with the computer-based protocol introduced here. In another example the false positive and false negative rates were significantly reduced by replacing a quantitative analysis technique that makes use of a global intensity threshold with our proposed method.

Index Terms—Bioelectric phenomena, biomembrane transport, cell membrane, drug delivery, electroporation, high-voltage pulses, HL-60 cells, transmembrane voltage.

I. INTRODUCTION

Image analysis is required to determine the presence or absence of these indicators when using microscopy to visualize the cells. Analysis based solely on visual inspection suffers from subjectivity in distinguishing between NEP cells and cells that undergo TEP with minimal internalization. A quantitative analysis using a fixed luminescence intensity threshold is also not ideal because stray light, such as coronas surrounding intensely fluorescing cells, can interfere and cause false positives (defined as the erroneous determination of electroporation for a NEP cell).

In this paper, we present an improved method of analyzing fluorescence microscopy images to distinguish between electroporation outcomes. This method uses quantitative analysis to determine if a cell is fluorescing by comparing each cell to the local background luminescence intensity. We illustrate this method using propidium iodide (PI) as a fluorescent membrane integrity indicator. PI is

normally a membrane impermeable molecule. It binds to intracellular nucleic acids when it crosses the cell membrane (either through electroporation or cell death), causing a significant increase in fluorescence. Thus, PI fluorescence is only detectable once the molecule has passed through the plasma membrane. In our illustrative example, we use trypan blue (TB) as the secondary indicator to distinguish TEP from IRE. (TB could be replaced by a second fluorescent membrane integrity marker if multiple fluorescence channels are available.) Images collected from HL-60 cells exposed to a 40 μs PEF over the range of 0 to approximately 8 kV/cm were independently analyzed by two researchers using both a purely visual identification method and our proposed local-intensity quantitative method to determine PI internalization. The results generated by the two independent observers demonstrate that the local-intensity quantitative analysis technique offers significant improvement in precision over visual identification. Additional results generated from a comparison of the local-intensity quantitative method to a quantitative method that uses a global fixed-intensity threshold demonstrate an improvement in accuracy of the electroporation outcome determination.

II. MATERIALS AND METHODS

A. Electroporation Protocol

Human promyelocytic leukemia cells (HL-60) (American Type Culture Collection, Manassas, VA, USA) were used for all electroporation experiments because their spherical shape eliminates the dependency of the electroporation outcome on the cell's orientation relative to the electric field. The HL-60 cells were cultured at 37°C and 5% CO2. The incubation medium was RPMI-1640 with L-glutamine (Mediatech, Inc., Manassas, VA, USA), supplemented with 10% fetal bovine serum (VWR, Philadelphia, PA, USA) and 2% penicillin and streptomycin (Global Cell Solutions, Inc., Charlottesville, VA, USA).

Slides were treated with poly-L-lysine adhesion coating (Sigma-Aldrich, Madison, WI, USA) at least one day prior to experimentation and then allowed to dry for at least 24 hours. Immediately before experimentation, cells were counted, pelleted, and re-suspended in Hank's balanced salt solution (HBSS) (Thermo Scientific, Waltham, MA, USA) (1.42 S/m conductivity) at a concentration of 2 million cells per milliliter. The count was used to determine the percentage of dead cells at the beginning of each trial. PI (MP Biomedicals, Solon, OH, USA) was used as the primary membrane integrity indicator. PI was dissolved in HBSS and added to the cell/HBSS mixture resulting in a final PI concentration of 30 μM.

A BTX Model ECM 830 Square Wave Electroporation System (Harvard Apparatus, Holliston, MA, USA) was used to deliver the PEF. Cells were electroporated in a 2-mm electroporation cuvette designed for this electroporation system. Square, monopole, 40 μs pulses with voltages up to 1.5 kV were used for this study. After electroporation, cells remained in the cuvettes undisturbed for 30 minutes to allow for transient pores to close.

TB (Lonza, Walkersville, MD, USA) was added 30 minutes after electroporation as the second membrane integrity indicator. Five minutes after the addition of TB, 13 μL of the cell/HBSS/PI mixture was injected onto a poly-L-lysine coated slide with a nylon washer placed in the middle to form a well for the cells. The cells were allowed to settle on the slide for 7 min, after which bright field and fluorescence images were taken. PI fluorescence was monitored using fluorescence microscopy at 535 nm excitation and 617 nm emission wavelengths. A Lambda DG-4 excitation lamp and high-speed wavelength switcher (Sutter Instrument, Novato, CA, USA) were used to excite the PI. Control of the lamp and CCD camera was done with custom software (Prairie Technologies Inc., Madison, WI, USA). A Nikon Eclipse TE200 microscope (Nikon USA, Melville, NY, USA) equipped with a Hamamatsu C4742-95 Digital charge-coupled device (CCD) camera (Hamamatsu Photonics,

Bridgewater, NJ, USA) was used to capture all images taken in this study. A timeline of the experimental procedure is provided in Table 4-1.

Table 4-1

TIMELINE OF EXPERIMENTAL ELECTROPORATION PROCEDURE.

Time	Task
T = -24 h	At least one day prior to the start of the experiment prepare Poly-L-Lysine coated slides.
T = 0 min	Count cells to determine the percentage that are living. Place cells into centrifuge tube. Centrifuge until pellet forms. Re-suspend cells in HBSS at a concentration of 2 million cells per ml. Mix with equal parts of 2x (60 µm) PI solution. Incubate for 10 min.
T = 10 min	Place 200 µL of cell/PI mixture into a 2-mm cuvette. Electroporate cells. Leave cells undisturbed for 30 min.
T = 40 min	Add 2 µL of TB to the cuvette. Allow to sit for 5 min.
T = 45 min	Place 13 µL of cells on slide inside the nylon washer. Allow to settle for 7 min.
T = 52 min	Take snapshots of bright field and fluorescence images. Save files as 16-bit .tiff images to analyze in MATLAB®.

B. Analysis Method – Visual Techniques

TB internalization was determined by visually inspecting the bright field images as seen in Figure 4-1(a). Any in-focus cells darker than the norm were counted as having internalized TB. For example, in Figure 4-1(a), cells labelled 1 through 5 were identified as having internalized TB. Any cells considered TB-positive were counted as IRE. The precision of this visual inspection technique was tested using two independent observers. The results were then compared to determine if visual inspection was reliable for determining TB internalization.

The approximate percentage of dead cells at the beginning of the experiment was identified using TB and a hemocytometer using a standard cell counting protocol. As part of the analysis protocol, the percentage of cells identified as dead at the beginning of the experiment was subtracted from the

percentage of cells identified as IRE. This minimizes the effect that a variable number of dead cells at the start of the experiment has on the IRE determination.

A similar technique was performed to illustrate the difficulty of visually determining PI internalization. Two researchers independently counted the number of fluorescing cells using visual inspection. Images were displayed using MATLAB® (The MathWorks, Natick, MA, USA). The colormap for the fluorescence image was adjusted to provide better contrast for dimly fluorescing cells. A cell was counted as fluorescing (and thus having internalized PI) if an observer perceived it to be visually brighter than the surrounding background. Results using the same colormaps were compared and the variability between observers was reported.

C. Analysis Method – Quantitative Techniques

The methods for performing quantitative analysis on fluorescence microscopy images (as opposed to analysis based purely on visual inspection) involve analyzing optical images acquired following the addition of TB. Cells that internalized both TB and PI were counted as IRE, cells that internalized PI but excluded TB were counted as TEP, and cells that excluded both TB and PI were counted as NEP.

The location of each cell was manually identified via visual inspection of bright field images acquired during the electroporation procedure. A representative bright field image is shown in Figure 4-1(a). We also used the bright field images to visually determine TB internalization.

To distinguish between fluorescing and non-fluorescing cells, we used MATLAB® to quantitatively analyze the fluorescence images. First, we compared each cell's internal fluorescence intensity to a global fixed-intensity threshold. Second, we used our proposed method whereby we compared the cell's internal fluorescence intensity to several local intensities in the background region surrounding the individual cell. The fluorescence intensity inside the cell was determined by selecting a pixel near the center of the cell and then averaging the intensity throughout an M×M area centered

on the chosen pixel, where M was chosen to be 11 pixels. Hereafter, these M×M areas are referred to as pixel blocks.

In order to measure the background fluorescence, we sampled three external regions, approximately evenly spaced around the cell. In preliminary trials, we found that using fewer than three regions created too much sensitivity in the determination of whether a cell was classified as fluorescing to the specific location of the regions (particularly near bright cells which had a visible corona surrounding them). Using more than three regions did not result in any notable benefit. The locations of the pixel blocks were chosen to be roughly equidistant from each other at a distance of approximately 10 microns from the outside border of the cell. The center of each of these pixel blocks is marked with an "x" as shown in Figure 4-1. The cell was determined to be fluorescing if its average internal fluorescence value exceeded a threshold of T times the local average external luminescence intensity.

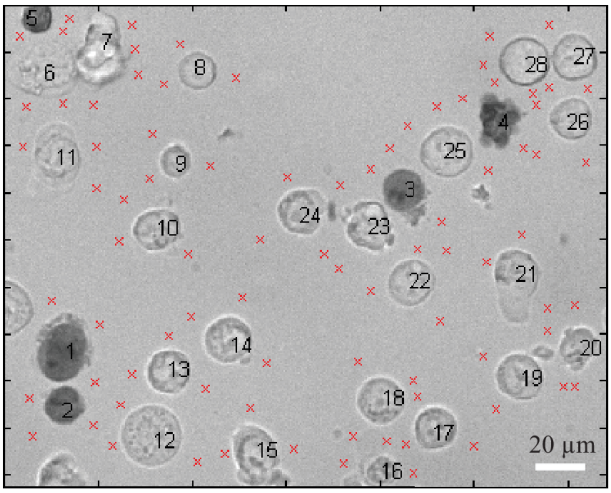

(a)

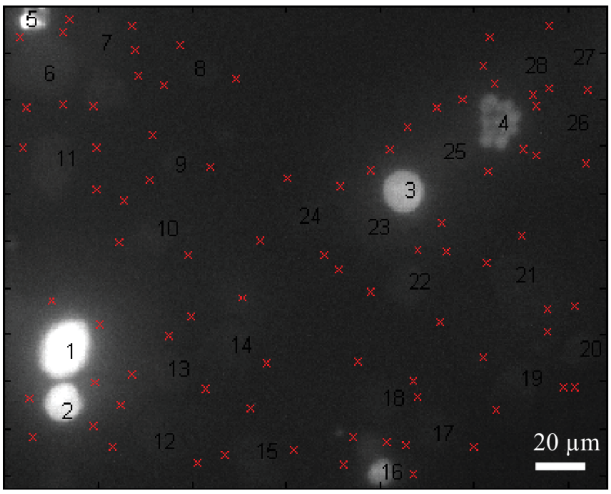

(b)

Figure 4-1. A representative bright field and fluorescence image illustrating the quantitative image analysis method used in this study. Fluorescence intensity inside each cell was determined by comparing an M×M pixel block inside the cell, in the region of the cell number label, and comparing it to three M×M pixel blocks surrounding the cell, the center of which is marked with the red x. Any cell exhibiting fluorescence above a chosen threshold was recorded to have internalized PI, the membrane integrity indicator. Cells internalizing both TB and PI were considered to be IRE, cells internalizing only PI were considered to be TEP, and cells excluding both membrane integrity indicators were considered to be NEP. IRE cells typically exhibit higher amounts of fluorescence than TEP cells. (a) is the bright field image and (b) is the fluorescence image. The scale bar represents 20 µm.

The threshold intensity, T, was chosen by examining the results of experiments with no externally applied electric field, for which the ground truth is known. Namely, these experiments should have IRE outcome determinations (i.e. cells identified to have internalized both TB and PI) equal to the number of dead cells at the beginning of the experiment and no TEP outcomes (i.e. no cells that internalized PI but excluded TB). Thus, a determination of TB internalization without PI internalization is defined as a false negative, while a determination of PI internalization without TB internalization (i.e. a determination of TEP) is defined as a false positive. A range of thresholds were tested, and the number of cells identified to be fluorescing was recorded. The results of changing T are shown in Figure 4-2. As threshold T increased, the number of false positives decreased. However, increasing the threshold also resulted in an increase in false negatives. For this series of experiments, threshold T was chosen such that there were as few false negatives as possible; this occurred over the threshold range of 1.05 through 1.15. A specific value within this range was chosen by considering where the false negatives were lowest, i.e. at 1.125 through 1.15 in this range. Therefore, in our specific experiments, the threshold was chosen to be T=1.125. This threshold matches well with the cutoff range for normally distributed NEP cells, as shown in Figure 4-3. In this figure, cells not exposed to electric fields, yielding mostly NEP cells, with some percentage appearing as IRE due to dead cells in the sample. In total, 50 cells in this sample were visibly stained with TB. Therefore, with a threshold of 1.125, 6 cells out of >330 sampled would be falsely labeled as RE, or less than a 2% error rate, most of which was caused by artifacts in the image (such as floating IRE cells above the focal plane). This is a close match to previous results in our lab, such as those shown in Figure 3-1c.

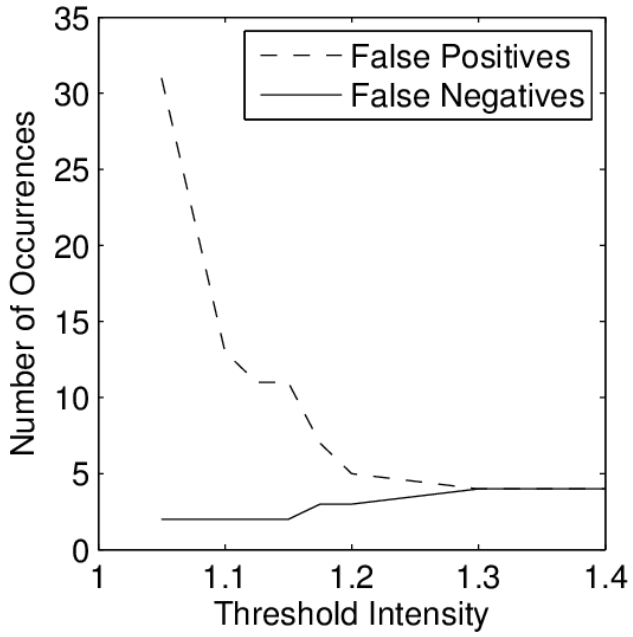

Figure 4-2. The effect of changing the intensity threshold on false negative and false positive determinations of PI internalization. The threshold intensity (T) multiplied by the local background luminosity is the value that a cell's internal luminosity must exceed in order to be considered to have internalized PI. The number of occurrences represents the total number of false positives or false negatives counted in the sample.

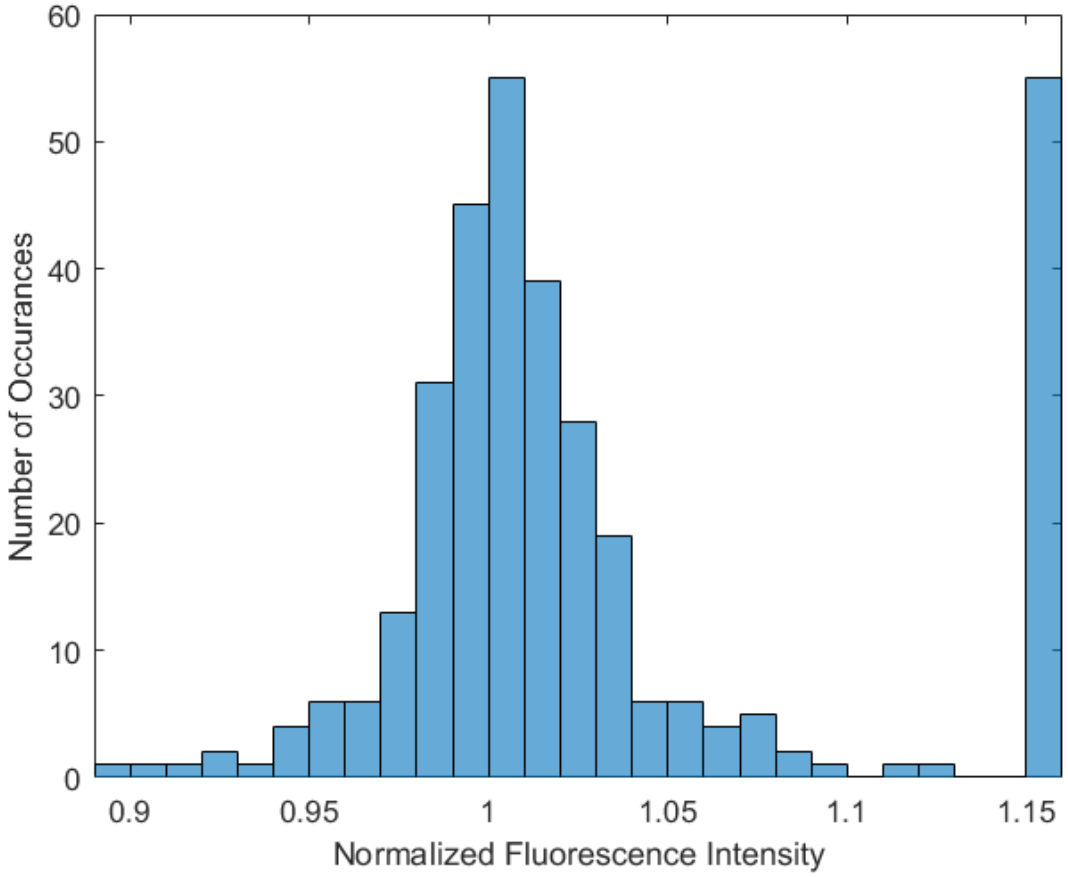

Figure 4-3 Histogram of internal fluorescence intensity divided by local background luminescence. The leftmost bin represents all values less than 0.9, and the rightmost bin represents all values greater than 1.15. NEP cells are normally distributed around 1, most falling between 0.9 and 1.1. Samples contained only NEP and dead cells only. 50 cells in this group were stained with TB out of 56 total cells with greater than 1.125x the background luminescence, resulting in <2% false positive RE cells.

There were several reasons why we chose to prioritize minimizing false negatives rather than minimizing the total number of cells incorrectly counted. In general, IRE and dead cells will have a higher level of PI internalization compared to TEP. This means that if this method results in any false negatives when labeling dead cells, it will also miss many TEP cases. Additionally, false positive identification can be the result of artifacts in the image, such as cells reflecting light from brightly fluorescing cells.

A t-test was used to confirm that average intracellular pixel intensities exceeding 1.125 times the local average external luminescence intensity were reliably indicative of cell luminescence, and not a

result of background noise ($p<0.001$). This was done using randomly selected background areas and comparing to three nearby points. In general, the process described above can be used to establish an appropriate discrimination threshold. A similar approach was used to determine the threshold value used in the global fixed-intensity threshold analysis.

D. Analysis of Precision and Accuracy

Precision was evaluated by comparing the results generated by two independent observers analyzing the same images. The variation in detecting both TB and PI internalization visually was determined for a sample set of approximately 280 cells. This same batch of experiments was analyzed by the same two observers using the quantitative technique (with three manually selected background regions) as described in Section II-C. Accuracy was evaluated using the known ground truth case (no externally applied electric field) as described in Section II-C.

III. RESULTS

Cells were electroporated at 0, 411, 775, 1170, 1362, 1544 V (with a standard deviation of ≤ 1.6%) in cuvettes with a gap size of 2 mm. When using 2-mm cuvettes, any voltage higher than ~1550 V resulted in an arc (when using HBSS as the electroporation medium). Therefore, experiments were not performed at any higher voltages. All electric field strengths are reported in kV/cm, calculated by dividing the gap voltage by the gap spacing of 0.2 cm. Fourteen samples were taken at each voltage setting.

To compare the precision of our computer-based quantitative image analysis method relative to that of the purely visual technique, two experimenters conducted independent visual determinations of fluorescing cells on six different samples, using the method described in Section II-B. The precision

of the results was quantified using the procedure outlined in Section II-D. Of the cells sampled, approximately 25% were identified differently between the two experimenters, likely due to several factors, including screen brightness. Additionally, humans are known to be inconsistent in color shade matching [189]. These same experiments were analyzed using the new method, which resulted in less than 0.5% of cells being identified differently between the same two experimenters. The method described in Section II-B was also performed to test the precision of visually determining TB internalization. The two observers' determinations of TB internalization disagreed for 4% of the cells sampled. To account for this variation and reduce the effect of the observer, we averaged the results of two independent observers' determinations of TB internalization.

Accuracy was optimized using a range of thresholds, as described in Section II-C, for the new local-intensity quantitative analysis method and a global fixed-intensity threshold quantitative technique. Using the three background-region analysis, with the tuned threshold of T=1.125, we identified that there were 11 false positives and two false negatives out of 333 total cells analyzed using the local-intensity quantitative analysis method. We then analyzed the same samples using the global fixed-intensity threshold method. To fairly compare the two, we chose a global intensity threshold such that the number of false positives obtained with the global fixed-intensity threshold method matched the number of false positives obtained with the fixed-intensity threshold method at T=1.125. At this global threshold value, there were 29 false negatives. Thus, the new method resulted in 62% fewer false negatives than a global fixed-intensity-threshold quantitative method.

Figure 4-4, 4-5, and 4-6 show the results for NEP, TEP, and IRE outcomes, which are presented as a demonstration of the technique presented in this paper. The central line in these boxplots represents the median, and the edges of the box represent the 25th and 75th percentiles. The whiskers extend to cover data within a 99.3% confidence interval, assuming normally distributed data. The 99.3% confidence interval corresponds to the default whisker length in MATLAB® of 1.5. Outliers

are marked with a + sign. Figure 4-4 shows the percentage of cells identified as NEP at the tested electric field strengths. The percentage of cells identified as NEP decreases as field strength is increased, which is consistent with existing literature. Figure 4-5 shows the TEP results. With these specific experimental parameters, the highest TEP percentage is 58% and occurs at 5.9 kV/cm. When used in gene transfer, electroporation has a survival rate of 20-60% [1], [8], so our TEP results are also consistent with existing literature. Figure 4-6 shows IRE results, where the percentage IRE increases with increasing field strength, as expected.

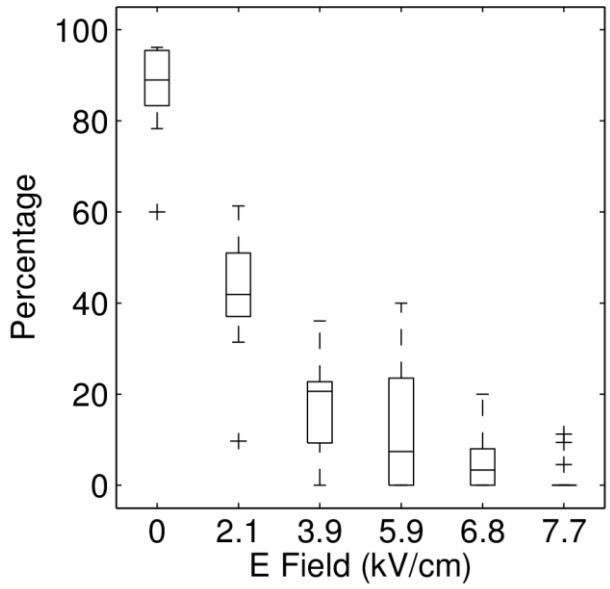

Figure 4-4. Percentage of cells that did not internalize TB or PI. Cells that excluded both membrane integrity markers were deduced to be NEP. Pulse duration was 40 μs. The edges of the box represent the 25th and 75th percentiles and the whiskers extend to the most extreme non-outlier data points. Outliers are denoted by the + symbol.

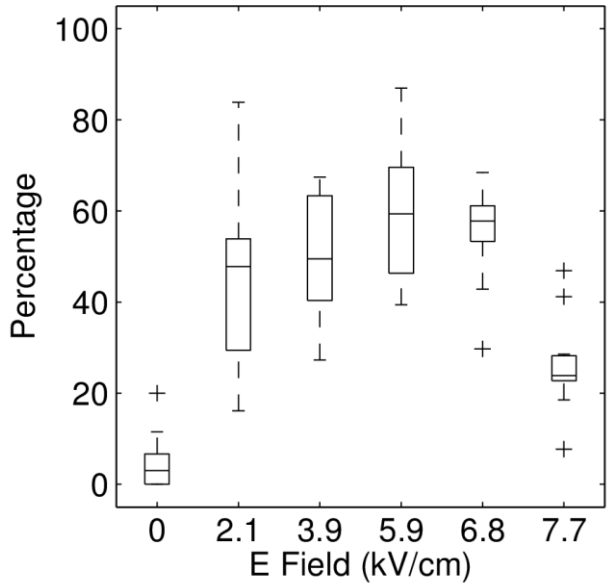

Figure 4-5. Percentage of cells that internalized PI and excluded TB. Cells that excluded both TB but included PI were deduced to have undergone TEP. Pulse duration was 40 μs. The edges of the box represent the 25th and 75th percentiles and the whiskers extend to the most extreme non-outlier data points. Outliers are denoted by the + symbol.

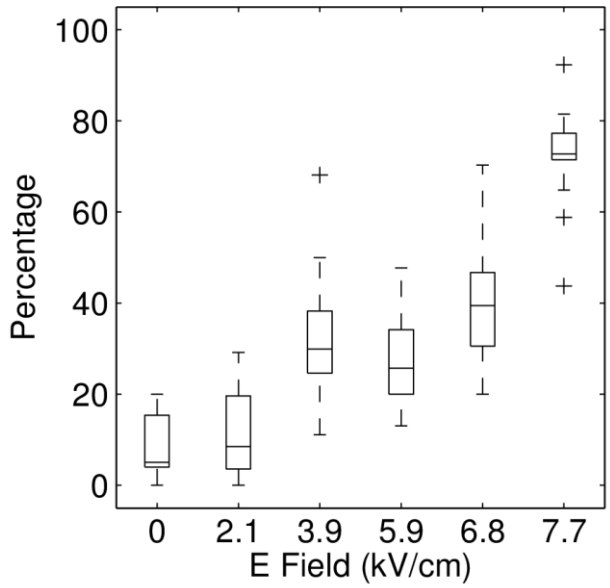

Figure 4-6. Percentage of cells that internalized both TB and PI after removing the average percentage of cells determined to be dead prior to the start of each experiment. These cells were

deduced to have undergone IRE. Pulse duration was 40 μs. The edges of the box represent the 25th and 75th percentiles and the whiskers extend to the most extreme non-outlier data points. Outliers are denoted by the + symbol.

IV. DISCUSSION

There exists some inherent error when using TB and PI internalization to identify which type of electroporation had occurred. At 0 kV/cm an ideal situation would result in 100% of the sample being identified as NEP. As evident in Figure 4-4, a small percentage of the cells internalized TB and/or were fluorescing enough to be determined as PI positive. This small percentage is likely the result of variability in the number of dead cells in the sample at the beginning of each data acquisition period, despite measures taken to remove dead cells from consideration. Additionally, TB molecules are slightly larger than PI, meaning it is possible for pores to open that are large enough to allow PI internalization, but still exclude TB. Also, as previously discussed, while this method was designed to reduce PI false positives, it cannot completely eliminate them without inducing an unacceptable number of PI false negatives. These issues may be the cause of the small number of TEP cells identified at 0 kV/cm (shown in Figure 4-5).

Data gathered using the techniques outlined in this paper can be used to determine electroporation parameters for specific applications. In our specific example, the highest electric field of 7.7 kV/cm yielded approximately 70% IRE and ~25% TEP (with less than 2% NEP outcomes); this type of outcome is appropriate for applications that require maximizing the IRE outcomes from a single pulse. Another useful trend to note is that with these specific settings, the percentage of cells identified as TEP is relatively consistent between 2.1 kV/cm and 6.8 kV/cm. Therefore, when TEP is the desired outcome, the electric field strength can be selected from within this range at a level that best accommodates the more nuanced needs of a specific application (i.e. choosing whether it is better for the alternate outcome to be NEP or IRE).

V. CONCLUSION

The quantitative analysis procedure developed for determining PI internalization the local-intensity quantitative analysis method presented in this paper provides a significantly less subjective and more accurate method for determining electroporation outcomes using single channel fluorescence microscopy. This method can be combined with visual identification of TB to create a computer-based method for quantitatively analyzing single channel fluorescence microscopy images to distinguish between NEP, TEP, IRE cells.

This method offers an improvement over other microscopy techniques that determine electroporation outcomes because it reduces the error caused by different observers when using visual techniques. The method described in this paper improves precision over visual identification of PI and TB internalization and is more accurate than a fixed intensity threshold method. For example, in an illustrative comparison, the observer-to-observer outcome assessment variability was reduced from 25% to 0.4% between a purely visual inspection of fluorescence images and the local-intensity quantitative analysis protocol introduced here. The number of false positive for PI cells was reduced by 62% from a fixed intensity threshold method.

This procedure can be useful for predicting the approximate distribution of cells that were NEP, TEP, and IRE at a given electric field strength and thus aid in determining the proper electroporation parameters for a desired outcome. This technique allowed us to process more samples within our existing laboratory setup. It was designed specifically to function well with our existing laboratory setup.

4.2 Automated detection of cells and image analysis

To process more samples quickly, we decided to develop a program that would automate our image analysis. To do this, we needed a program capable of identifying unstained cells in a bright field microscope image, stores the coordinates, compares to an after image which determines if a cell has moved, then for cells which remained stationary, analyzes internal fluorescence of the cell and compares it to the local background fluorescence, and detects TB within bright field images. We chose to use MATLAB® to achieve this. All staining procedures are the same as discussed in Chapter 4.1. We used bright field and fluorescent images like those in 4.1.

To detect cells in a bright field image, we decided to identify edges within the images. First, we filtered the images using Gaussian and average filters to smooth the background noise. Cell edges were then identified on bright field images using the Sobel edge detection method (part of MATLAB's Image Processing Toolbox), where the threshold was determined by testing numerous images generated from our lab to minimize false positives. Cell outlines were generated from the edge detection by a combination of removing small objects (i.e. remaining background noise), dilating, filling, thinning, and using the Sobel edge detection on the filtered image to re-find edges. This process is depicted in Figure 4-7. We also removed any cells touching the border of the image at this stage. We then identified the center and radius of every remaining enclosed area, which after the correct tuning parameters (such as cell size and values for how much noise to include) were input, outlined single and small clusters of cells. Large clusters of cells appeared as a single large cell and were therefore removed from the analysis, since detecting an individual cell's fluorescence is difficult if the cell is part of a large cluster.

Figure 4-7. Automatic cell detection. This figure provides an example of how cells were detected using this method. From left to right: Bright field image of cells, Sobel edge detection, dilate and remove small objects, outline, and smooth outlines shown on original images.

This method was highly effective at identifying single cells and cell groups of two, however larger clusters of cells would appear as one large area. To rectify this problem, we removed any objects significantly larger than normal (later in the procedure) and adjusted procedures within the lab to avoid this, particularly by being careful of the final concentration of cells. This is a good general practice, since it can be difficult to identify an individual cell's fluorescence within a large cluster of cells regardless of the analysis method used.

After cells were detected using edge detection, the cell movement between a before and an after image was determined. Any cells with more than 50% overlap between the before and after images were kept.

The local background fluorescence was determined by removing the areas in the image for all detected cells (even those on the boarders of the image) plus a small margin around them. These areas were replaced with NaN values, which are not counted when averaging using MATLAB's® nanmean function. Anything brighter than a pre-determined threshold was counted as fluorescing.

Cells in the 'before' image were analyzed based on their darkness to determine if TB was internalized. Cells which internalized both TB and were counted as fluorescing were determined to be IRE, cells which did not internalize TB and were fluorescing were determined to be RE, and cells

which did not internalize TB and were not determined to be fluorescing were determined to be NEP. Any cells which were identified as internalizing TB but not fluorescing were labeled with an Error tag to be analyzed individually, which rarely happened, and was generally the result of foreign objects getting into the sample. We adjusted parameters, including allowed cell size, fluorescence intensity for PI detection, and pixel darkness for TB detection in this method to allow it to match our existing results. In a random selection of samples, the average difference between the automated method and the existing method was 3.9%, with an aggregate difference of 0.2% across all samples tested. Additionally, the standard deviation of the automated method was 6.7% compared to 8.3% for the existing method, indicating that the automated method reduces variance. Development of this automated method improved our results from Aim 1 and significantly improved our internal lab operation, reducing labor by hundreds of hours per project and reducing the chances of human error.

Chapter 5: **Ionomycin-Induced Changes in Membrane Potential Alter Electroporation Outcomes in HL-60 Cells**

Since the work with cationic peptides was primarily focused on IRE [12], we decided to investigate the effects of changing the resting membrane potential on electroporation outcomes with a specific focus on RE outcomes. Improving RE outcomes could be useful in a wide range of applications since the widespread use of RE as a molecule delivery technique is largely limited by its relatively low efficiency [1], [8], [190]. We also reviewed the mechanisms of electroporation causing cell death (IRE) to find ways to reduce IRE therefore further improve RE outcomes.

In order to reduce IRE it is important to recall that cell death resulting from electroporation is caused by either apoptosis or necrosis [56], [127], [128]. The type of cell death is primarily dependent

on pulse duration, with short duration pulses primarily causing apoptosis, and long duration pulses resulting in more necrosis [56], [127], [128]. Short duration pulses affect not only the plasma membrane, but also intracellular structures, such as the nucleus, plasma membrane, endoplasmic reticulum, and Golgi complex [127]. Reducing the externally applied PEF intensity may help reduce damage to these structures, thereby reducing apoptosis, and improving RE at certain pulse durations/intensities. Therefore, we hypothesized that one way to do so is hyperpolarizing the cell membrane, which would increase RE at lower PEF durations/intensities. More specifically, it would cause less apoptosis from organelle damage due to lower applied electric fields required to cause electroporation on the outer membrane. At higher PEF intensities, we hypothesized that the mechanism for cell death changes and we expect more cell death due to plasma membrane destruction when hyperpolarized. We conducted the following experiment to test these hypotheses. Completion of this section satisfied Aim 2 of this dissertation.

5.1 Ionomycin-Induced Changes in Membrane Potential Alter Electroporation Outcomes in HL-60 Cells

E. J. Aiken, B. G. Kilberg, S. Yu, S. C. Hagness, and J. H. Booske

The Department of Electrical and Computer Engineering, University of Wisconsin-Madison, Madison, Wisconsin, United States of America

As accepted by Biophysical Journal, DOI: 10.1016/j.bpj.2018.05.018

5.2 Abstract

Previous studies have shown greater fluorophore uptake during electroporation on the anode-facing side of the cell than on the cathode-facing side. Based on these observations, we hypothesized that hyperpolarizing a cell prior to electroporation would decrease the requisite pulsed electric field (PEF) intensity for electroporation outcomes, thereby yielding a higher probability of reversible electroporation (RE) at lower electric field strengths and a higher probability of irreversible electroporation (IRE) at higher electric field strengths. In this study, we tested this hypothesis by hyperpolarizing HL-60 cells using ionomycin prior to electroporation. These cells were then electroporated in a solution containing propidium iodide, a membrane integrity indicator. After 20 min, we added trypan blue to identify IRE cells. Our results showed that hyperpolarizing cells prior to electroporation alters the PEF intensity thresholds for RE and IRE, allowing for greater control and selectivity of electroporation outcomes.

5.3 Introduction

A pulsed electric field (PEF) applied across a cell membrane causes positive and negative charges to accumulate at opposite sides of the membrane, increasing the transmembrane voltage [71]. If sufficient charge accumulates for a long enough time, pores will open in the cell membrane [1], [12], [67], [71], [191]. This phenomenon is referred to as electroporation [1], [12], [191]. There are three potential outcomes of electroporation. It can cause irreparable damage to the cell membrane resulting in cell death. This outcome is denoted as irreversible electroporation (IRE) [1], [12], [191]. Alternatively, the pores generated during electroporation may close after a short delay, allowing the cell to remain viable [81] - an outcome known as reversible electroporation (RE) [1], [12], [191]. A

third possible outcome of PEF exposure occurs when the energy delivered is insufficient to open a significant number of pores or the pores opened are of negligible size. Cells under this condition are considered non-electroporated (NEP) [1], [12], [191].

IRE and RE both have important clinical applications. IRE shows promise as a non-thermal technique for ablating tissue [7], [105], [106]. In contrast to thermal ablation techniques such as radio-frequency (RF) ablation, IRE-based ablation is not impeded by heat sink effects of nearby veins and arteries [7], [105], [106], [192], [193]. Additionally it leaves the extracellular matrix intact [7], [194] and avoids an inflammatory response [195]. It is also useful due to its short treatment time compared to RF ablation and cryosurgery [77]. RE is a promising technique for delivering macromolecules such as proteins, DNA, RNA [1]–[3], [149], [196]–[198], antibodies [4], and nanoparticles [5], [6] into a cell's cytoplasm. In contrast to viral delivery techniques, RE does not invoke an immune response and can transfect larger DNA molecules [8], [36], [58], [199]. One limitation of current RE procedures is the relatively low survival rate of the treated cells [8], [199]. Improving cell viability will make RE more attractive for therapeutic applications involving the insertion of DNA, proteins, enzymes, or drugs into cells [90], [200].

There is interest in developing methods that increase the probability of RE or IRE depending on pulse parameters. In this paper, we are focusing on a potential method that exploits manipulating the transmembrane potential across cell's plasma membrane prior to electroporation. Previous studies have indicated a correlation between transmembrane electric potential and pore creation. One of the earliest studies reported the discovery that more fluorophores entered the cell through the membrane the facing positive electrode (anode) than through the opposing side [126]. The inner portion of cells are normally negatively charged, which is balanced by charges on the external face of the plasma membrane from protons or cations, resulting in a natural anion-membrane-cation transmembrane potential [101], [102]. This naturally occurring phenomenon has been attributed to the increase in pore

formation near the anode [126], [201]. This suggests that altering the transmembrane potential prior to electroporation could decrease the applied PEF threshold for electroporation and increase the probability of RE or IRE depending on pulse parameters. Kennedy *et al.* demonstrated that cationic peptides could be used to increase the cytoplasmic transmembrane voltage (resulting in membrane hyperpolarization) and reduce the threshold for IRE [12]. However, the cationic peptides used in that study have a high toxicity and are therefore not good candidates for RE applications.

Transmembrane voltage can also be regulated by the concentration of ions and their permeability inside and outside the cell [202]. The ions with the strongest effect on transmembrane potential are potassium (K^+), sodium (Na^+) and chloride (Cl^-). Changing the concentration of ions outside the cell or activating ion pumps within the cell membrane alters the transmembrane potential. For example, Brent *et al.* showed that HL-60 cells exposed to the drug ionomycin, a Ca^{++} ionophore, underwent membrane hyperpolarization for several minutes [130]. This group observed a similar effect using adenosine triphosphate (ATP), with a shorter duration [130]. They did not report any toxic effects from the either method over the seven-day duration of their experiments, suggesting that low concentrations of ionomycin or ATP are non-toxic to HL-60 cells.

We present a comprehensive study designed to test the hypothesis that hyperpolarizing cell membranes prior to electroporation reduces electroporation PEF thresholds and increases electroporation outcome efficiencies. We specifically hypothesized that decreasing the threshold for electroporation would make conditions for RE more favorable at lower PEF intensities and therefore improve the ratio of RE to IRE cells in a sample, while at higher PEF intensities, decreasing the threshold would cause more membrane damage to occur, thereby increasing IRE outcomes without increasing the externally applied PEF intensity. Membrane hyperpolarization of HL-60 cells was achieved using ionomycin. We elected to model our experimental results with cubic spline data fit models in anticipation of nonlinear relationships between PEF intensity or pulse duration and the

three possible outcomes. An interaction between ionomycin and PEF or pulse duration was also allowed in the models. Significant effects were determined using an analysis of variance (ANOVA) procedure. We observed significant increases in RE for shorter pulse durations and lower PEF intensities, and increases of IRE for all higher PEF intensities. This suggests that RE is effectively achieved over a select window of pulse durations, while IRE performance is pulse-duration independent.

5.4 Materials and Methods

A. Cell Preparation, Electroporation Protocols, and Design

HL-60 human promyelocytic leukemia cells (American Type Culture Collection, Manassas, VA, USA) were used for all experiments because their spherical shape eliminates the dependency of the electroporation outcome on the cell's orientation relative to the electric field. HL-60 cells were cultured at 37°C and 5% CO_2 in RPMI-1640 containing 2% glutamine supplemented with 10% fetal bovine serum (FBS) and 2% penicillin and streptomycin. Propidium Iodide (PI) (MP Biomedicals, Solon, OH, USA) and Trypan Blue (TB) (Lonza, Walkersville, MD, USA) were used as membrane integrity indicators. PI is visible using fluorescence microscopy, fluorescing after it enters a cell. TB is visible using bright field microscopy, staining cells with compromised membranes.

At least one day prior to conducting experiments, slides were treated with a poly-L-lysine adhesion coating (Sigma-Aldrich, Madison, WI, USA) and then allowed to dry. Immediately prior to experimentation, a sample of cells was counted, using TB to distinguish between live and dead cells. Cells were pelleted and re-suspended in Hank's balanced salt solution (HBSS) without phenol red, calcium, or magnesium, containing 5.3 mM KCl, 0.44 mM KH_2PO_4, 4.17 mM $NaHCO_3$, 137.93 mM NaCl, 0.34 mM Na_2HPO_4, and 5.56 mM D-glucose (dextrose) (Thermo Scientific, Waltham, MA, USA) (1.42 S/m conductivity) at a concentration of 2 million cells per milliliter. The cell count was

used to quantify the percentage of dead cells at the beginning of each trial. An equal quantity of 60 μM PI solution (Fisher Scientific International, Pittsburgh, PA, USA) (dissolved in HBSS) was added to the cell/HBSS mixture resulting in a final PI concentration of 30 μM. For the treatment group (HBSS + ionomycin experiments), the control solution (PI + HBSS) was supplemented with 100 nM ionomycin (Fisher Scientific, Pittsburgh, PA, USA). After addition of PI (and ionomycin when applicable), cells were incubated for ten minutes at 37°C and 5% CO_2. After incubation, ionomycin was added again to the HBSS + PI + ionomycin samples because under these conditions the effects of the ionomycin on the transmembrane electric potential started to diminish after approximately ten minutes. In order to estimate causal effects of hyperpolarization on electroporation outcome, we randomized samples of cells to treatment and control levels.

A BTX Model ECM 830 Square Wave Electroporation System (Harvard Apparatus, Holliston, MA, USA) was used to deliver the PEF. The PEF was delivered to cells in an electroporation cuvette with a 2.0 mm gap between parallel plate electrodes. Square monopolar pulses with voltages up to 1.5 kV were used for this study. Pulse durations ranged from 20-100 μs. After electroporation, cells remained in the cuvettes undisturbed for 20 minutes to allow transient pores to close. We selected the 20 minute interval based on the understanding that pore resealing in RE cells typically lasts up to a few minutes [1], [68], [69], [79]–[83]; hence, a 20 minute interval allows sufficient time for transient pores to close.

TB was added 20 minutes after electroporation. Two minutes after TB addition, 13 μL of the cell/HBSS/PI mixture was then placed onto a poly-L-lysine coated slide with a nylon washer placed in the middle to form a well for the cells. The cells were allowed to settle on the slide for five minutes, after which bright field and fluorescence images were taken. PI fluorescence was monitored using fluorescence microscopy at 535 nm excitation and 617 nm emission. A Lambda DG-4 excitation lamp and high-speed wavelength switcher (Sutter Instrument, Novato, CA, USA) was used to excite the PI.

Control of the lamp and CCD camera were done with custom software (Prairie Technologies Inc., Madison, WI, USA). A Nikon Eclipse TE200 microscope (Nikon USA, Melville, NY, USA) equipped with a Hamamatsu C4742-95 Digital charge-coupled device (CCD) camera (Hamamatsu Photonics, Bridgewater, NJ, USA) was used to capture all images taken in this study. A timeline of the experimental procedure is provided in Table 5-1.

Table 5-1. Timeline of experimental procedure

Time	**Task**
Prep	At least one day prior to the start of the experiment, prepare Poly-L-Lysine coated slides.
0 min	Count cells to determine the percent living. Place cells into centrifuge tube. Centrifuge until pellet forms. Re-suspend cells in HBSS at a concentration of 2 million cells per milliliter. Mix with equal parts of 2x (60 μm) PI solution. Add ionomycin for ionomycin + HBSS experiments. Incubate for 10 minutes.
10 min	Add second dose of ionomycin for the ionomycin + HBSS experiments. Place 200 μL of cell/electroporation medium mixture into a 2 mm cuvette. Electroporate cells. Leave cells undisturbed for 20 minutes.
30 min	Add 2 μL of TB to the cuvette.
32 min	Place 13 μL of cells on slide inside the nylon washer.
37 min	Take snapshots of bright field and fluorescence images.

We performed three sets of experiments. The first was fixing the pulse duration at 40 μs and varying the amplitude of the PEF from 0 – 7.5 kV/cm. We chose the 40 μs pulse duration because previous work in our lab had determined it is well suited for RE in HL-60 cells (unpublished work). We then repeated the experiments at a pulse duration of 100 μs, which was chosen because it is commonly used for IRE applications [14], [77], [203], [204]. Lastly, we fixed the PEF amplitude at 2.06 kV/cm (which is approximately where the peak percentage of RE was previously observed) and varied the pulse duration from 20-100 μs to investigate the range of pulse durations that are effective for increasing RE.

5.4.1 Transmembrane Potential Measurements

The transmembrane potential was measured using the potential-sensitive dye $DiBAC_4(3)$. We created a calibration curve to establish a direct relationship between the internalized concentration of $DiBAC_4(3)$ and the respective measured fluorescence intensity. We then used this relationship to determine the concentration of $DiBAC_4(3)$ within any cell of interest. The transmembrane potential was calculated using the Nernst equation (eq. 1) with the fluorescence-determined intracellular dye concentration and the known extracellular dye concentration.

$$V = \frac{RT}{F} \ln\left(\frac{D_i}{D_e}\right) \qquad (1)$$

where R is the universal gas constant, T is the absolute temperature, F is the Faraday constant, D_i is the concentration of $DiBAC_4(3)$ internalized by the cell, and D_e is the external concentration of $DiBAC_4(3)$.

The calibration curve was created by depolarizing cells with 0.5 μg/mL gramicidin (Fisher Scientific, Pittsburgh, PA, USA) [205] and incubating with various concentrations of $DiBAC_4(3)$ (Fisher Scientific, Pittsburgh, PA, USA) ranging from 1 μM to 15 μM. This depolarization caused the intracellular and extracellular $DiBAC_4(3)$ concentrations to be equal. The cells were incubated for 30 minutes after the addition of $DiBAC_4(3)$ and gramicidin. After incubation, the fluorescence of $DiBAC_4(3)$ was then sampled using the same microscope setup as described in Section II-A using a 470 nm excitation/525 nm emission filter cube with an exposure time of 750 ms. The calibration experiments were run three times and the internal fluorescence was calculated using MATLAB® (The MathWorks, Natick, MA, USA), and thus we were able to establish a relationship between the amount of $DiBAC_4(3)$ internalized to fluorescence intensity. Using this curve, shown in Supplementary Materials Figure 5-S1, we were able to calculate the concentration of $DiBAC_4(3)$ internalized for an

unknown sample by measuring its fluorescence intensity. Each experiment was run as a pair of one control and one hyperpolarized, and the difference was recorded to minimize effects of day to day variation. This provided improved accuracy over averaging across all recorded values. The transmembrane potential was then calculated using eq. 1. Finally, the calibration measurements were replicated using a 10-minute incubation after addition of $DiBAC_4(3)$ and gramicidin. The results of the 10-minute incubation time protocol matched the results of the 30-minute incubation protocol, confirming the accuracy of calibrations and confirming that a 10-minute incubation protocol was sufficient for our purposes.

When measuring the effects of ionomycin on transmembrane potential, the same (10-minute) procedure was followed as described above, except no gramicidin was used, 11 μM $DiBAC_4(3)$ solution was used, and the cells were incubated in HBSS plus 0.1 μM ionomycin solution. Additional ionomycin was also added immediately following incubation to match the conditions of the electroporation experiments.

Throughout the duration of the electroporation experiments, a sample of the cells was periodically tested with 11 μM $DiBAC_4(3)$ solution to confirm that ionomycin was continuing to affect the transmembrane potential. Any experiments that were tested that resulted in negligible change in the transmembrane potential were discarded, and new ionomycin was used. The measured change in transmembrane potential across all (kept) experiments was 13.2 ± 6.1 mV (more negative).

$DiBAC_4(3)$ was also used to determine the time response of ionomycin by collecting snapshots over the course of 30 min after ionomycin addition. The transmembrane potential effects of 100 nM ionomycin wore off between 10 & 15 min. However, if ionomycin was added again after 10 min, the effects lasted much longer (>20 min). Additionally, it took 5-10 min for the cells to adjust their transmembrane potential after HBSS was added. Taking these both into account, we chose to incubate

the cells in HBSS (or HBSS + Ionomycin) for 10 min prior to applying the PEF and adding a second dose of Ionomycin approximately one minute prior to applying the PEF.

5.4.2 Analysis Method

PI and TB were used to distinguish between NEP, RE, and IRE outcomes. PI is normally a membrane impermeable molecule which binds to intracellular nucleic acids when it crosses the cell membrane (either through electroporation or cell death), causing a significant increase in fluorescence. Thus, PI fluorescence is only detectable once the molecule has passed through the plasma membrane. TB stains any cells with compromised membranes, and thus when added after reversible pores have had time to close only stains IRE cells. TB is detectable using standard bright field microscopy. Cells which internalized both TB and PI were counted as IRE, cells that internalized PI but excluded TB were counted as RE, and cells that excluded both TB and PI were counted as NEP. Cells that were dead prior to electroporation also internalize PI and TB, and thus appear as false positive IRE cells with this method. To account for this, we determined the live/dead ratio of the samples immediately prior to electroporation, and adjusted the IRE counts accordingly so the reported numbers reflect what happened to the living cells.

The center of each cell was identified using the bright field images, acquired during the procedure. A representative bright field image is shown in Figure 5-1(a). We also used the bright field images to visually determine TB internalization.

To distinguish between fluorescing and non-fluorescing cells, we used MATLAB® to quantitatively analyze the fluorescence images by comparing each cell's *internal* fluorescence intensity to several local luminescent intensities *external* to the individual cell. The fluorescence intensity *inside* the cell was measured near the center of the cell. This was compared to the average external luminescence intensity, determined by sampling the background near to the cell. In order to measure the background fluorescence, we sampled three external regions, approximately evenly spaced around the cell. In

preliminary trials, we found that using fewer than three regions created too much sensitivity in the determination of whether a cell was classified as fluorescing to the specific location of the regions (particularly near bright cells which had a visible corona surrounding them). Using more than three regions did not result in any notable benefit. The cell was determined to be fluorescing if the average measured internal fluorescence value exceeded a threshold of T times the average value of the surrounding background luminescence intensities. Unpublished work in our lab determined that, for our setup, T equal to 1.125 gave the highest accuracy (least number of false negatives and positives). We present a representative fluorescence image in Figure 5-1(b).

5.4.3 Statistical Analysis

In the 40 μs and 100 μs experiments described in section A, we implemented a cubic splines regression using the lm package in R® [206] to estimate effects on the electroporation outcome. We modeled the treatment effect of hyperpolarization with ionomycin as linear. The effect of PEF intensity and its interaction with treatment were modeled using a nonlinear cubic spline regression generated using the ns function in R® [206]. We chose cubic splines because they allow for incorporation of nonlinear effects with more than one point of inflection using a relatively small number of parameters [180], [188]. Knots were chosen to reflect known underlying trends in the results [183]. Specifically, we expected the primary electroporation outcome to change depending on the applied PEF intensity. At low PEF intensity, NEP was expected to be the dominant term, followed by a region where RE is dominant, then IRE. We selected knots to be in transition areas to allow for the best representation of the data. Prior findings establish that this approach is best for describing the expected nonlinear biological dependence of electroporation type on field strength [182]–[184]. Specifically, the biological mechanisms that rule this relationship are highly nonlinear [207], justifying the use of splines. The interaction term was included to explore the hypothesis that the effects of membrane hyperpolarization using ionomycin would vary depending on PEF intensity. Significance

of effects was determined using ANOVA. Interaction effects that were not deemed significant (meaning the effect of PEF intensity was not significantly different for different levels of ionomycin) were excluded from the model. Three separate regressions were performed, one for each possible outcome as a percent of cells (i.e. percent NEP, RE, or IRE). In the experiments where we fixed PEF at a constant value and varied the pulse duration, the statistical model was fitted similar to the one described above but substituting PEF intensity with pulse duration. In our analysis, we considered $P < 0.05$ as significant. We calculated means and standard error (SE) for all combinations of treatment and PEF, shown in the figures.

5.4.4 Viability Studies

We investigated whether the experimental conditions were toxic to cells by performing live/dead counts on groups of cells in both the control group (HBSS/PI solution) and the treatment group (HBSS/PI/ionomycin solution). For both cases, we did not detect any decrease in cell viability within the first two hours. The treatment group resulted in 1.11% ± 0.59% standard deviation (SD) dead, while the control resulted in 1.72% ± 0.65% SD. This resulted in $P = 0.1508$, and therefore we concluded that the percentage of dead cells is not significantly different between the two groups.

Cells in the control group did not show any increase in cell death during the two-hour duration of the experiment. At the working concentration of ionomycin, cells in the treatment group did not show any change in cell viability over the course of two hours. Live/dead counts were comparable to cells incubated in HBSS without ionomycin at each time point sampled during the two hours.

However, cells incubated in a solution with double the working concentration of ionomycin (i.e. 200 nM ionomycin, added at t = 0 and t = 10 min) for two hours resulted in a twofold increase in cell death and lower proliferation rate of about half when compared to cells incubated for the same amount of time in HBSS. These samples were then washed, and the cells which were exposed to

ionomycin proliferated normally (doubling approximately every 24 hours) once the ionomycin was removed.

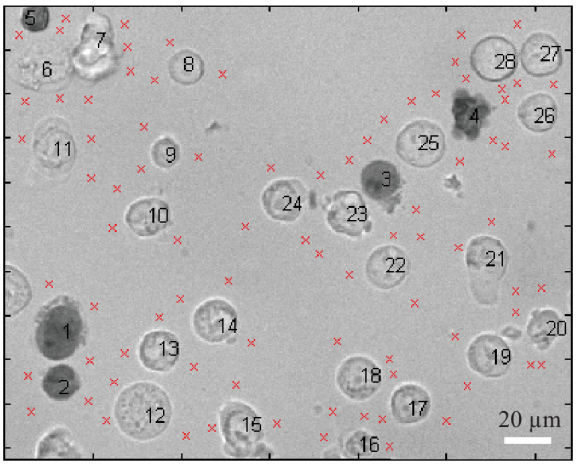

(a)

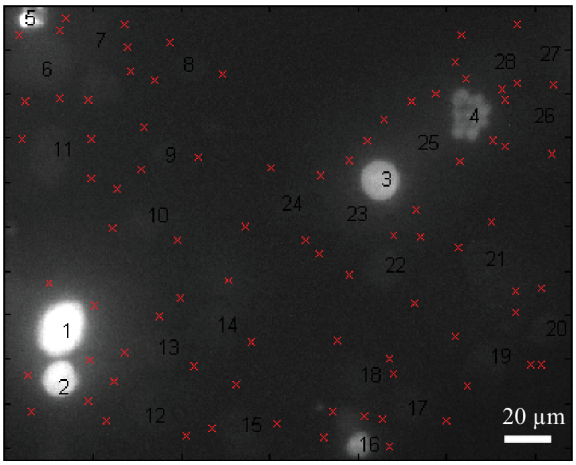

(b)

Fig. 5-1. A representative bright field and fluorescence image illustrating the analysis method used in this study. PI fluorescence intensity inside each cell was determined by comparing an area inside of the cell to three nearby points external to the cell, (marked with the red x). Cells internalizing both TB and PI were considered IRE (cells 1-5), cells internalizing only PI were considered RE (6, 8, 11, 14-20, 22, 25), and cells excluding both membrane integrity indicators were considered NEP (cells 7, 9, 10, 12, 13, 21, 23, 24, 26-28). (a) is the bright field image and (b) is the fluorescence image. The scale bar represents 20 µm.

5.5 Results

5.5.1 40 μs Results

Cells were electroporated at approximately 200-1500 V in cuvettes with a gap size of 2.0 mm. When using these cuvettes, any voltage higher than 1500 V resulted in an arc (with HBSS as the medium). Therefore, we did not perform experiments at higher voltages. All electric field strengths (PEF intensities) were calculated from the applied voltage and gap size and therefore reported in kV/cm, calculated by dividing the gap voltage by the gap spacing of 2.0 mm. The PEF intensities for the 40 μs experiments ranged from 0-7.5 kV/cm. We took a minimum of fourteen samples at each voltage setting. These results are shown in Figures 5-2 through 5-5.

At low PEF intensities (1.8, 2.0, and 3.0 kV/cm), the addition of ionomycin significantly increased the percentage of RE cells while decreasing the number of NEP cells. The peak RE percentage increased from 57.5% ± 17.7 SD at 3 kV/cm to 71.85% ± 11.7 SD at 2 kV/cm. It is worth noting that the window of PEF intensities that attain close to peak RE decreased for the hyperpolarized cells. The hyperpolarized cells are close to the peak RE percentage in the range of 1.77 kV/cm to 4 kV/cm, while the control cells peak RE range is 2 kV/cm to 7 kV/cm. Here we define close as overlapping 95% confidence intervals. At higher PEF intensities (6.0 and 6.9 kV/cm), the addition of ionomycin significantly increased the percentage of IRE cells, while decreasing the number of RE cells.

We analyzed the results for the 40 μs pulse durations using a cubic spline regression with three knots, located at 1.5, 2.5, and 6.5 kV/cm. These results are shown in the next three sections.

i. NEP Regression Results

Results from the regression analysis for NEP outcomes indicated that the direct effect of treatment with ionomycin, PEF intensity, and the interaction between treatment and PEF intensity were significant, meaning they all resulted in statistically significant changes in electroporation percentage.

The significance of the interaction term between the electroporation spline and treatment means the effects of ionomycin change depending on the PEF intensity. This is specifically seen in the 1.75 – 3 kV/cm range. The results of the regression are shown in Figure 5-2 (fitted lines) and Table 5-2. We flipped the NEP results to show the percent electroporated in Figure 5-2. Results confirm that hyperpolarizing the cellular membrane decreased NEP, and therefore increased the chances for electroporation at certain ranges of PEF intensities with 40 μs pulse durations.

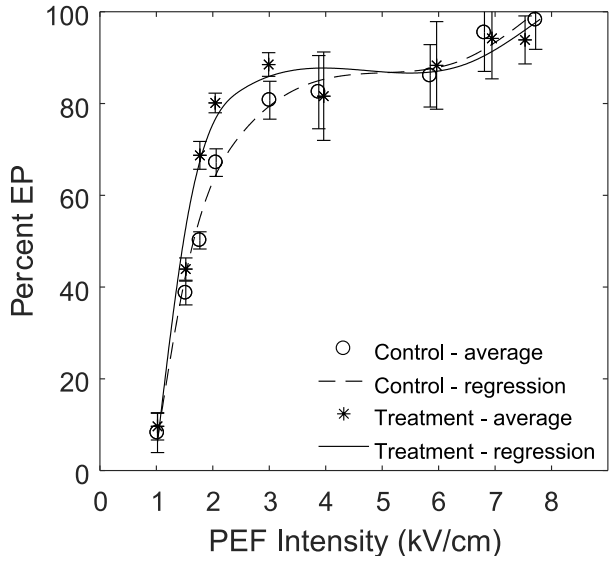

Fig. 5-2. Percentage of sample determined to be electroporated (EP) with a 40 μs pulse duration. The control group was electroporated in HBSS and the treatment group was electroporated in HBSS supplemented with 100 nM ionomycin. The average values of each sampled PEF intensity are depicted by 'o' for control and '*' for treatment. The error bars represent a 95% confidence interval. PEF intensities of 1.8 and 2.0 kV/cm resulted in significant differences in the percent of electroporated cells. Regression lines represent the fitted cubic splines.

Table 5-2. 40 μs NEP regression ANOVA results

	Degrees of Freedom	Sum of Squares	P Value
Direct Effect	1	2279	< 0.0001
Spline of PEF	4	181169	< 0.0001
Interaction	4	2751	0.0003

ii. RE Regression Results

Results from the regression analysis for RE outcomes indicated that the direct effect of treatment with ionomycin was not significant for the electroporation outcome. But both the effect of PEF intensity and the interaction between treatment and PEF intensity were. This suggests, respectively, that PEF intensity has an effect on electroporation outcome, and that hyperpolarizing the cellular membrane changed RE outcomes differently depending on the PEF intensity (i.e. interaction). Specifically, hyperpolarizing the membrane increased the chances for RE at lower PEF intensities and decreased the chances for RE at higher PEF intensities using 40 μs pulse durations. This increase in RE was observed for a smaller range of PEF intensities in the hyperpolarized case (1.75 – 3 kV/cm, with between 62.3% and 71.9% fluorescing), while a more constant effect across PEF intensities was observed for non-hyperpolarized membranes, as seen in the window between 2 – 7 kV/cm (with between 42.7% and 57.4 % fluorescing). The results of the regression are shown in Figure 5-3 (fitted lines) and Table 5-3. We flipped the NEP results to show the percent electroporated in Figure 5-3. No departures of normality or heterogeneity of variances were found in the residual and variance check.

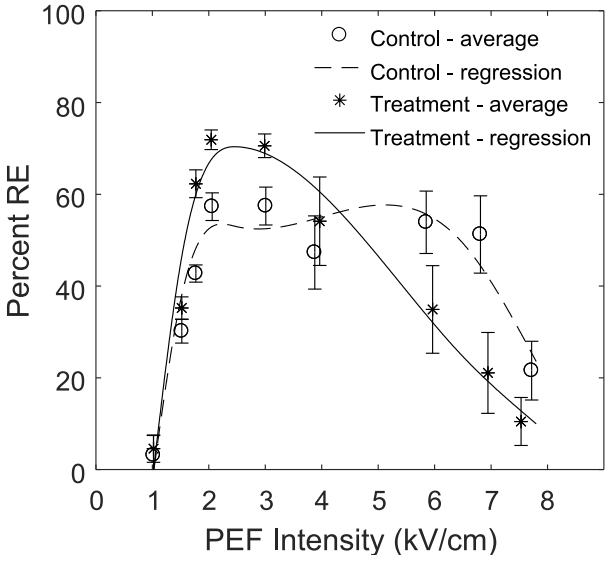

Fig. 5-3. Percentage of sample determined to be RE with a 40 µs pulse duration. The control group was electroporated in HBSS and the treatment group was electroporated in HBSS supplemented with 100 nM ionomycin. The average values of each sampled PEF intensity are depicted by 'o' for control and '*' for treatment. The error bars represent a 95% confidence interval. PEF intensities of 1.8 and 2.0 kV/cm resulted in significant increase in the percent of RE cells in the treatment samples, while at 6.0 and 6.9 kV/cm had a statistically significant reduction in RE in the treatment samples. Regression lines represent the fitted cubic splines.

Table 5-3. 40 µs RE regression ANOVA results

	Degrees of Freedom	**Sum of Squares**	**P Value**
Direct Effect	1	364	0.1780
Spline of PEF	4	108475	< 0.0001
Interaction	4	16422	< 0.0001

iii. IRE Regression Results

Results from the regression analysis for IRE outcomes indicated that the direct effect of treatment with ionomycin, PEF intensity, and the interaction between treatment and PEF intensity were significant, meaning they all resulted in statistically significant changes in electroporation percentage.

Results of the regression are shown in Figure 5-4 and Table 5-4. Results suggest that hyperpolarizing the cellular membrane changed IRE outcomes differently depending on the PEF intensity. Specifically, hyperpolarizing the membrane increased the chances for IRE at higher PEF intensities using 40 μs pulse durations when compared to the control. We observed a slight increase in the regression for the control compared to the treatment at around 3 kV/cm, however this is not significant, as visualized by the overlapping 95% confidence interval bars.

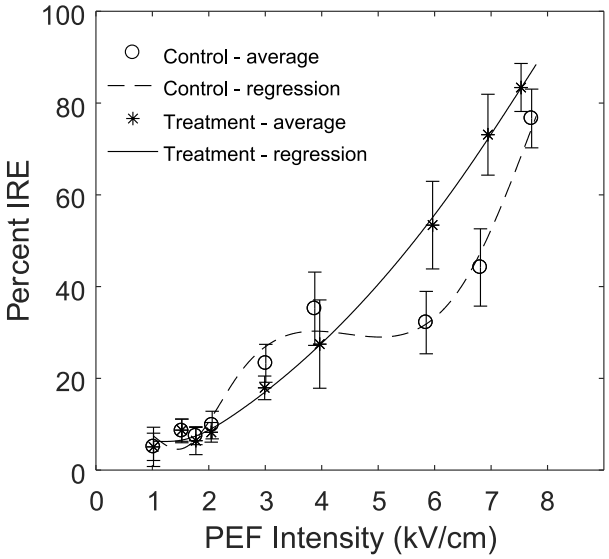

Fig. 5-4. Percentage of sample determined to be IRE with a 40 μs pulse duration. The control group was electroporated in HBSS and the treatment group was electroporated in HBSS supplemented with 100 nM ionomycin. The average values of each sampled PEF intensity are depicted by 'o' for control and '*' for treatment. The error bars represent a 95% confidence interval. PEF intensities of 6.0 and 6.9 kV/cm resulted in a statistically significant increase in IRE in the treatment samples. Regression lines represent the fitted cubic splines.

Table 5-4. 40 μs IRE regression ANOVA results

	Degrees of Freedom	Sum of Squares	P Value
Direct Effect	1	849	0.0036
Spline of PEF	4	174216	< 0.0001
Interaction	4	7858	< 0.0001

5.5.2 100 μs Results

We performed the second set of experiments using 100 μs pulse durations. Cells were electroporated at approximately 0-1150 V in cuvettes with a gap size of 2.0 mm. The longer pulses resulted in arcs when a voltage greater than 1150 V was supplied, therefore experiments were cut off at 1150 V. Electric field strengths (PEF intensities) were calculated from the applied voltage and gap size, therefore the PEF intensities used in this part of the study ranged from 0-5.75 kV/cm. These results are shown in Figures. 5-5 through 5-7. Unlike the 40 μs results, we did not observe any increase in overall EP. However, there was an increase of IRE at higher field strengths.

We analyzed the results for the 100 μs pulse durations using a cubic spline regression with three knots, located at 1.5, 2.5, and 5 kV/cm. These results are shown in the next three sections.

i. NEP Regression Results

Results from the regression analysis for NEP outcomes indicated that only the effect of PEF intensity was significant. The results of the regression are shown in Table 5-5. Unlike 40 μs, there was neither a statistically significant direct effect of treatment on NEP outcomes nor a significant interaction between treatment and PEF intensity. Therefore, we conclude that ionomycin did not significantly alter the NEP outcomes for 100 μs pulse durations and that the effect of treatment was not different for different levels of PEF intensity. For this reason and being concerned about

overfitting, we decided to exclude the interaction term from the model and refit the spline curve for PEF intensity without it (Figure 5-5), as it is a better representation of the data. The regression results without the interaction term are shown in Table 5-6.

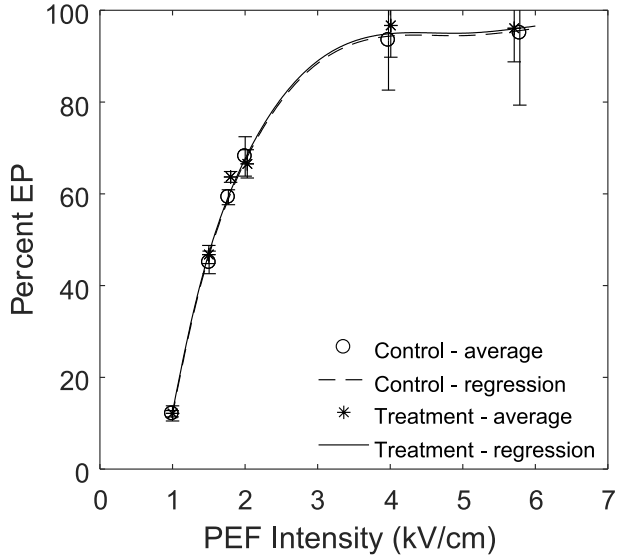

Fig. 5-5. Percentage of sample determined to be electroporated with a 100 μs pulse duration. The control group was electroporated in HBSS and the treatment group was electroporated in HBSS supplemented with 100 nM ionomycin. The average values of each sampled PEF intensity are depicted by 'o' for control and '*' for treatment. The error bars represent a 95% confidence interval. No PEF intensities resulted in a significant difference in the percent of electroporated cells. Regression lines represent the fitted cubic splines.

Table 5-5. 100 μs NEP regression ANOVA results

	Degrees of Freedom	Sum of Squares	P Value
Direct Effect	1	41	0.5111
Spline of PEF	4	140132	< 0.0001
Interaction	4	285	0.5526

Table 5-6. 100 μs NEP regression ANOVA results – without interaction

	Degrees of Freedom	Sum of Squares	P Value
Direct Effect	1	17	0.6701
Spline of PEF	4	140155	< 0.0001

ii. RE Regression Results

Results from the regression analysis for RE outcomes indicated that the direct effect of treatment with ionomycin was not significant, but the effect of PEF intensity and the interaction between treatment and PEF intensity were both significant. We conclude that hyperpolarizing the cellular membrane changes RE outcomes differently depending on the PEF intensity. Significant differences between the two curves occurred for specific portions of the plot, more precisely decreasing the chances for RE at higher PEF intensities using 100 μs pulse durations. The results of the regression are shown in Figure 5-6 and Table 5-6.

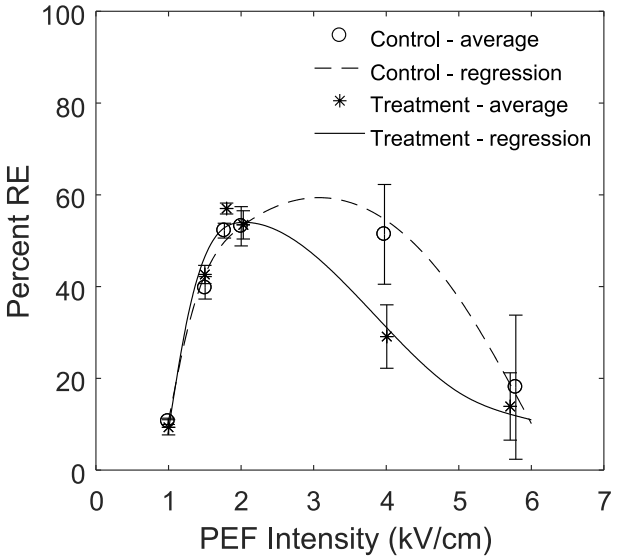

Fig. 5-6. Percentage of sample determined to be RE with a 100 µs pulse duration. The control group was electroporated in HBSS and the treatment group was electroporated in HBSS supplemented with 100 nM ionomycin. The average values of each sampled PEF intensity are depicted by 'o' for control and '*' for treatment. The error bars represent a 95% confidence interval. PEF intensities of 4.0 kV/cm had a statistically significant reduction in RE in the treatment samples. Regression lines represent the fitted cubic splines.

Table 5-7. 100 µs RE regression ANOVA results

	Degrees of Freedom	**Sum of Squares**	**P Value**
Direct Effect	1	274	0.2031
Spline of PEF	4	63172	< 0.0001
Interaction	4	4385	0.0001

iii. IRE Regression Results

Results from the regression analysis for IRE outcomes indicated that the direct effect of treatment with ionomycin, PEF intensity, and the interaction between treatment and PEF intensity were significant, meaning they all resulted in statistically significant changes in electroporation percentage.

Results of the regression are shown in Figure 5-7 and Table 5-8. They confirm that hyperpolarizing the cellular membrane changed IRE outcomes differently depending on the PEF intensity, specifically increasing the chances for IRE at higher PEF intensities using 100 μs pulse durations. No departures of normality or heterogeneity of variances were found in the residual and variance check.

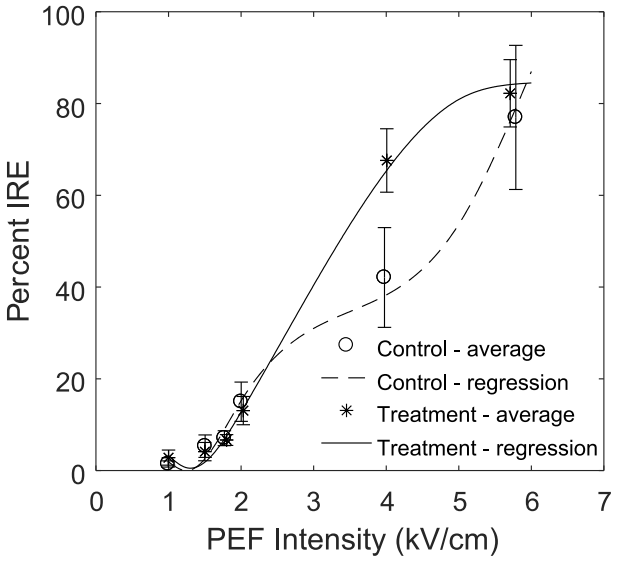

Fig. 5-7. Percentage of sample determined to be IRE with a 100 μs pulse duration. The control group was electroporated in HBSS and the treatment group was electroporated in HBSS supplemented with 100 nM ionomycin. The average values of each sampled PEF intensity are depicted by 'o' for control and '*' for treatment. The error bars represent a 95% confidence interval. PEF intensities 4.0 kV/cm resulted in a statistically significant increase in IRE in the treatment samples. Regression lines represent the fitted cubic splines.

Table 5-8. 100 μs RE regression ANOVA results

	Degrees of Freedom	**Sum of Squares**	**P Value**
Direct Effect	1	522	0.0149
Spline of PEF	4	146260	< 0.0001
Interaction	4	5785	< 0.0001

5.5.3 2.06 kV/cm Results

In the last set of experiments, we used a fixed PEF intensity of 2.06 kV/cm and pulse durations of 20, 40, 60, 80, and 100 μs. Results are shown in Figures. 5-8 through 5-10. Only the 40 μs pulse duration had a significant change in the electroporation outcome for both EP and RE compared to the control (no overlap in the 95% confidence interval). Overall, increased pulse duration yielded a small decrease in the percentage of EP and RE and an increase in IRE. There was no notable change in IRE between the control and treatment groups. We analyzed the results for 2.06 kV/cm experiments using a cubic spline regression with two knots, located at 30 and 90 μs.

i. NEP Regression Results

Results from the regression analysis for NEP outcomes indicated that the direct effect of treatment with ionomycin, pulse duration, and the interaction between treatment and pulse duration were significant, meaning they all resulted in statistically significant changes in electroporation percentage. These results are shown in Figure 5-8 and Table 5-9. We observed that each instance tested resulted in at least a slightly increased percent electroporated in the treatment group. Interestingly, while individually some NP values were not significant (overlapping 95% confidence intervals), when evaluated together they were deemed significant (i.e. the direct effect of treatment was significant). The significant interaction term suggests that the effect of treatment is different for different levels of pulse duration, in other words certain regions (specifically lower pulse durations) had an increased effect for the treatment when compared to the control.

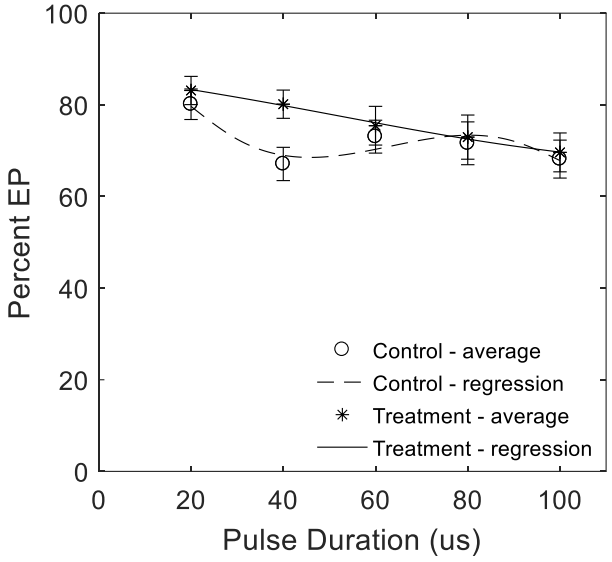

Fig. 5-8. Percentage of sample determined to be electroporated with a 2.06 kV/cm PEF intensity. The control group was electroporated in HBSS and the treatment group was electroporated in HBSS supplemented with 100 nM ionomycin. Only 40 µs pulses resulted in significant differences in the percent of electroporated cells. Error bars represent a 95% confidence interval. Regression lines represent the fitted cubic splines.

Table 5-9. Varied duration NEP regression ANOVA results

	Degrees of Freedom	**Sum of Squares**	**P Value**
Direct Effect	1	1539	0.0006
Spline of Duration	4	4874	< 0.0001
Interaction	4	1237	0.0228

ii. RE Regression Results

Results from the regression analysis for RE outcomes indicated that the direct effect of treatment with ionomycin, pulse duration, and the interaction between treatment and pulse duration were significant, meaning they all resulted in statistically significant changes in electroporation percentage.

These results are shown in Figure 5-9 and Table 5-10. Similar to the EP case, there is a visual trend of increases in RE for all but one pulse duration. The direct effect of treatment being significant agrees with the visual inspection. In addition, similar to EP results, the significant interaction term suggests that the effect of treatment is different for different pulse durations, in other words certain regions (specifically lower pulse durations) had an increased effect for treatment when compared to the control.

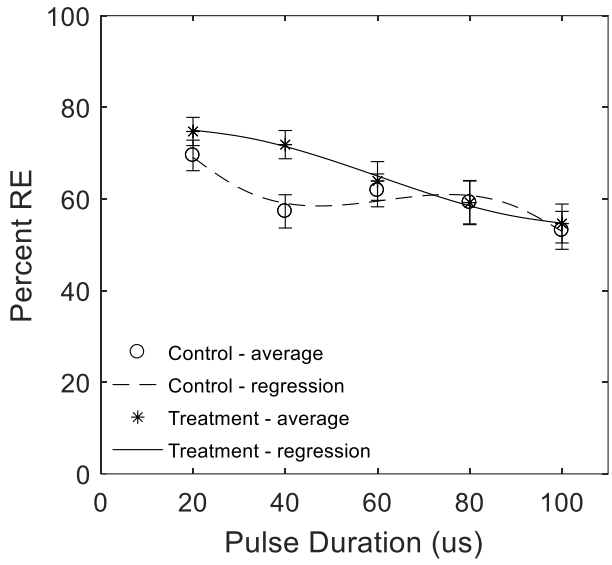

Fig. 5-9. Percentage of sample determined to be RE with a 2.06 kV/cm PEF intensity. The control group was electroporated in HBSS and the treatment group was electroporated in HBSS supplemented with 100 nM ionomycin. Only 40 µs pulses resulted in significant differences in the percent of RE cells. Error bars represent a 95% confidence interval. Regression lines represent the fitted cubic splines.

Table 5-10. Varied duration RE regression ANOVA results

	Degrees of Freedom	Sum of Squares	P Value
Direct Effect	1	1865	0.0012
Spline of Duration	4	11176	< 0.0001
Interaction	4	1823	0.0165

iii. IRE Regression Results

Results from the regression analysis for IRE outcomes indicated pulse duration had a significant effect on IRE outcomes, but treatment with ionomycin and the interaction between treatment and pulse duration did not. These results are shown including the interaction term in Table 5-11. As the interaction was not significant, we removed the interaction term and reanalyzed the regression to avoid overfitting the data. Results without the interaction term are shown in Figure 5-10 and Table 5-12. An increased pulse duration was shown to negatively affect IRE.

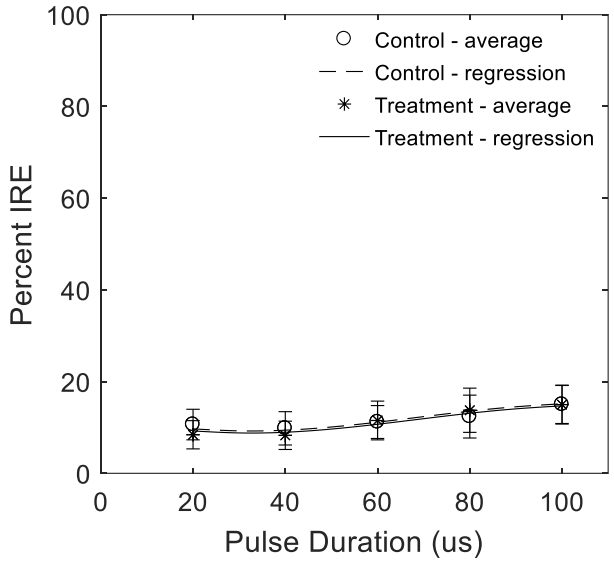

Fig. 5-10. Percentage of sample determined to be IRE with a 2.06 kV/cm PEF intensity. The control group was electroporated in HBSS and the treatment group was electroporated in HBSS supplemented with 100 nM ionomycin. There were no statistically different percentages of IRE cells. Error bars represent a 95% confidence interval. Regression lines represent the fitted cubic splines.

Table 5-11. Varied duration IRE regression ANOVA results

	Degrees of Freedom	**Sum of Squares**	**P Value**
Direct Effect	1	16	0.6046
Spline of Duration	4	1698	< 0.0001
Interaction	4	108	0.6175

Table 5-12. Varied duration IRE regression ANOVA results

	Degrees of Freedom	**Sum of Squares**	**P Value**
Direct Effect	1	16.1	0.6046
Spline of Duration	4	1698	< 0.0001

5.6 Discussion

Our results show that hyperpolarizing HL-60 cell membranes by adding ionomycin yields a statistically significant change in electroporation outcomes. In particular, making the transmembrane electric potential more negative by 13.2±6.1 mV resulted in:

- Increase of RE outcomes at low PEF intensities and 40 μs pulse duration (1.8, 2.0, and 3.0 kV/cm). The most significant increase was observed at 2.0 kV/cm with 62.3% RE compared to 42.7% of the control.
- Increase of IRE outcomes at high PEF intensities for both 40 and 100 μs pulse durations.
- No statistically significant difference for electroporated or RE outcomes with 100 μs pulse durations.

Finally, our results from the fixed PEF intensity and variable pulse duration experiments suggest a slight increase in EP and RE across all pulse durations in addition to the significant increase at 40 μs.

The most likely biological mechanism that justifies the results found in this analysis is that hyperpolarizing the cell membrane prior to electroporation increases the resting transmembrane electrostatic energy [106], thereby reducing the PEF intensity threshold needed to create and expand membrane pores. Since cell death (IRE) can be caused by multiple factors, such as immediate death due to substantial, irreparable plasma membrane damage, or delayed death due to internal organelle damage [56], [128], [208], [209], we further hypothesize that ionomycin only alters the external transmembrane potential, leaving the internal organelles' transmembrane potentials unaltered. Therefore, for a given externally applied PEF intensity, the plasma membrane is more likely to be

electroporated when the membrane is hyperpolarized. At lower applied electric field intensities (e.g., 40 μs and lower *E* field strengths between 1.8 and 3.0 kV/cm), this results in increasing RE while maintaining a similar level of IRE. Other studies have reported that for 40 μs pulses, the endoplasmic reticulum, the largest organelle in most eukaryotic cells, begins to experience electroporation at PEF intensities of around 2 kV/cm [56]. This is the region where we saw an increase of RE outcomes, suggesting that the increase in RE outcomes could be related to this phenomenon. At higher energy levels, we hypothesize that the main mechanism changes and more irreparable plasma membrane damage at a given field strength occurs when cells are hyperpolarized, causing the increase in IRE. This is consistent with existing knowledge that IRE (caused from high PEF intensities) is the result of rapid irreparable damage to the cell membrane [106], [107], [158], [191].

Results obtained in this analysis also support our initial claim that the relationship between PEF and electroporation outcome is non-linear [191], [207]. Since pore creation, and thus electroporation outcomes are nonlinear [191], using piecewise cubic splines is a more recommended method for modeling outcomes than simplified linear models [180], [181]. Alternative models such as low order polynomial regressions are likely to miss important details in the fitted curves, while higher order polynomial models can add artificial artifacts, potentially overfitting the model [180].

Cell membrane hyperpolarization achieved using ionomycin combined with 40 μs pulses resulted in an increase in RE outcomes at lower PEF intensities. When the membrane was hyperpolarized, the peak percentage of RE with a 40 μs pulse (71.9%) was higher than with 100 μs (57.0%), revealing that membrane hyperpolarization can improve the efficiency of the RE procedures at select pulse durations. Increasing the likelihood of RE outcomes could be instrumental for practical applications of the results presented in this study. For example, the increase in the peak percentage of RE could increase the efficiency of RE-based drug delivery therapies. When applying such therapies, one should also anticipate that the benefits of hyperpolarizing the cell membrane for RE applications appear to

be limited to a relatively small range of pulse durations. We note that the results presented here were based on *in vitro* experiments and some applications may require additional *in vivo* studies.

Similarly, cell membrane hyperpolarization achieved using ionomycin showed an increase in IRE outcomes at higher field strengths for both the 40 μs and 100 μs. The 100 μs experiments resulted in the highest peak percentage of IRE outcomes. The significant difference (> 2X) of pulse length between these two data sets demonstrates a wide window of parameter space in which membrane hyperpolarization effects can increase IRE outcomes. These results are interesting for practical applications, such as tumor ablation, where increasing the efficiency of IRE could either increase the size of the ablation zone if keeping all the pulse parameters the same or decrease the required field strength or pulse duration to achieve a particular treatment. For example, electroporation protocols using longer pulse durations encounter problems such as heating, arcing, thermal effects, etc. at lower PEF intensities than protocols using shorter pulse durations. In fact, from analyses such as those reported by Ji, et al., avoidance of thermal effects favors shorter pulses [210], thus decreasing thresholds for IRE reduces the likelihood of thermal effects. Additionally, similar to that discussed by Kennedy *et al* [12], if membrane hyperpolarization can be combined with targeting methods (i.e. specifically hyperpolarizing tumor cells while not affecting non-cancerous cells), techniques could be developed to improve tumor destruction while sparing nearby healthy tissues.

5.7 Conclusion

Addition of ionomycin caused a 13.2±6.1 mV (more negative) difference in transmembrane potential in HL-60 cells suspended in HBSS. This change in transmembrane potential prior to electroporation affected electroporation outcomes at both low and high pulsed electric field (PEF) intensities. The probability of reversible electroporation (RE) was increased at low PEF intensities and

short pulse durations (particularly 40 μs), while the probability of non-electroporated (NEP) outcomes decreased. At high PEF intensities, the probability of irreversible electroporation (IRE) increased while the probability of RE decreased.

Changing the transmembrane electric potential allows for improved control and selectivity of electroporation outcomes. Controlled, selective increase of RE outcomes could improve the efficacy of electroporation for *in vitro* procedures and *in vivo* therapies involving transfection or drug delivery. Controlled, selective increase of IRE outcomes could improve the efficacy of electroporation for IRE ablation therapies.

II. AUTHOR CONTRIBUTIONS

E.J.A: study design, data collection, cell culture, microscopy imaging, image analysis, data analysis and interpretation, and writing of manuscript. B.G.K: study design, data collection. S.Y.: data collection and interpretation. S.C.H: study design, data analysis and interpretation, and critical revision of the manuscript. J.H.B: study design, data analysis and interpretation, and critical revision of the manuscript.

III. ACKNOWLEDGMENTS

We express our gratitude to Vera Cardoso Ferreira for assistance with statistical analysis and interpretation of data.

This work was supported by the Duane H. and Dorothy M. Bluemke professorship and the Philip Dunham Reed professorship.

IV. SUPPLEMENTARY MATERIALS

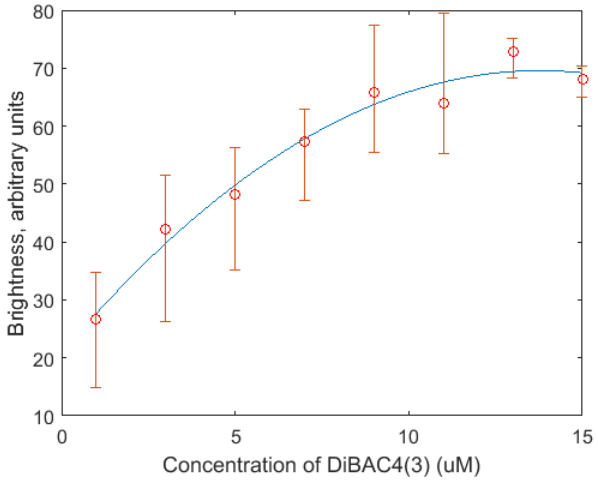

Fig. 5-S1. Calibration curve used to map brightness to known concentrations of internalized DiBAC4(3). The calibration curve, shown in blue, is a 3rd-order polynomial fit to the measured data shown in red. The circles represent the mean and the variability bars span the min and max of the three brightness measurements obtained at each concentration.

Chapter 6: **Electroporation aided delivery of AAV**

Together with colleagues at UW-Hospital, we identified the clinical need for an electroporation device and procedure capable of achieving RE in liver cells. Our colleagues had developed an AAV viral vector capable of delivering a gene which converted liver cells, allowing them to act as surrogate pancreas cells and therefore cure Type 1 diabetes. However, this method was only practical in small animals such as mice. This is because scaling gene therapy methods to large animals is difficult for three reasons. First, viral gene transfer is inefficient, requiring cost-prohibitive gene vector doses [140]. Second, larger doses result in an increase in vector-neutralizing antibodies against the virus capsid (which contains the curative gene), which at best interferes with transfection and at worst can trigger

significant–possibly fatal– immune responses in the patient [145], [211]. Third, systemic injection of the vector creates adaptive immunity, causing subsequent treatments to be less efficient, requiring even more of the virus than earlier treatments [211]. We hypothesized that electroporation could be used to overcome all of these challenges by providing a localized treatment that significantly reduces the quantity of virus necessary to achieve the therapeutic goal of around 5% of liver cells transfected [212]. To meet this requirement, we hypothesized that we could combine AAV-mediated transfection of the gene with electroporation to boost efficiency, therefore only requiring a small dose of AAV, and reducing or avoiding the major drawbacks of viral gene transfer. The first step in testing this was showing electroporation could improve AAV uptake of a gene.

6.1 Electroporation aided delivery of *Adeno-associated virus*

Erik Aiken[1], John Booske[1], and Susan Hagness[1]

[1]Department of Electrical and Computer Engineering, University of Wisconsin–Madison

* Erik Aiken

E-mail: aiken@wisc.edu

6.2 Abstract

Adeno-associated virus **(AAV) is a virus commonly used to transport DNA through cell membranes to treat genetic disorders. Once the new DNA is transducted through the cell membrane, it travels to the nucleus and replaces target portions of the existing DNA with the modified version, potentially altering protein production which can be beneficial in many diseases. However, clinical use of AAV to transduce DNA is limited due to the large doses required to deliver genes in large sized animals (including humans), resulting in high costs, low efficiency, and safety concerns. Targeted, localized delivery of AAV is one promising way to overcome these issues, however low efficiency is still an area that needs to be improved. Regarding that concern, we hypothesize that electroporation can improve AAV transfection efficiency for targeted delivery, significantly reducing the quantity of viral vector needed for a given treatment. In this study we present results showing that electroporation greatly improves expression of green fluorescent protein (GFP) using the AAV complex CMV.GFP-AAV2/8 transfection with a short delivery time across multiple cell types.**

6.3 Introduction

Gene therapy is a promising technique for treating a wide variety of diseases. In 2017, the U.S. Food and Drug Administration (FDA) announced a landmark approval of gene therapy for the treatment of Acute Lymphoblastic Leukemia in humans [213]. This *ex vivo* gene therapy method removes hematopoietic cells from the patient, alters them, and reinfuses genetically modified cells that are capable of combating the tumor cells. On the other hand, many other diseases (e.g. solid tumors, hemophilia, and diabetes) require *in vivo* delivery of the vector directly to the target organ or tissue. *In vivo* gene therapy clinical trials have been approved for a large number of diseases and conditions [78], [214]–[218], which use a variety methods for getting the altered genes into target cells [11]. The central

issue preventing the broad use of gene therapy is that existing methods of getting the genes into cells have severe limitations, such as size of the gene, efficiency, ease of use, and safety. [139], [219], [220].Of the currently available methods, viral vectors are the most commonly used for delivering DNA.

The process of introducing foreign DNA into a cell using viral vectors is called transduction [221]. Many different virus vectors exist for this purpose. *Adeno-associated virus* (AAV) is one of widely used viral vectors for gene transduction in humans [135] and animal models [212], [222]. While trials using AAV to transduct cells in small animals have been successful [212], scaling it to larger animals (such as humans) has three major limitations. First and most significantly, large quantities of viral vectors can invoke potentially fatal immune response [8], [145]. Second, adaptive immunity may limit effectiveness of subsequent treatments [211]. Third, inefficient transduction requires large, cost-prohibitive doses [140].

Non-viral techniques have been explored to attempt to overcome the above mentioned challenges [4], [108], [134], [146], [198], [217]. More generally, the process of introducing foreign DNA into a cell (generally using non-viral methods) is called transfection [220]. Reversible electroporation (RE), the use of short duration pulsed electric fields (PEF) to open temporary pores in cell membranes, is one technique that may be able to overcome many of the aforementioned challenges with delivery of macromolecules. These transient pores make it easier for macromolecules, like DNA, to pass into the cell. However, currently RE is hindered by low efficiency. For example, with DNA delivery rates ranging from 20 to 60% of the treated cells in different studies that used current electroporation techniques [1], [9].

One way to overcome this issue is to increase the efficiency of uptake while localizing the injection of the viral vector to the target tissue. This would result in reducing the quantity of the viral vector needed and therefore make gene transfection more applicable in fields like medicine or veterinary

sciences Electroporation has been used to assist adenovirus uptake in kidneys [47], [110], and may be useful in aiding the localized delivery of other viral vectors, such as AAV, in different cell types. In this paper, we present a method for improving viral aided gene transfection by combining electroporation with AAV delivery *in vitro*. We examined a range of electroporation parameters and AAV concentrations to determine the ranges that obtained the most successful uptake outcomes. We successfully established a range of parameters *in vitro* for virus concentration (titers) and electric field settings that significantly improved transfection. These results can potentially have practical application in gene therapy as they showed that this combined method of AAV and electroporation greatly improve AAV uptake, addressing the limitations outlined above.

6.4 Materials and methods

6.4.1 Cell Preparation and Electroporation Protocols

We used HL-60 human promyelocytic leukemia cells (HL-60) (American Type Culture Collection, Manassas, VA, USA) for initial experiments. These cells are well suited for these experiments because their low autofluorescence levels improves our ability to detect fluorophores and their spherical shape eliminates the dependency of the electroporation on the cell's orientation. HL-60 cells were cultured at 37°C and 5% CO_2 in RPMI-1640 (Mediatech, Inc, Manassas, VA) containing 2% glutamine supplemented with 10% fetal bovine serum (FBS) and 2% penicillin and streptomycin.

Mus musculus, mouse hepatoma cells (Hepa 1-6) (ATTC, Manassas, VA, USA) were used as a second cell type. Hepa 1-6 cells were cultured at 37°C and 5% CO_2 in DMEM with 4.5 g/L glucose, L-glutamine, and sodium pyruvate (VWR International, Radnor, PA), supplemented with an additional 1% glutamine dipeptide and penicillin and streptomycin and 10% FBS.

To test our hypothesis that electroporation could aid AAV uptake, we used *adeno-associated virus 2/8* (AAV 2/8) combined with green fluorescent protein (GFP) (CMV.GFP-AAV2/8, Waisman,

Madison, WI) as our test for viral gene delivery. The experimental procedure we used to test for increased GFP expression is described below.

At least one day prior to conducting experiments, slides were treated with a poly-L-lysine adhesion coating (Sigma-Aldrich, Madison, WI, USA) and then allowed to dry. Immediately prior to experimentation, a sample of cells was counted, using Trypan Blue (TB) (Lonza, Walkersville, MD, USA) to distinguish between live and dead cells. Cells were pelleted and re-suspended in Hank's balanced salt solution (HBSS) (Thermo Scientific, Waltham, MA, USA) (1.42 S/m conductivity) at a concentration of 1 million cells per milliliter. Prior to electroporation, CMV.GFP-AAV2/8 was added to each sample at a predetermined concentration (either 10,000 vg/cell or 10 vg/cell). Cells were then incubated for five minutes at 37°C and 5% CO_2.

A BTX Model ECM 830 Square Wave Electroporation System (Harvard Apparatus, Holliston, MA, USA) was used to deliver the PEF. The PEF was delivered to cells in an electroporation cuvette with a 2.0 mm gap between parallel plate electrodes. These cuvettes were designed for this electroporation system. Previous research has shown both μs and ms pulses have been used for gene transfection, with better performance in the 20-50 ms range [103], [122], [147], [149], [150], therefore we tested 40 μs, 100 μs, and 50 ms pulses. Electric field intensities were varied through a wide range of values. Preliminary testing was done in the range of 75-275 V/cm, with further testing at regions with less than approximately 50% cell death and notable GFP expression. HL-60 cells were used first to determine efficient pulse parameters because of their round shape and low levels of autofluorescence which were expected to give more easily interpretable results, and Hepa 1-6 cells were tested after to test a different cell type. Preliminary testing indicated that 125 – 250 V/cm was the best range for HL-60 cells and 75 – 200 V/cm was the best range for Hepa 1-6. Square monopole pulses were used for this study.

After electroporation, a 20 μL portion of the cells were removed from the samples to determine cell counts. The remaining cells were centrifuged and washed to remove excess CMV.GFP-AAV2/8 from the samples. Cell counts were performed using TB and a hemocytometer.

Samples were taken from the incubated cells and analyzed using a fluorescent microscope daily for up to four days. GFP were detected using fluorescence microscopy with a 470 nm excitation/525 nm emission filter cube with an exposure time of five sec.

Our preliminary testing showed little to no increased effect using 40 μs and 100 μs pulses compared to CMV.GFP-AAV2/8 without electroporation. Single pulses of 50 ms durations showed an increase (on the order of 10-30%) but wasn't high enough to be worthwhile for many practical applications. To increase GFP expression, we decided to use multiple pulses on the same sample, testing multiple 50 ms pulses, and 40 or 100 μs pulses followed by a single 50 ms pulse. Preliminary testing for both 40 μs and 100 μs pulses followed by a single 50 ms pulse did not provide any apparent increase in GFP uptake, and thus we did not further pursue these parameters.

We repeated these experiments using 8 pulses with a 50 ms pulse duration and varying electric field strength. Peak values of cells expressing GFP were similar to the 2x pulses, however the 2x pulses resulted in a wider window of electric field strengths where the percent expressing GFP was close to the peak value, therefore we did not pursue further 8x pulsed experiments for this project.

6.4.2 Analysis Method

TB, which stains any cells with compromised membranes and is detectable using standard bright field microscopy, was used to determine the amount of cell death after electroporation. We determined the quantity of cells killed during the electroporation procedure by counting the electroporated samples and comparing the number of surviving cells (i.e. cells still excluding TB) to the non-electroporated controls.

To distinguish between fluorescing and non-fluorescing cells, we used MATLAB® to quantitatively analyze the fluorescence images by comparing each cell's *internal* fluorescence intensity to several local luminescent intensities surrounding (*external* to) the individual cell. We developed a customized automatic cell identification script, based off the image segmentation method [223]. Our program automatically detected cells on bright field images, tracking any movement by comparing a before and after image. Cells which had their centers move by more than a half radius were discarded from the sample. We did this by modifying existing open source code for circle movement detection and snipping vectors [224], [225]. The fluorescence intensity *inside* the cell was measured near the center of the cell. This was compared to the average external luminescence intensity, determined by sampling the background near the cell. A cell was determined to be fluorescing if the average measured internal fluorescence value exceeded a threshold of T times the average value of the surrounding background luminescence intensities.

The threshold T for distinguishing between fluorescing and non-fluorescing cells was determined by allowing no more than 25 percent of false positives on the non-electroporated, non CMV.GFP-AAV2/8 control groups. Note that some percentage is expected due to normal cell autofluorescence, especially in liver cells. Natural autofluorescence was partly blocked in Hepa 1-6 cells by supplementing with 0.5 mM CuSO4 prior to fluorescence images being taken. The percentage of false positive cells in a given sample was determined using a non-electroporated, no CMV.GFP-AAV2/8 control. This percentage of fluorescing cells were subsequently subtracted from the samples which included CMV.GFP-AAV2/8. We monitored GFP fluorescence for three days after electroporation for HL-60 cells and four days for Hepa 1-6 cells, since beyond those thresholds high levels of cell death were noted, likely caused by GFP exposure [226]. The peak average (mean) percentage fluorescing for each field strength was used to determine the number of cells transfected. The percentage killed, otherwise known as irreversibly electroporated(IRE) was analyzed using a

hemocytometer after electroporation. The average IRE percentage at a given pulse duration/intensity was included when determining the percentage of the sample transfected.

A completely randomized control trial was conducted to test the hypothesis that electroporation improves the cellular uptake of AAV. Cells were randomized to all possible combinations of the two treatments: titer level (10 or 10,000 vg/cell) and of the above mentioned electric field parameters. All cells were evaluated for the percent of cells expressing GFP.

6.4.3 Statistical Analysis

The experimental data was analyzed using a linear regression combined with an Analysis of Variance (ANOVA) to determine significance of effects. First order effects for titer were allowed and first and second order effects were allowed for electric field, as well as an interaction between electric field and titer in the model as follows:

$$y_{ijk} = \mu + \alpha_1 I_i + \beta_1 E_j + +\beta_2 E_j^2 + \gamma_1 I_i E_j + \gamma_2 I_i E_j^2 + \varepsilon_k \quad (1)$$

where y_{ijk} is the percentage of cells which expressed GFP; μ is the overall intercept; I_i is the treatment level with either 10 or10,000 vg/cell titer; and E_j is the electric field strength. α_1 is the direct effect of treatment, and β_1 and β_2 is the linear and quadratic electric field effects, respectively. γ_1 and γ_2 is the interaction effect between electric field (linear and quadratic, respectively) and titer. ε_k is a random disturbance term associated to each sample.

We allowed higher order terms because electroporation is non-linear with respect to electric field [207]. Our range was restricted to a relatively small window which reduced the complexity of the model, allowing us to use a lower order polynomial (as opposed to a more complex method such as splines or higher order polynomials). We tested models using the 1st through 3rd order polynomials, and used Akaike Information Criterion (AIC) [63] and Bayesian Information Criterion (BIC) [185],

[186] to penalize these models. AIC and BIC assign penalties for increased complexity, and are widely used in model selection [63], [185]–[187], [227]–[229]. Both AIC and BIC indicated that the 2nd order model was the best choice.

Model assumptions were checked and met for all models. P-values are presented for all statistical tests performed and values below 0.05 were deemed significant. If the quadratic interaction effect was not deemed significant, it was excluded from the model, which was refit without it. Means and standard deviations were calculated for all combinations of titer and EF and presented as a boxplot.

6.5 Results

For the HL-60 cells, two 50 ms pulses, spaced 5 min apart resulted in a wide window of electric field intensities that significantly enhanced CMV.GFP-AAV2/8 transfection. As mentioned in the methods section, preliminary testing showed that the range of 125 – 250 V/cm was the best region for electroporation with this cell type and pulse parameters, so we focused on these values. Results for this region are shown in Figure 6-1. Both 10 vg/cell and 10,000 vg/cell titers had increases in GFP expression compared to non-electroporated samples, indicating that electroporation can increase AAV delivery of a gene, even at relatively low concentrations of the virus. The maximum fluorescence increased greater than 5 times the control in the treatment of 10 vg/cell of CMV.GFP-AAV2/8, and greater than 10 times the control with the addition of 10,000 vg/cell of CMV.GFP-AAV2/8, showing that while both titers were efficient at increasing GFP expression, 10,000 vg/cell had a more significant impact. These results also show a wide range of electric field strengths that caused an increase in GFP expression.

In the linear model regression for the RE outcomes of the HL-60 cells, the effect of titer ($P = 0.0043$), the second order electric field ($P < 0.0001$) as well as the interaction effect between linear

electric field and titer (P = 0.0444) were deemed significant (P-value < 0.05). These results are shown in Table 6-1. This provides significant evidence to reject the null hypothesis that effects are equal zero and accept the alternative hypothesis that the there is an effect and that the effect of titer is different for different levels of electric fields.

In Figure 6-2 we provide a visualization of the results for the polynomial regression. Results for titer indicate that there was a significant difference in GFP expression between the 10 and 10,000 vg/cell concentrations of CMV.GFP-AAV2/8, with higher titer yielding a higher percentage of cells that express GPF. For the effect of the intensity of the applied electric field, the significance of the 2nd order term reiterates our hypothesis that the effect of electric field on GFP expression is better suited by a nonlinear model, as expressed by the curve in the graph. Overall, we see a decreasing trend in the percentage of cells fluorescing as we increase the electric field strength in the range observed, likely due to increased cell death at higher electric field strengths. This figure also allows visualization of the difference in curves for different treatment effect (i.e. interaction).

When combined, the above results confirm that electroporation significantly increases the amount of GFP transfected across the range of electric fields tested, that the effect of titer is important, as was the interaction between both. Our results suggest that the window of applied electric field strengths between 125 and 225 V/cm is effective at increasing CMV.GFP-AAV2/8, with better results at the lower end of this range.

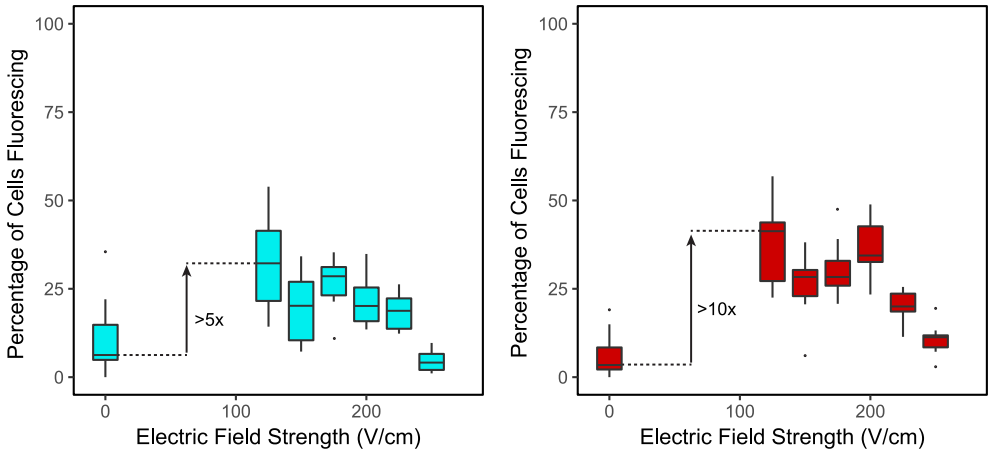

Fig. 1. **Percentage of HL-60 cells expressing GFP when exposed to two 50 ms pulses and two different titers of CMV.GFP-AAV2/8.** (a) 10 vg/cell concentration of CMV.GFP-AAV2/8. (b) 10,000 vg/cell concentration of CMV.GFP-AAV2/8. Both titers had a large increase in percentage of cells fluorescing. The maximum fluorescence increased greater than 5 times the control in the treatment of 10 vg/cell of CMV.GFP-AAV2/8, and greater than 10 times the control with the addition of 10,000 vg/cell of CMV.GFP-AAV2/8.

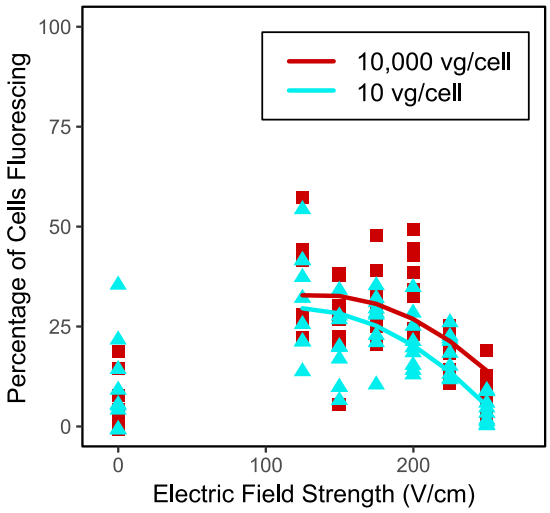

Fig. 2. Regression results for HL-60 cells pulsed twice. Regression lines for 10 and 10,000 vg/cell presented for treatment levels in comparison to the control.

Table 6-1. HL-60 cells 2x Pulses ANOVA Results

	Df	Sum of Squares	P-Value
Titer	1	706	0.0043
EF	1	151	0.1810
EF^2	1	9551	< 0.0001
Titer × EF	1	345	0.0444

For Hepa 1-6 cells, overall, similar results were obtained at the 10,000 vg/cell titer (though at slightly lower PEF intensities, probably due to the larger cell size), however there was very little detectable uptake of GFP in the 10 vg/cell titer. Results for the Hepa 1-6 cells are shown in Figure 6-3. This difference indicates that electroporation can increase AAV delivery of GFP, but only at a high concentration of CMV.GFP-AAV2/8 for Hepa 1-6 cells. The maximum fluorescence increased greater than 3 times the control in the treatment of 10,000 vg/cell of CMV.GFP-AAV2/8 but decreased by approximately 50 percent for the 10 vg/cell titer. This decrease could be related to general autofluorescence interfering with our ability to detect low levels of GFP in this cell type. These results also show a wide range of electric field strengths that caused an increase in GFP expression for the 10,000 vg/cell titer.

In the linear model regression for the RE outcomes of the Hepa 1-6 cells, the effect of titer ($P < 0.0001$), the first order electric field ($P = 0.0102$), the second order electric field ($P = 0.0003$) as well as the interaction effect between second order electric field and titer ($P = 0.0003$) were deemed significant (P-value < 0.05). These results are shown in Table 6-2. Note that the model choice was slightly different for Hepa 1-6 cells, compared to the HL-60 cells described above since the quadratic interaction term was deemed significant. This difference is caused by the inability to detect any increase in GFP expression at the 10 vg/cell titer, requiring additional terms in the model to accurately account for this difference. This provides significant evidence to reject the null hypothesis that effects are equal

zero and accept the alternative hypothesis that the there is an effect and that the effect of titer is different for different levels of electric fields.

In Figure 6-4 we provide a visualization of the results for the polynomial regression for the Hepa 1-6 cells. Following a similar approach to the above stated for HL-60 cells, results provide evidence to reject the null hypothesis of no effect of titer and EF on the percentage of cells which expressed GFP and accept the alternative hypothesis that there is an effect. More specifically, this analysis indicated that the effect of titer was different between the 10 and 10,000 vg/cell concentrations of CMV.GFP-AAV2/8. Regarding the intensity of the applied electric field, for the 10,000 vg/cell we observed a nonlinear trend of decrease in the of fluorescing cell as we increased the EF. For the 10,000 vg/cell, there was a linear trend of decrease that was not significant. Regarding the interaction effects, results suggest that the effect of EF was different for different levels of titer on the quadratic level only. This is different from the linear interaction results observed for the HL-60 cells.

The above results confirm that electroporation significantly increases the amount of GFP transfected across the range of electric fields tested, that the effect of titer is important, as was the interaction between titer and electric field strength. Only the 10,000 vg/cell concentration produced a detectable increase in GFP expression in Heap 1-6 cells. Regression results suggest that the most optimized electric field strength for GFP uptake using CMV.GFP-AAV2/8 and Hepa 1-6 cells is between 75 and 175 V/cm, with better uptake at the lower end of that range.

Overall, we observed an increase of GFP expression, which was sensitive to titer, in both cell types tested. This sensitivity to titer indicates that one should be careful selecting the proper dosage based on the cell type. The window of electric fields that were effective was approximately the same size, with fields between 125 and 225 V/cm for HL-60 cells and fields between 75 and 175 V/cm for Hepa 1-6 cells resulting in large increases of GFP expression in at least one titer. The difference in magnitude is most likely a result of the difference in cell size

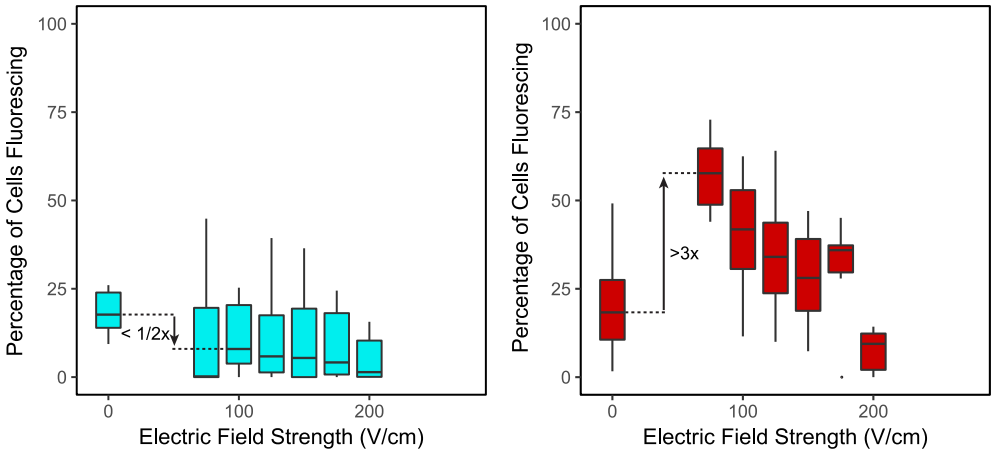

Fig. 3. **Percentage of Hepa 1-6 cells expressing GFP when exposed to two 50 ms pulses and two different titers of CMV.GFP-AAV2/8.** (a) 10 vg/cell concentration of CMV.GFP-AAV2/8. (b) 10,000 vg/cell concentration of CMV.GFP-AAV2/8. Only 10,000 vg/cell resulted in a detectable increase in fluorescence. The maximum fluorescence *decreased* by approximately 50% compared to the control in the treatment of 10 vg/cell of CMV.GFP-AAV2/8, while a greater than 3 times increase was detected using 10,000 vg/cell of CMV.GFP-AAV2/8.

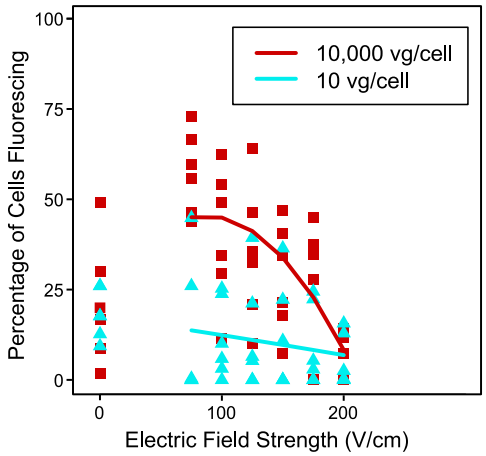

Fig. 4. Regression results for Hepa 1-6 cells pulsed twice. Regression lines for 10 and 10,000 vg/cell presented for treatment levels in comparison to the control

Table 6-2. Hepa 1-6 cells 2x Pulses ANOVA Results

	Df	Sum of Squares	P-Value
Titer	1	8436	< 0.0001
EF	1	1422	0.0102
EF^2	1	2955	0.0003
Titer × EF	1	6	0.6143
Titer × EF^2	1	2877	0.0003

6.6 Discussion

Our 2x pulse procedure produced the highest percentage of cells transfected and the widest window of PEF intensities that achieved similar levels of transfection. This was expected since the mechanism for DNA entry into a cell through electroporation requires the presence of an electric field, so increasing the number of pulses increases the exposure to the DNA [4]. Somewhat surprisingly, it was more effective than the 8x pulse protocol we tested. Six to eight pulses is a common range cited in literature as a useful number of pulses for gene transfection [108], [133], [216], [230]. However, it is possible that the amount of damage caused by electroporation in the eight pulse experiments was too much at higher electric field strengths, reducing the window of effective electric field strengths. This will need to be explored more in *in vivo* experiments to determine the optimal number of pulses.

Our results showed significant increases in GFP expression in both cell types using 10,000 vg/cell of the vector. This confirms our hypothesis that electroporation can increase gene delivery of AAV, similar to reported using other viruses [110]. The peak level of transfection occurred in HL-60 cells at 125 V/cm, resulting in an average value of 37% of the samples fluorescing. For Hepa 1-6 cells, this

peak occurred at 75 V/cm, with an average value of 58% of the sample fluorescing enough to overcome autofluorescence. This efficiency is on the upper limits of existing techniques (not counting techniques involving direct contact with individual cells) [1], [9].

10 vg/cell of the vector resulted in significant GFP expression in HL-60 cells but did not result in a significant increase in Hepa 1-6 cells. We postulate that this was caused by an inability to discern between innate autofluorescence of liver cells and fluorescence from GFP, due to the limitations of the autofluorescence blocking we attempted in this study. Specifically, with a lower titer value, (i.e.10 vg/cell) we hypothesize that fluorescence was not strong enough to overcome this effect during the four-day duration of these experiments, while the 10,000 vg/cell titer resulted in a strong enough fluorescence signal to overcome the background noise. This is supported by the average time it took for samples to reach the peak percentage fluorescing, which was 44.6 hours (± 5.1 standard error (SE)) for the 10,000 vg/cell titer while the 10 vg/cell titer was 96 (± 0.0 SE). 96 hours was the cutoff duration for these experiments due to cell viability concerns. The percent fluorescing peak at the end of the experiments suggests that the percentage fluorescing was still increasing by the end of the experimental window, and therefore would have likely further increased had the duration of these experiments been extended further. These results would not have been indicative of the actual percent fluorescing however, since GFP has a high toxicity which resulted in significant cell death after three to four days [226].

The difference in the significance of the EF and interaction terms between HL-60 and Heap 1-6 cells is also likely related to this phenomenon. Since the 10 vg/cell titer did not result in any detectable increase in GFP, the results are flat, while the 10,000 vg/cell case followed the parabolic function, causing this difference in the shape of the curves, and therefore the difference in significance in the related terms.

6.7 Conclusion

Electroporation significantly increased CMV.GFP-AAV2/8 transfection in both HL-60 cells and Hepa 1-6 cells for a wide range of electric field strengths. These results show a viable way to increase AAV uptake in a wide range of applications, potentially reducing the quantity of AAV needed to achieve transfection and therefore improving clinical outcomes by decreasing immune effects of AAV and reducing costs of treatments. The a wide window of electric field strengths which increase AAV uptake that we have shown in this study is valuable for *in vivo* applications, where tissues can be exposed to different field strengths dependent on probe positioning [103].

6.8 Acknowledgements

Hepa 1-6 cells and CMV.GFP-AAV2/8 were kindly provided by Dr. Hans Sollinger and Dr. Tausif Alam, Department of Surgery, Division of Organ Transplantation, University of Wisconsin Hospital and Clinics, Madison, WI. We also express our gratitude to Vera Cardoso Ferreira for assistance with statistical analysis and interpretation of data. This work was supported by the Duane H. and Dorothy M. Bluemke professorship and the Philip Dunham Reed professorship.

Chapter 7: **Device development**

After determining that electroporation significantly aided AAV-mediated transfection of a gene, we began testing various designs for a minimally invasive device capable of causing RE deep into the liver tissue. Catheter designs were the logical device type choice since the catheter could be used to

inject the AAV-capsid locally and is minimally invasive, only requiring a small incision. As stated in Chapter 2.11, existing catheter electroporation devices involved a single catheter and were used to treat tissue near or within blood vessels. To reach deeper into tissue, it would be necessary to either extend a guidewire down a nearby vein or use a second catheter. We decided to pursue the second catheter design since it would be easier to implement clinically and resulted in larger volumes electroporated than a guidewire model did in preliminary electromagnetic simulations. We then focused on this two-catheter design in our electromagnetic simulations.

In addition to electromagnetic simulations, we tested a prototype design of this device in excised swine livers, which were catheterized and injected with dye-containing fluid with varying volumes and rates of injection and monitored the extent of perfusion. These data allowed us to ensure the volume of cells exposed to the AAV particles (combined with RE exposure) would be sufficient for gene therapy treatments.

7.1 In Vivo Gene Therapy Delivery Electroporation Device and Procedure

Erik Aiken[1], Ashley Zagaros[1], Paul Laeseke[2], Tausif Alam[3], Hans Sollinger[3], John Booske[1], and Susan Hagness[1]

1 Department of Electrical & Computer Engineering, University of Wisconsin-Madison, Madison, Wisconsin, United States of America

2 Department of Radiology, University of Wisconsin-Madison, Madison, Wisconsin, United States of America

3 Department of Surgery, University of Wisconsin-Madison, Madison, Wisconsin, United States of America

7.2 Abstract

Inherited genetic diseases severely affect hundreds of millions of people around the world. Gene therapy has the potential to cure many of these diseases. One of the common methods for getting genes into target cells (transduction) is the use of a virus, where the viral load has been replaced with the therapeutic gene. When inside the cell the therapeutic gene goes to the nucleus, where it replaces portions of the DNA sequence fixing functions that cause the disease. While this technique has shown promise, it currently faces significant challenges in efficiency, cost, and safety. Many of these challenges are related to the large quantities of viral vector needed to successfully transduct enough cells to have an effect. We have developed a device and procedure capable of significantly reducing the quantity of vector needed for successful gene therapy. By combining viral gene therapy with electroporation, or the use of pulsed electric fields to open pores in cell membranes, we can significantly increase the uptake of a viral vector. This can be combined with a double balloon catheter to localize treatment, decreasing the necessary quantity of viral vector, therefore reducing cost and the probability of adverse side effects. In this paper, we present a combination of *ex vivo* and electromagnetic field simulation results tested in liver tissue to demonstrate the potential applications of this device. Our results indicate that this technique is capable of delivering RE-inducing electric fields and injectate to a sufficient volume of liver tissue to potentially treat several genetic diseases, such as hemophilia and type 1 diabetes. This device also has the capability to be used to cure numerous other genetic diseases.

7.3 Introduction

Inherited genetic mutation-based metabolic diseases significantly reduce quality of life for hundreds of millions of people in the world and account for 70% of child hospitalizations and 10% of adult hospitalizations [211], [231]. There are hundreds of types of such diseases, including diabetes, cystic fibrosis, sickle cell anemia, hemophilia, and thalassemia. Many of them involve the liver due to its central role in metabolism [211], [232], [233]. Developed countries spend trillions of dollars each year for patient care, with over $800B spent annually on type 1 diabetes alone. The recent advent of gene therapy has potential to provide a cure for many of these diseases. However, for many diseases, it can only occur if practical, cost-effective, *in vivo* methods existed to transport a normal single curative gene into a small portion of the liver cells. More specifically, for gene therapy to work, a gene, defined as the functional portion of a DNA sequence, needs to be transferred into a target cell. From there, the foreign gene enters the nucleus and is incorporated into the cell's DNA sequence [131]. When the altered sequence then replicates, it will produce different functional or regulatory proteins, changing the function of the cell.

A variety of methods exist to aid in gene transduction (the transfer of genetic material into a cell) including direct injection, viral delivery, plasmid liposome complexes, cationic lipids, and electroporation [11], [76], [110], [133]–[135]. Most non-viral treatments suffer from poor efficiency, therefore many applications have used viral delivery for gene therapy [217], [234]. Viruses can enter the cell either directly through the plasma membrane or from binding to cellular receptors and triggering pathways into the cell [25], [34]–[39]. All viruses consist of at least two parts, the viral genome or genetic material (DNA/RNA) and a capsid which protects the viral genome and is involved with transport through the membrane [40]. Naturally occurring viruses can be stripped of their original viral genome and replaced with a new genome, called a cassette, to help transport new genomes through the membrane [41]. Successful treatments of viral aided gene therapy have been reported with systemic injection of the viral vector, but these have been primarily for small mammals [211], [212].

The notable exception is a report of systemic injection for treatment of hemophilia, which had a prohibitively high cost on the order of $1 million per treatment [140].

However, this is not the only hurdle that gene therapy faces. Three major obstacles have prevented success of systemic injection *in vivo* gene therapy for large mammals. First, as mentioned above, inefficient transduction of target cells necessitates large, cost prohibitive gene vector doses [140]. Second, neutralizing antibodies form against the virus capsid containing the curative gene and can interfere with or prevent transduction [211]. Third, systemic injection of large quantities of the virus vector can trigger adaptive immunity that destroys the transduced transgene-producing cells [211].

Another method for gene delivery which could be useful in overcoming these challenges is electroporation. Electroporation is a technique that uses an externally applied pulsed electric field to induce pore formation in cells, and has also been used for gene therapy [54], [73], [214]. We have developed a revolutionary approach that could be a single-procedure, complete, permanent and cost-effective cure for many liver-based genetic metabolic diseases. This approach combines localized, intravenous targeted delivery of viral vectors containing modified genes with intravenous reversible electroporation (RE) – achieved simultaneously in the liver using a minimally invasive balloon catheter – to increase the efficiency by which curative genes get transducted into hepatocytes. This approach addresses the core issues of gene therapy: inefficient transfection of target tissue cells resulting in either failure or suboptimum transgene expression, and the requirement of large, expensive, and pathogenic viral loads often resulting in an immune response to the vector.

Previous research supports the idea that electroporation can improve viral gene delivery. A study by Terada et al. has shown that electroporation combined with adenovirus could greatly increase the gene transfer of Smad7, which was used to prevent renal fibrosis in kidneys [110]. Based on these results, we showed in our lab that electroporation could improve AAV uptake CITATION.

Our overarching hypothesis is that combining *in vivo* RE – the use of pulsed electric fields to open temporary pores in the cellular membrane – with adeno-associated virus (AAV) vector delivery will enhance transfection rates to achieve the therapeutic goal of transducing a significant fraction (≥3-8%) of available hepatocytes. AAV is a commonly used viral vector that has already been used for gene therapy treatments of a variety of diseases including hemophilia B [138]–[142], lipoprotein lipase deficiency (LPLD) [143], Parkinson's disease [10], among others [135], [144]. The range of ≥3-8% of available hepatocytes was chosen because it was the target conversion rate for gene therapies such as curing hemophilia and type I diabetes [138], [139], [141], [212]. The estimates for treating hemophilia ranged from a 3-8% conversion rate [138], [139], [141] and the estimates for treating diabetes were around a 5% conversion rate [212].

In this paper, we present a design for an effective electrode configuration for delivering electric fields capable of achieving RE in hepatocytes/liver tissue, quantify the PEF dose variability due to electrode positioning uncertainty, and determine perfusion of injectate into liver tissue. Computational electromagnetic simulations and *ex vivo* experiments with pig livers have been designed to a) develop electroporation electrodes for intravenous catheter introduction in the liver which expose a significant hepatocytes volume (≥3-8%) to the pulsed electric field intensities needed for RE, and b) determine relationships between electrode positioning, applied voltage, and tissue volume receiving a pulsed electric field dose that achieves hepatocyte RE. Our hypotheses are: (i) a well-defined mapping between electrode orientation/position/voltage and pulsed electric field intensity spatial distribution will enable an interventional radiologist to position the electrodes using real-time imaging and choose a suitable voltage to yield the desired RE-exposed volumes, and (ii) the uncertainty in electrode positioning will be small enough to ensure that any unintended variability in pulsed electric field dose is negligible. We have established the relationship between electrode spacing, angle, and voltage required to maximize the amount of tissue that receives both RE and the injectate. During *ex vivo*

experiments with commercial catheters, we have investigated insertion, manipulation, and positioning of prototype catheter-based electrodes in excised pig livers.

7.4 Materials and Methods

7.4.1 Electroporation Range

We used a combination of *in vitro* laboratory results and existing literature to determine the effective range of electric field strengths which result in RE. Higher intensity electric field strengths can cause cell death through irreversible electroporation (IRE) and should generally be avoided for molecule delivery applications. Our *in vitro* testing on mouse hepatocyte cells showed a significant increase in AAV uptake compared to non-electroporated controls in the range of 75-175 V/cm when using two pulses spaced 5 min apart with a pulse duration of 50 ms. While these numbers provide a good starting point, *in vivo* results can often differ from *in vitro*. An extensive literature review of *in vitro* electroporation for gene therapy showed a larger range of electric field intensities reported to result in RE for gene uptake. Previous studies have shown an effective range of 70-250 V/cm for transferring genes into liver tissue using 50 ms pulses [142], [230], [235]–[237]. In other tissues, the range is from around 60-300 V/cm for pulse durations in the 10-150 ms range [147], [238]–[241]. Based on these results, we anticipate the most RE to occur in the range between 100 and 200 V/cm and some uptake in the 60-100 and 200-275 V/cm range when using 50 ms pulses *in vivo* for liver tissue.

7.4.2 Ex Vivo Experiments

In order to develop a device capable of achieving clinically relevant volumes of molecule delivery inside target cells, we needed to determine the region where this equipment would be capable of delivering the molecule of interest. To do this, we performed *ex vivo* experiments to investigate

insertion, manipulation, and positioning of prototype balloon-catheter-based probes in excised porcine livers to confirm and refine the electrode orientations.

We used porcine livers provided by the University of Wisconsin-Madison Meat Science program to test injectate perfusion. Immediately prior to catheter experiments, livers were perfused with a saline solution. To test the distribution of the injectate (in practice the injectate would contain the curative AAV-gene), we used a green India ink to visualize regions where the injectate can perfuse to for different catheter locations. Initial tests were performed with single and double balloon catheter setups. Catheters were inserted into the hepatic vein in an isolated lobe of the liver. Dye was injected either upstream or downstream from single balloons and between double balloon setups. Early observations indicated that a double balloon design was superior to single balloon delivery, since it required less volume of dye injected to reach tissue where the electrode would be positioned. More precisely, the single balloon design was poor because most of the dye either returned up the vein (if the balloon was downstream from the injection site) or ended up far from the balloon (if injected downstream from the balloon). Therefore, we decided to focus on the two-balloon design for simulations and further experimentation.

After dye was injected, the liver was cut perpendicular to the vein in which the dye was injected. The regions where the electrode would be positioned were analyzed for dye distribution in various contours, as shown in Figure 7-1. In this figure we can identify the injectate flow based on the green dyed region. In total, seven separate total lobes from three different pig livers were used for this analysis.

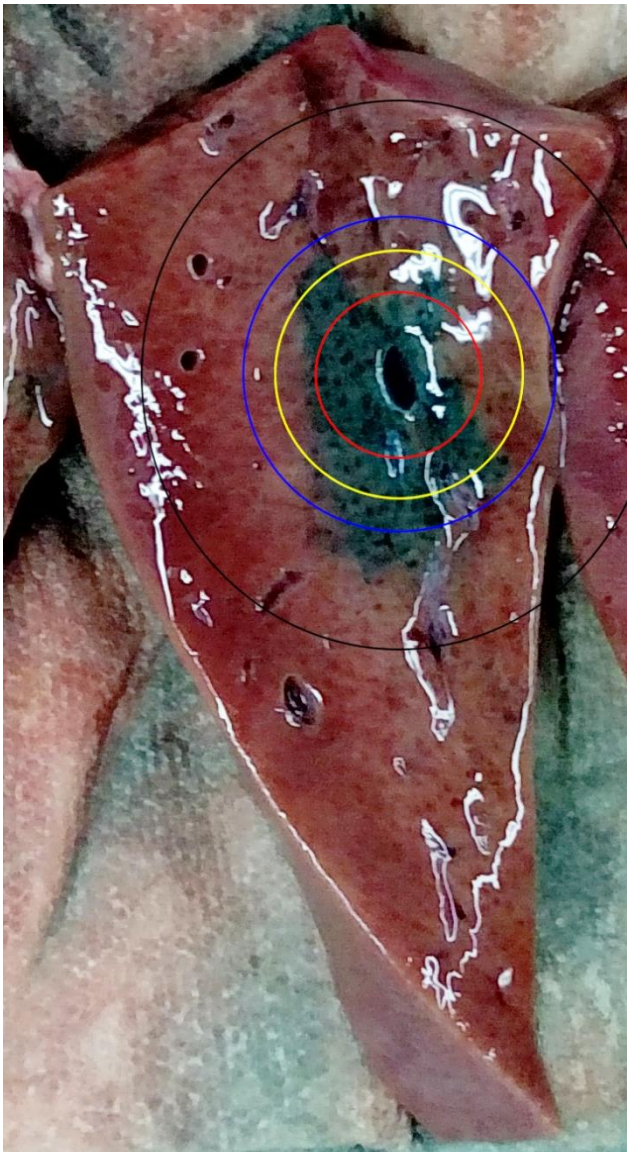

Figure 7-1. Illustrative image of dye distribution in cross-section of liver. The red (innermost) contour has a 0.8 cm radius, the yellow contour (second from center) has a 1.2 cm radius, the blue contour (third from center) has a 1.5 cm radius, and the black (outermost) contour has a 2.5 cm radius. The amount of dye enclosed by each of the contours were used to determine idealized pulse parameters for electroporation depending on electrode spacing.

7.4.3 Electromagnetic Simulations

This catheter device is designed to enter two nearby veins or arteries. In the case of liver, it could be inserted down the hepatic vein and into sub-branches such as those depicted in Figure 7-2. Figure 7-3 depicts a diagram of the intended device, with key components labeled.

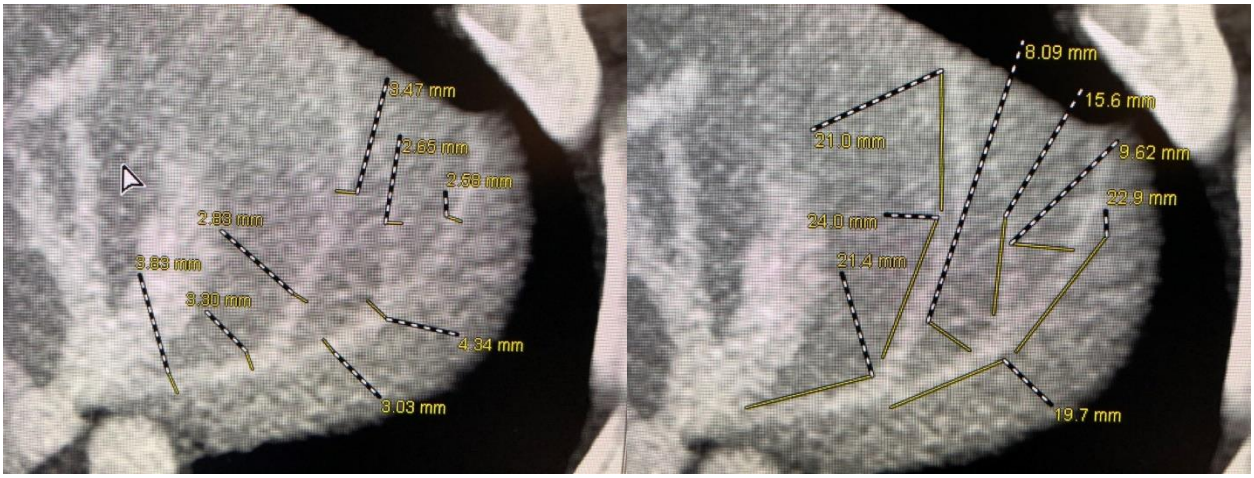

(A) (B)

Figure 7-2. Single pig liver lobe ultrasound image. This device would be positioned in nearby, roughly parallel veins. Measured lengths are depicted in yellow, with a dashed line drawn to the measurement. (A) Vein width measurements. (B) Lengths of straight segments.

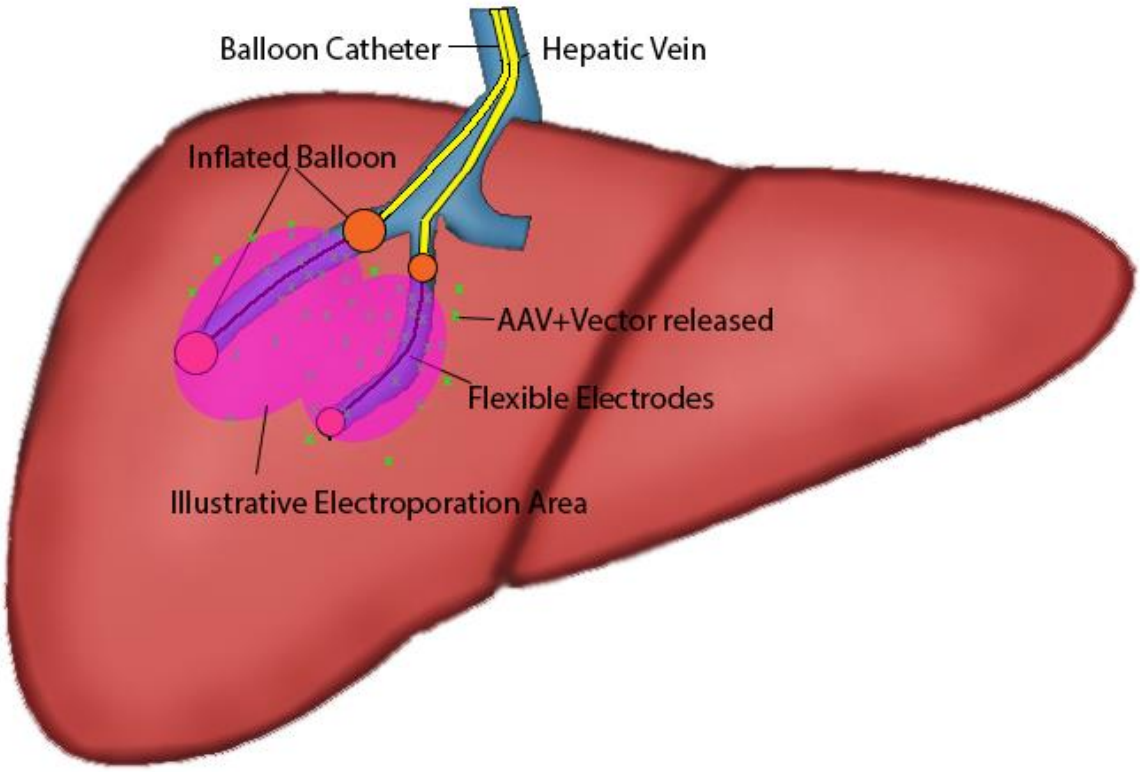

Figure 7-3. Diagram of catheter electrode layout. The catheters are represented by the yellow lines, with the inflated balloons represented by the orange circles. The active portion of the electrode is the black line between the balloons, with an illustrative electroporation region shown in pink. The estimated perfusion of the injected viral vector, here represented by AAV, is shown by the green 'x' characters. Successful transfection is expected to occur in the region where the electroporation range overlaps the injected viral vector.

After determining the radii of injectate perfusion, we used the electromagnetic simulation software CST Studio [242] to simulate electric field distributions in liver tissue with different electrode configurations to determine the voltage-spacing relationship required to cause the most RE in the area where the injectate reaches. All material properties used in this simulation were CST Studio default properties unless otherwise noted.

In CST Studio, we designed this device to have a coaxial conductor inside a catheter leading up to the active element. The coaxial conductor was chosen because it reduces stray electric fields in the tissue. In the active portion of the device (between the balloons), the inner conductor is extended,

while the polytetrafluoroethylene (PTFE) dielectric and outer conductor stopped at the balloon. A prototype of this design either could use a semi-rigid coaxial cable or layered medical tubing (such as nitinol inner and outer layers with a dielectric in-between). The inner conductors were connected to a voltage generator port, and the shields were shorted together, which prevented any stray fields from the source from entering the area of interest. The structure of this device is labeled in detail in Figure 7-4a.

As previously mentioned, we decided to use a double balloon catheter on each probe. Double balloon catheters have two inflatable balloons which can be used to block flow in a blood vessel. A fluid can be injected between the balloons, which helps localize the injectate to that region. We simulated the expanded balloons using air to fill them, however saline could also be used for the same purpose. The catheter was simulated using PTFE for its material and had an outer radius of 0.835 mm and an inner radius of 0.4445 mm, consistent with a 5 Fr catheter. A single hole was included the catheter in the center of the region between the balloons was added to allow injectate to flow to the target region. All metal components were simulated using perfect electrical conductors. We used blood as the material inside the veins, and the liver properties were chosen to be the built-in liver tissue properties included with CST Studio. We adjusted the angle of the veins to determine the impact of a non-parallel environment on results, as is likely to be encountered in an *in vivo* setting. Figure 7-4 shows the probes and simulation domain used in CST, with Figure 7-4a and 4b showing the parallel configuration and Figure 7-4c and 4d showing the 30º configuration.

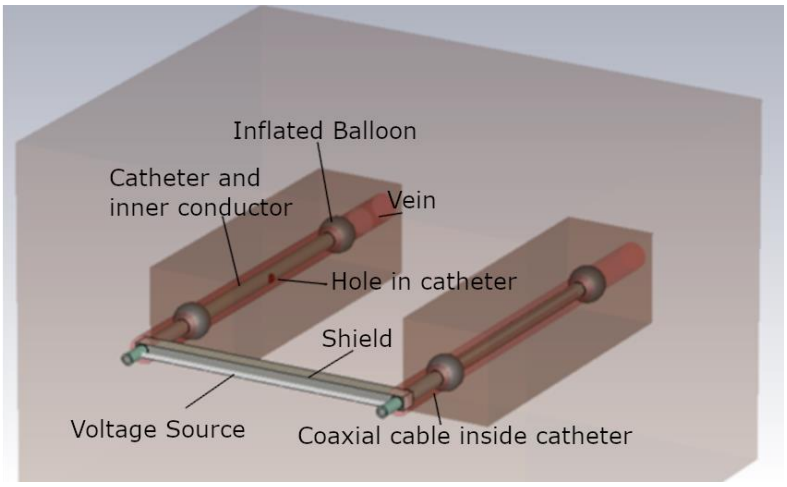
Inflated Balloon
Catheter and
inner conductor
Vein
Hole in catheter
Shield
Voltage Source
Coaxial cable inside catheter

(A)

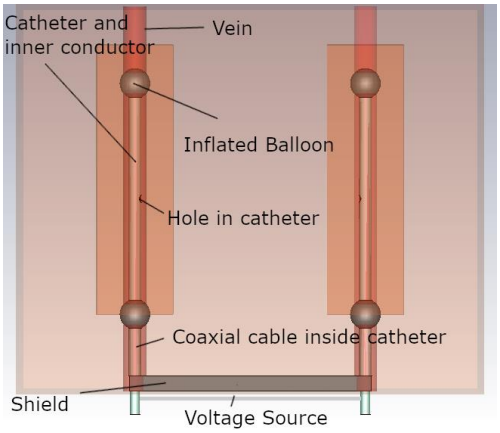
Catheter and
inner conductor
Vein
Inflated Balloon
Hole in catheter
Coaxial cable inside catheter
Shield
Voltage Source

(B)

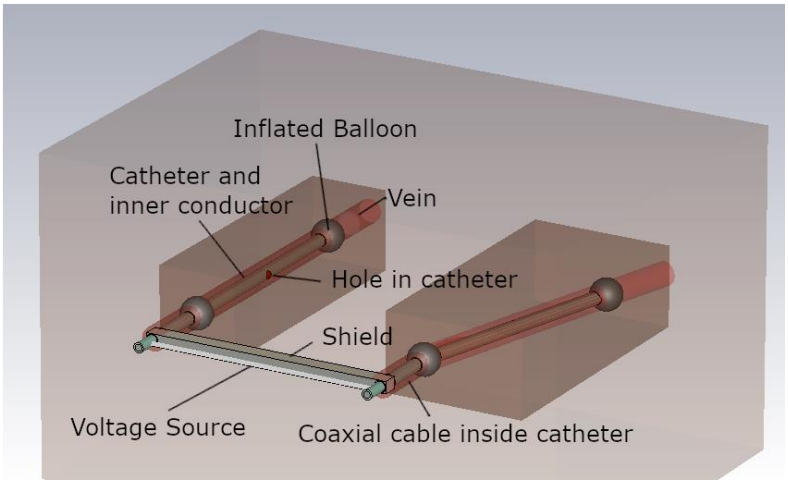
Inflated Balloon
Catheter and
inner conductor
Vein
Hole in catheter
Shield
Voltage Source
Coaxial cable inside catheter

(C)

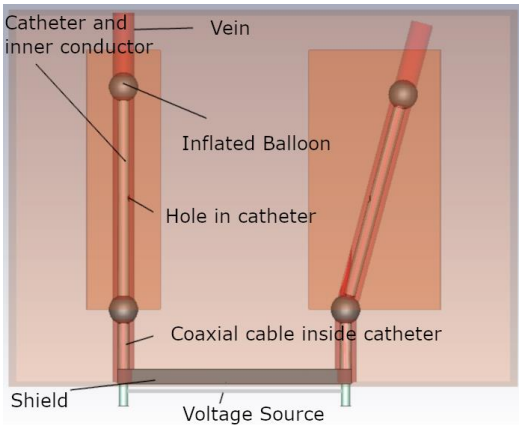

(D)

Figure 7-4. Device layout in CST. A) 3D view of parallel configuration with labels. B) Top view of parallel configuration. C) 3D view of angled configuration. D) Top view of angled configuration.

7.5 Results and Discussion

Results presented in this section were designed to simulate and predict field strengths capable of achieving RE outcomes in liver tissue. More precisely, as above mentioned, the device developed here must be capable of delivering sufficient electric fields to attain RE in a significant volume of tissue and a sufficient quantity of the desired injectate must be present at the time of the electric field exposure. In the previously mentioned example of treating diabetes with gene therapy for example, it is estimated that approximately 5% of liver cells must successfully uptake the modified gene to produce insulin and thus behave as surrogate pancreas cells [212]. For moderate and mild hemophilia in humans, the estimated volume to achieve considerable reduction in frequency and severity of hemorrhaging is approximately 3 to 8% of hepatocytes. [141]. To predict the volume of liver exposed to both RE and the curative gene we analyzed how dye perfused when injected between two balloons

in a branch of the hepatic vein within the liver, and then compared these results to electromagnetic simulations.

7.5.1 Liver Dye Perfusion

We analyzed the dye flow in two cross sections between balloons (except in a single case where only one cross section was used). Balloon spacings were 3-5 cm apart for all measurements. We measured dye flow within four different radii of the vein: 0.8, 1.2, 1.5, and 2.5 cm for the 2-3 separate lobes from three different pig livers (in total seven lobes). Averages for Radius (in cm), Dyed Area (cm^2) as well as its respective SD, Total Area (cm^2) and the percentage of the area that was dyed (% of Area) are shown in Table 7-1. We noticed that the dyed area increases as we increase radius (from 1.6 cm^2 at 0.8 radius to 6.7 cm^2 at 2.5 radius), but there is also increase in the variation (SD ranges from 0.37 at 0.8 radius to 2.0 at 2.5 radius). It is also noticeable that the percentage of area decreases with increase in the radius (from 80.3% at 0.8 radius to 34.3% at 2.5 radius).

Table 7-1. Dye perfusion in excised liver in seven separate lobes

Radius (cm)	Dyed Area (cm^2)	S.D.	Total Area (cm^2)	% of Area
0.8	1.615	0.37	2.01	80.32
1.2	2.88	0.78	4.52	63.67
1.5	4.00	0.95	7.07	56.57
2.5	6.74	2.037	19.63	34.34

In order to understand the linear association between radius (in cm) and the percentage of area dyed (more precisely the change observed in the measured dyed area given a change in radius) we used a simple linear regression. Results of the regression are shown in Table 7-2. These results indicate that there is a significant ($P < 0.0001$) association between radius and the dyed area. More precisely, for every 1 cm change in radius we expect to observe 3.01 cm^2 increase in the dyed area. Results from the

regression were used to predict values for dyed area in the full range of radii analyzed from 0.8-2.5 cm. The calculated R^2 value for this regression was high and equal to 0.726, meaning that 72.6% of variance in the dyed area is explained by the radius.

Table 7-2. Dye perfusion regression coefficients

	Estimate	S.E.	P Value
Intercept	-0.70	0.42	0.1061
Radius	3.01	0.26	< 0.0001

This provided us with a simple linear equation for predicting the area dyed within a given radius, described in Equation 1

$$A = -0.70 + 3.01R \quad (1)$$

where A is the dyed area, the overall mean is equal to -0.70, and R is the radius. Results for the linear prediction of dyed area, given the radius are illustrated in Figure 7-5. The predicted value is represented by the red line and individual datapoints are represented by the blue dots.

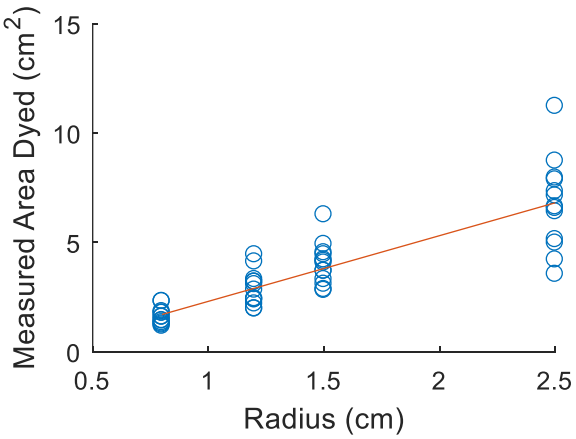

Figure 7-5. Fitted results for radius and measured area dyed. The line indicates the fitting of equation 1 and the circles indicate individual measurements.

7.5.2 Electromagnetic Simulations

We used CST Studio to perform electromagnetic simulations of the device as described in the methods section. We tested a range of spacings from 5-30 mm between probes, angles from 0 degrees to 45 degrees, and applied voltages of 250-1025 V. These simulations gave us the electric field distributions for these different parameters. Results are shown for 0 degrees in Figure 7-6 and 30 degrees in Figure 7-7. The spacing for the angled probes was measured at the closest spacing between the two electrodes.

As seen in Figure 7-6a, in the parallel configuration the RE area reaches 15 cm^2 (represented by the yellow region) at 30 mm spacing and 1000 V. In contrast, as seen in Figure 7-7a, there is a larger set of parameters where the 30º electrodes exceeds 15 cm^2 (also represented by the yellow region). The reason for this difference is that there is on average a larger spacing in the angled case than the parallel case. If the angled measurements are instead measured from the center point of the conductor, the results are a closer match for the parallel and angled case, as seen by comparing Figure 7-6a and 7-6b to Figure 7-7c and 7-7d. If measuring from the midpoint of the electrode, small spacings are not valid in the angled case since the closer points would overlap and have therefore been omitted from the

figure (represented as the white region in Figures 7-7c and 7-7d). The percent difference in area RE was evaluated from 15-30 mm spacings and is shown in Figure 7-8. At approximately 600 V, the different spacings converge to a similar response, with the minimum difference at around 600 V and gradually increasing. The percent differences in RE area are all within 10% of the parallel case up to 950 V. The angled probes resulted in larger areas in all measurements, indicating that the parallel configuration is a good baseline measurement for expected RE area.

At angles of 45° we started noticing higher amounts of IRE near the closest spacing, likely due to edge effects of the electric field, because electric fields tend to concentrate near sharp edges, and therefore we did not continue simulating angles ≥ 45°. The total area exposed to electric fields which cause RE was similar for most relevant spacings and voltages (within 10% area, as shown in Figure 7-8), if measured from the midpoint instead of closest location in the angled probes. Figure 7-9 shows a representative top view of a parallel and angled probe.

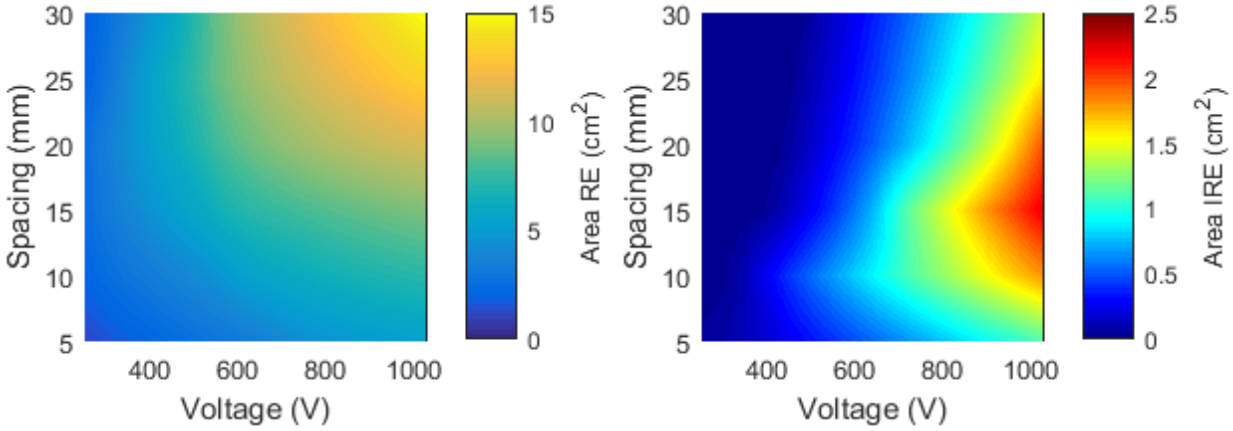

(A) (B)

Figure 7-6. Cross sectional area between probes that received RE or IRE for a parallel probe configuration. A) The area of tissue that received RE field strengths (60-275 V/cm). B) The area of tissue that received IRE field strengths (>275 V/cm).

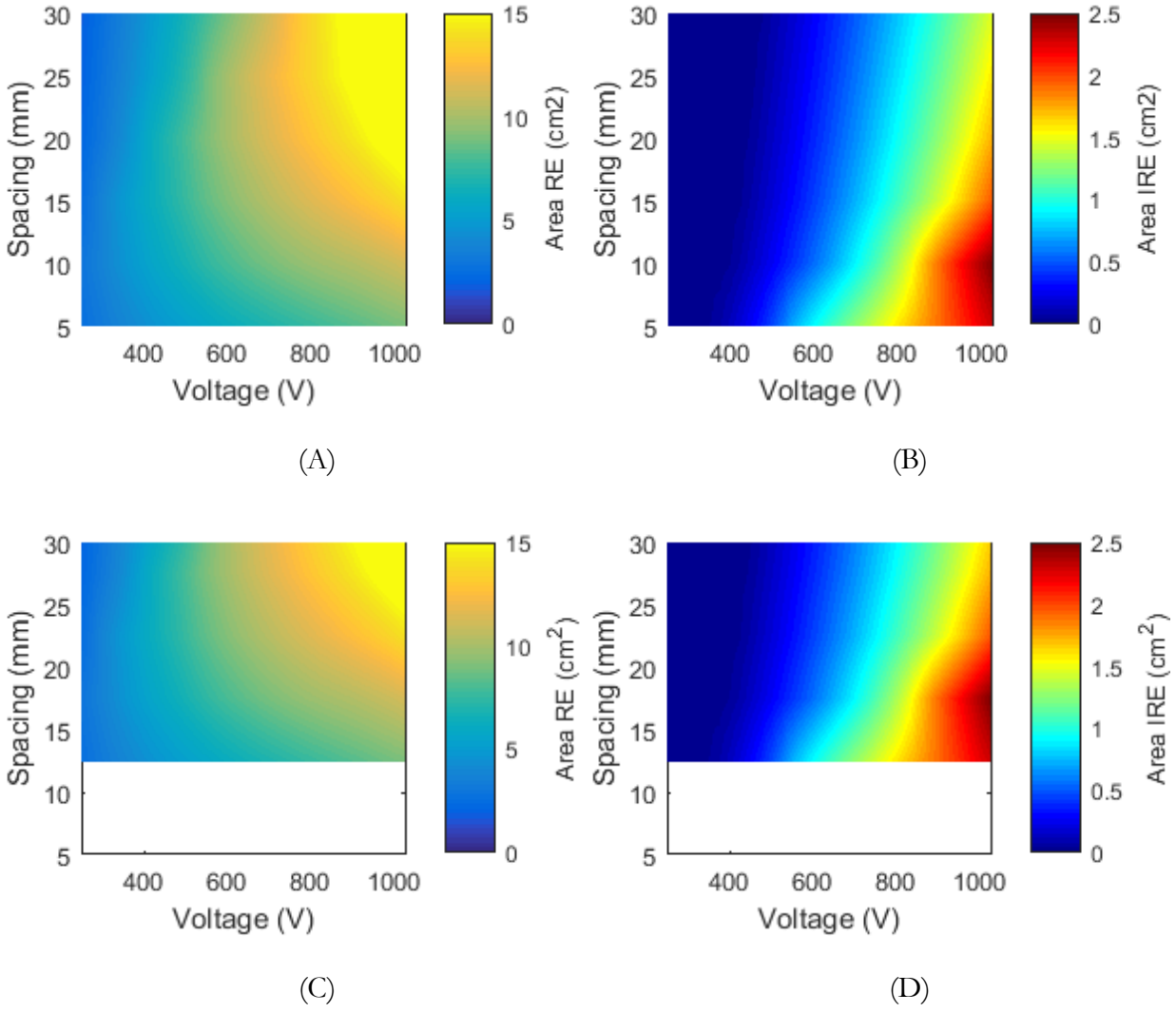

Figure 7-7. Cross sectional area between probes that received RE or IRE for the 30-degree angled probe configuration. A) The area of tissue that received RE field strengths (60-275 V/cm). B) The area of tissue that received IRE field strengths (>275 V/cm). C) RE, adjusted to show center spacing. D) IRE, adjusted to show center spacing. Small spacings are not valid in the angled case when measured from the midpoint and have therefore been omitted from the figure, as seen in the white regions of part C and D.

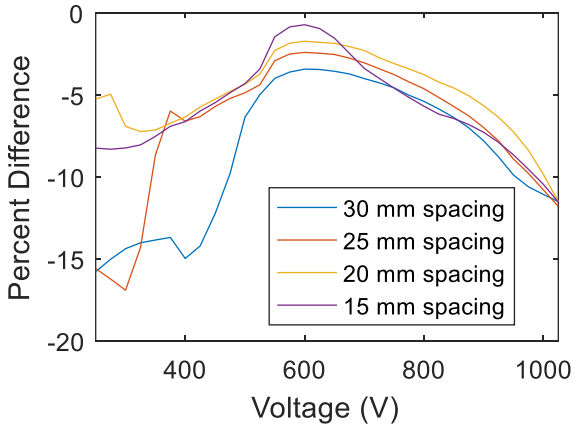

Figure 7-8. Percent difference in Area RE between parallel and 30º angled probe. The angled probe spacing measurement is taken at the midpoint. The angled probe resulted in more RE area for all measurements. For voltages between 600-950 V there was little difference between the different spacings and less than 10% difference for the RE area.

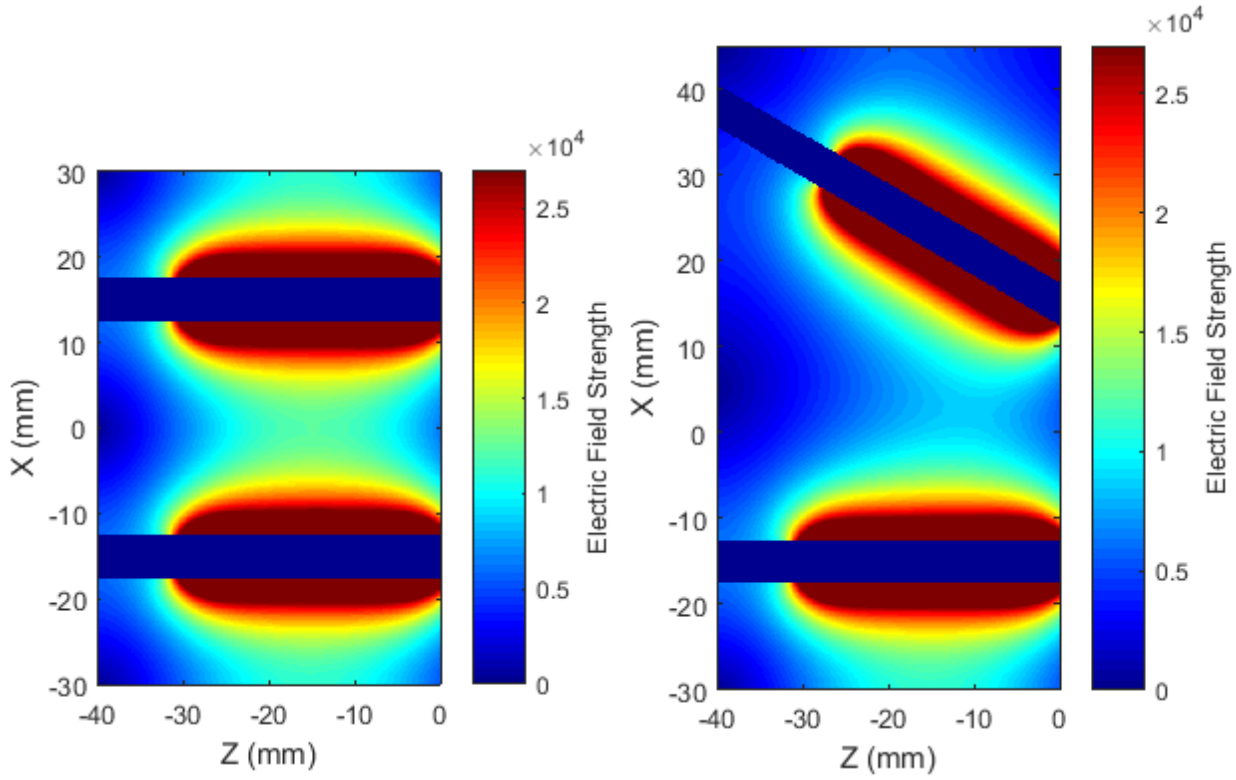

(A) (B)

Figure 7-9. Top view of electric field distribution for parallel and angled electrodes at 30 mm spacing and 1000 V. The electric field intensity has been set to 0 V/m inside the vein areas so as not to be included in area or volume calculations. (A) parallel probed. (B) 30° probes. The total volume RE was 42.22 cm^3 in the parallel case and 45.15 cm^3 in the 30° case.

7.5.3 Combined Results

To determine the area that would receive a dose of an injected drug, we combined the dye perfusion results with the electromagnetic simulations. Since the density of dye decreased with increasing radius, we calculated the percentage of tissue in the RE region that received dye using equation 1 and multiplied that by the RE area for a given field strength and voltage. To do this, we determined the approximate radius of the IRE area from the simulation results and used equation 1 to calculate the area of injectate that would be within that radius. We then did the same calculation with the approximate radius of the RE area, which provided the area of injectate in the entire

electroporated area. Subtracting the amount in the IRE region provided the amount of dye only in the RE area. This was compared to the total area of circle of the same radius minus the IRE region to provide the proportion of cells in the RE area that received dye and did not die and would therefore be expected to receive an injected drug for gene therapy. Results of these calculations are shown in Figure 7-10. The amount of tissue that received both dye and RE strength fields ranged from 1.2-6.6 cm^2 in the parallel case, where 1.2 cm^2 is seen as the blue regions in Figure 7-10a and 6.6 cm^2 is the yellow region and 1.8-6.9 cm^2 in the 30º configuration where 1.8 cm^2 is seen as the blue regions in Figure 7-10b and 6.9 cm^2 is in the yellow region. The parallel configuration results in approximately 4.8-6.6 cm^2 volume of cells with both RE and the vector for spacings larger than 10 mm, while the 30º angled probes had at approximately 5.8 to 6.9 at the same spacings.

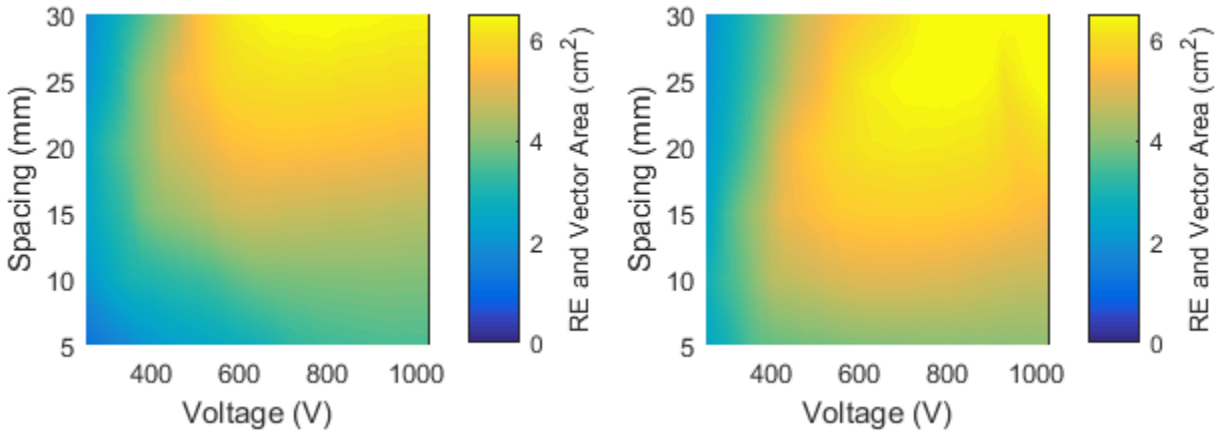

(A) (B)

Figure 7-10. Area of RE times the probability of dye reaching that area. The color indicates the area expected to receive both RE and the injected vector. (A) parallel probe configuration. (B) 30° angled probe configuration.

7.6 Practical applications, limitations, and advantages

As previously stated, treatment of diabetes and hemophilia with gene therapy require 3-8% of the liver to be transducted [138], [139], [141], [212]. In a small pig, the total volume of a liver is around 440-640 cm^3 [243], [244]. For larger pigs, the volume is on the order of 1400-1800 cm^3 [244]. Human livers have a volume of 998-2067 cm^3 [245], [246]. This means that to attain clinically relevant volumes of around 5% treated, 22-32 cm^3 would need to be treated for small pigs and 70-90 cm^3 would need to be treated for large pigs and humans. We must also consider that RE can result in approximately 50% of cells in the range transfected [1], [8], [9], and therefore these volumes should be doubled to account for this possible inefficiency.

These results can be used for several purposes. In a case where an entire liver could be exposed to a vector, the results shown in Figure 7-6 provides the expected area RE and IRE for given spacing and voltages. These values could predict the amount of tissue exposed for a given length of electrode. For example, in the case of a 3 cm electrode an 800 V pulse would result in approximately 30 cm^3 of tissue exposed to RE field strengths. In this case, it would be easy to attain clinically relevant volumes of tissue with few pulses. The downside to this is that it would require a large volume of an injectate to expose the liver, which as previously stated can result in large costs [140].

It is often desirable to keep the injectate close to the electrodes to reduce costs and other adverse effects such as immune responses [211]. The results shown in Figure 7-9 provide a map for determining the expected volume of tissue that will receive both RE and an injected vector for this double balloon catheter electrode design. In this case, to treat clinically relevant volumes of tissue, this method can be applied along the length of several parallel veins in a liver. Assuming a minimum combined treatment of RE and Vector area of 5 cm^2 (which as shown in Figure 7-7 is possible for all spacings larger than 15 mm), a total length of 36 cm would need to be treated to treat a large pig or human. Therefore, using a probe design using a 3 cm spacing between balloons, a total of 12 locations

per liver would need to be chosen to reach this threshold, while a 4 cm spacing would require 9 positions. In a smaller liver, a three cm probe would need approximately 5 positions, and a 4 cm probe would need approximately four positions. These results indicate it is possible to attain clinically relevant volumes of transduction while reducing the cost and chances of adverse effects. In the case of a small pig, over 5% of the volume can be transducted with 4-5 different probe positionings with a 3 cm electrode. In a larger pig and human sized liver, it could require up to 12 total locations to achieve the desired volume, though that number can be reduced by several factors. If the spacing is around 30 mm between probes, it is possible to attain 6.5 cm^2 area of both RE and the injectate, and therefore the maximum number of positionings would fall to ten. Using a 5 cm electrode instead of 3 cm would further reduce this to 6 locations. *In vivo* studies will be needed to determine the actual efficiency of RE for this device, and the realistic spacings and designs.

7.7 Conclusion

We have developed a design for an effective electrode configuration for RE of hepatocytes in liver tissue, that when combined with the appropriate procedure is capable of exposing a clinically significant volume of hepatocytes to the PEF intensities and an injected drug. In the case of gene therapy for treating either hemophilia or Type 1 diabetes with gene therapy, this device is easily capable of delivering a gene therapy to the minimum 3 or 5% necessary for treatment. We also demonstrated that this procedure is relatively stable for slight variations in probe angle and spacing, with angled configurations resulting in slightly more RE on average. We showed that correct electroporation parameters can be determined based on knowing the approximate spacing

Chapter 8: Conclusions and Future Work

8.1 Conclusions

Electroporation has a wide variety of clinical and research purposes. During this PhD thesis, I investigated underlying principles of electroporation with the focus on improving electroporation treatments, and to specifically address gaps in electroporation-based healthcare applications. The research projects I pursued demonstrate this progression, starting with improving the ability to process a high number of samples with our existing laboratory setup. Then I investigated ways to increase reversible electroporation (RE) outcomes, and finished by providing the groundwork, including the preliminary research and device development, for using a newly developed combination electroporation/viral delivery technique for locally improving gene therapy delivery. This device is minimally invasive and could ultimately change the way gene therapy is performed in healthcare applications.

In satisfying the previously mentioned specific aims, we have shown different ways to improve electroporation-mediated delivery of macromolecules. The first was through adjusting the cellular environment by modifying the plasma membrane potential prior to electroporation. We specifically wanted to focus on the effect of modifying the plasma membrane potential on RE outcomes, since this had never been done before and could have important clinical and research applications. This work led to the conclusion that even a slight change in the plasma membrane potential influenced electroporation outcomes at certain pulse parameters. If further advancements can be made in adjusting the membrane potential without harming the cell, it could have significant impact, with uses ranging from improving uptake in a laboratory setting to targeted clinical delivery. The second technique for improving electroporation-mediated delivery of macromolecules was related to the development of a minimally invasive *in vivo* electroporation device capable of localized delivery of RE. This development addressed one of the major obstacles in gene therapy: successful and efficient

transfection of the therapeutic gene into target cells. This device and procedure can deliver electric fields capable of performing RE to a clinically relevant volume of tissue for gene therapy treatment of several diseases. Therefore, we conclude that with our combined viral-electroporation technique and the catheter device presented in this dissertation that it is feasible to perform localized electroporation/viral mediated gene therapy. Furthermore, we discovered that the electroporation device is relatively robust to uncertainty in electrode position, which is beneficial for clinical use.

8.2 Possible Future Work

This thesis presented promising results in the area of electroporation for improve cellular AAV-gene uptake, and a device for delivering electroporation *in vivo* was successfully tested in an *ex vivo* and a simulation environment. Both the membrane potential study and the device development study have potential future work.

While we determined that hyperpolarizing cells affected RE outcomes, additional studies may improve this method. For example, more significant changes in membrane potential could be useful, especially for the RE case. Additionally, for this technique to be used in a wider variety of applications, more research could be done investigating the range of pulse durations where hyperpolarization is effective for increasing RE. Lastly, for *in vitro* applications, it would be useful to combine membrane potential adjustments with cell targeting techniques, which was not investigated in this project.

The next step for this the device development is to test this device *in vivo* to show electroporation improves AAV uptake in larger animals. The long-term goal is for this device to be successful in humans.

There are several short-term goals for *in vivo* testing of this device. First is to determine the actual RE efficiency *in vivo* and the region where RE occurs around the veins. While the simulations presented in this dissertation provide a starting point and present encouraging results, these need to be tested in

a living animal to further validate these claims. The next testing goal is to confirm long lasting modified cell function. This technique most useful clinically if the cells continue to express the modified gene and function long after treatment. Lastly, there should be minimal immune/inflammatory response, which as previously stated would be detrimental to subsequent treatments (if needed) and could pose additional serious health concerns. If this device and procedure can overcome these challenges, it could be a gamechanger in the field of gene therapy.

Chapter 9: **Works Cited**

[1] E. Neumann, A. E. Sowers, and C. A. Jordan, *Electroporation and Electrofusion in Cell Biology*, no. 1. New York, NY: Plenum Press, 1989.

[2] F. André and L. M. Mir, "DNA electrotransfer: its principles and an updated review of its therapeutic applications.," *Gene Ther.*, vol. 11, pp. S33–S42, 2004.

[3] T. Nishi *et al.*, "High-efficiency in vivo gene transfer using intraarterial plasmid DNA injection following in vivo electroporation," *Cancer Res.*, vol. 56, no. 5, pp. 1050–1055, 1996.

[4] J. Gehl, "Electroporation: Theory and methods, perspectives for drug delivery, gene therapy and research," *Acta Physiologica Scandinavica*, vol. 177, no. 4. pp. 437–447, 2003.

[5] J. Lin *et al.*, "Rapid delivery of silver nanoparticles into living cells by electroporation for surface-enhanced Raman spectroscopy," *Biosens. Bioelectron.*, vol. 25, no. 2, pp. 388–394, 2009.

[6] Z. A. Schelly, "Subnanometer size uncapped quantum dots via electroporation of synthetic vesicles," *Colloids Surfaces B Biointerfaces*, vol. 56, no. 1–2, pp. 281–284, 2007.

[7] M. Phillips, E. Maor, and B. Rubinsky, "Nonthermal irreversible electroporation for tissue decellularization.," *J. Biomech. Eng.*, vol. 132, no. 9, p. 091003, 2010.

[8] G. D. Schmidt-Wolf and I. G. H. Schmidt-Wolf, "Non-viral and hybrid vectors in human gene

therapy: An update," *Trends in Molecular Medicine*, vol. 9, no. 2. pp. 67–72, 2003.

[9] X. Xie, A. M. Xu, S. Leal-Ortiz, Y. Cao, C. C. Garner, and N. A. Melosh, "Nanostraw-electroporation system for highly efficient intracellular delivery and transfection," *ACS Nano*, vol. 7, no. 5, pp. 4351–4358, 2013.

[10] M. G. Kaplitt *et al.*, "Safety and tolerability of gene therapy with an adeno-associated virus (AAV) borne GAD gene for Parkinson's disease: an open label, phase I trial," *Lancet*, vol. 369, pp. 2097–2105, 2007.

[11] T. Niidome and L. Huang, "Gene Therapy Progress and Prospects: Nonviral vectors," *Gene Ther.*, vol. 9, no. 24, pp. 1647–1652, 2002.

[12] S. M. Kennedy *et al.*, "Cationic peptide exposure enhances pulsed-electric-field-mediated membrane disruption," *PLoS One*, vol. 9, no. 3, pp. 1–17, 2014.

[13] D. M. Soden *et al.*, "Successful application of targeted electrochemotherapy using novel flexible electrodes and low dose bleomycin to solid tumours," *Cancer Lett.*, vol. 232, no. 2, pp. 300–310, 2006.

[14] E. Maor, A. Ivorra, J. J. Mitchell, and B. Rubinsky, "Vascular smooth muscle cells ablation with endovascular non thermal irreversible electroporation," *J. Vasc. Interv. Radiol.*, vol. 21, no. 11, pp. 1708–1715, 2011.

[15] J. B. Martin, J. L. Young, J. N. Benoit, and D. A. Dean, "Gene Transfer To Intact Mesenteric Arteries by Electroporation," *J Vasc Res*, vol. 37, no. 5, pp. 372–380, 2000.

[16] C. R. Lin *et al.*, "Electroporation for direct spinal gene transfer in rats," *Neurosci. Lett.*, vol. 317, no. 1, pp. 1–4, 2002.

[17] N. B. Dev, G. A. Hofmann, S. B. Dev, and D. P. Rabussay, "Intravascular Electroporation Markedly Attenuates Neointima Formation After Balloon Injury of the Carotid Artery in the Rat," *J. Interv. Cardiol.*, vol. 13, no. 5, pp. 331–338, 2000.

[18] C. V. Desimone *et al.*, "Novel balloon catheter device with pacing, ablating, electroporation, and drug-eluting capabilities for atrial fibrillation treatment - Preliminary efficacy and safety studies in a canine model," *Transl. Res.*, vol. 164, no. 6, pp. 508–514, 2014.

[19] S. B. Dev, N. B. Dev, and G. A. Hofmann, "Electroporation-mediated intravascular delivery." Google Patents, 1999.

[20] H. Lodish *et al.*, *Molecular Cell Biology*, 6th ed. New York, NY, NY: W. H. Freeman and Company, 2008.

[21] B. Alberts, A. Johnson, J. Lewis, M. Raff, K. Roberts, and P. Walter, *Molecular Biology of the Cell*. 2002.

[22] C. Chen, S. W. Smye, M. P. Robinson, and J. A. Evans, "Membrane electroporation theories: A review," *Medical and Biological Engineering and Computing*, vol. 44, no. 1–2. pp. 5–14, 2006.

[23] I. Budin and N. K. Devaraj, "Membrane assembly driven by a biomimetic coupling reaction," *J. Am. Chem. Soc.*, vol. 134, no. 2, pp. 751–753, 2012.

[24] J. M. Meacham, K. Durvasula, F. L. Degertekin, and G. Fedorov, Andrei, "Physical Methods for Intracellular Delivery: Practical Aspects from Laboratory Use to Industrial-Scale Processing," *J Lab Autom*, vol. 19, no. 1, pp. 1–18, 2014.

[25] N. J. Yang and M. J. Hinner, "Getting Across the Cell Membrane: An Overview for Small Molecules, Peptides, and Proteins," *Methods Mol Biol*, vol. 1266, pp. 29–53, 2015.

[26] G. M. Cooper and R. E. Hausman, "The Cell: A Molecular Approach 2nd Edition," *Sinauer Associates*. pp. 1–820, 2000.

[27] D. M. Copolovici, K. Langel, E. Eriste, and Ü. Langel, "Cell-penetrating peptides: Design, synthesis, and applications," *ACS Nano*, vol. 8, no. 3. pp. 1972–1994, 2014.

[28] M. Lindgren, M. Hällbrink, a Prochiantz, and U. Langel, "Cell-penetrating peptides.," *Trends Pharmacol. Sci.*, vol. 21, no. 3, pp. 99–103, 2000.

[29] K. M. Stewart, K. L. Horton, and S. O. Kelley, "Cell-penetrating peptides as delivery vehicles for biology and medicine," *Org. Biomol. Chem.*, vol. 6, no. 13, pp. 2242–2255, 2008.

[30] R. J. Collier, "Membrane translocation by anthrax toxin," *Molecular Aspects of Medicine*, vol. 30, no. 6. pp. 413–422, 2009.

[31] S. Friebe, F. G. van der Goot, and J. Bürgi, "The ins and outs of anthrax toxin," *Toxins*, vol. 8, no. 3. 2016.

[32] K. L. Thoren and B. A. Krantz, "The unfolding story of anthrax toxin translocation," *Molecular Microbiology*, vol. 80, no. 3. pp. 588–595, 2011.

[33] P. Falnes and K. Sandvig, "Penetration of protein toxins into cells," *Current Opinion in Cell Biology*, vol. 12, no. 4. pp. 407–413, 2000.

[34] A. V. Nicola, H. C. Aguilar, J. Mercer, B. Ryckman, and C. M. Wiethoff, "Virus entry by endocytosis," *Advances in Virology*, vol. 2013, 2013.

[35] J. Mercer and A. Helenius, "Virus entry by macropinocytosis," *Nature Cell Biology*, vol. 11, no. 5. pp. 510–520, 2009.

[36] L. Sun, J. Li, and X. Xiao, "Overcoming adeno-associated virus vector size limitation through viral DNA heterodimerization - Nature Medicine," *Nat. Med.*, vol. 6, no. 5, pp. 599–602, 2000.

[37] C. L. Moyer and G. R. Nemerow, "Viral weapons of membrane destruction: Variable modes of membrane penetration by non-enveloped viruses," *Curr. Opin. Virol.*, vol. 1, no. 1, pp. 44–49, 2011.

[38] J. Johnson and M. Banerjee, "Activation, Exposure and Penetration of Virally Encoded, Membrane-Active Polypeptides During Non-Enveloped Virus Entry," *Curr. Protein Pept. Sci.*, vol. 9, no. 1, pp. 16–27, 2008.

[39] B. Tsai, "Penetration of Nonenveloped Viruses into the Cytoplasm," *Annu. Rev. Cell Dev. Biol.*, vol. 23, no. 1, pp. 23–43, 2007.

[40] M. F. Naso, B. Tomkowicz, W. L. Perry, and W. R. Strohl, "Adeno-Associated Virus (AAV) as a Vector for Gene Therapy," *BioDrugs*, vol. 31, no. 4. pp. 317–334, 2017.

[41] S. D. Patil, D. G. Rhodes, and D. J. Burgess, "DNA-based therapeutics and DNA delivery systems: A comprehensive review," *AAPS J.*, vol. 7, no. 1, pp. E61–E77, 2005.

[42] J. Wang *et al.*, "Predominant cell-mediated immunity in the oral mucosa: Gene gun-based vaccination against infectious diseases," *J. Dermatol. Sci.*, vol. 31, no. 3, pp. 203–210, 2003.

[43] Y. Khan, "The gene gun: Current application in cutaneous gene therapy," *Journal of Pakistan Association of Dermatologists*, vol. 12, no. OCT./DEC., pp. 167–170, 2002.

[44] N. S. Yang, J. Burkholder, B. Roberts, B. Martinell, and D. McCabe, "In vivo and in vitro gene transfer to mammalian somatic cells by particle bombardment.," *Proc. Natl. Acad. Sci. U. S. A.*, vol. 87, no. 24, pp. 9568–72, 1990.

[45] N. Zilony, A. Tzur-Balter, E. Segal, and O. Shefi, "Bombarding cancer: Biolistic delivery of therapeutics using porous si carriers," *Sci. Rep.*, vol. 3, pp. 1–6, 2013.

[46] S. Hernot and A. L. Klibanov, "Microbubbles in ultrasound-triggered drug and gene delivery," *Advanced Drug Delivery Reviews*, vol. 60, no. 10. pp. 1153–1166, 2008.

[47] Y. Isaka, "Gene therapy targeting kidney diseases: Routes and vehicles," *Clin. Exp. Nephrol.*, vol. 10, no. 4, pp. 229–235, 2006.

[48] J. S. Soughayer, T. Krasieva, S. C. Jacobson, J. M. Ramsey, B. J. Tromberg, and N. L. Allbritton, "Characterization of cellular optoporation with distance," *Anal. Chem.*, vol. 72, no. 6, pp. 1342–1347, 2000.

[49] A. A. Davis, M. J. Farrar, N. Nishimura, M. M. Jin, and C. B. Schaffer, "Optoporation and Genetic Manipulation of Cells Using Femtosecond Laser Pulses," *Biophys. J.*, vol. 105, no. 4, pp. 862–871, 2013.

[50] I. B. Clark *et al.*, "Optoinjection for efficient targeted delivery of a broad range of compounds

and macromolecules into diverse cell types," *J. Biomed. Opt.*, vol. 11, no. 1, p. 014034, 2006.

[51] D. J. Stevenson, F. J. Gunn-Moore, P. Campbell, and K. Dholakia, "Single cell optical transfection," *J. R. Soc. Interface*, vol. 7, no. 47, pp. 863–871, 2010.

[52] M. Antkowiak, M. L. Torres-Mapa, D. J. Stevenson, K. Dholakia, and F. J. Gunn-Moore, "Femtosecond optical transfection of individual mammalian cells," *Nat. Protoc.*, vol. 8, no. 6, pp. 1216–1233, 2013.

[53] K. Rhodes, I. Clark, M. Zatcoff, T. Eustaquio, K. L. Hoyte, and M. R. Koller, "Cellular Laserfection," *Methods in Cell Biology*, vol. 82. pp. 309–333, 2007.

[54] R. Heller, "Overview of electroporation.," *Technology in cancer research treatment*, vol. 1, no. 5. pp. 317–318, 2002.

[55] T. Matsuda and C. L. Cepko, "Electroporation and RNA interference in the rodent retina in vivo and in vitro," *Proc. Natl. Acad. Sci.*, vol. 101, no. 1, pp. 16–22, 2004.

[56] J. C. Weaver, K. C. Smith, A. T. Esser, R. S. Son, and T. R. Gowrishankar, "A brief overview of electroporation pulse strength-duration space: A region where additional intracellular effects are expected," *Bioelectrochemistry*, vol. 87, pp. 236–243, 2012.

[57] S. Somiari *et al.*, "Theory and in Vivo Application of Electroporative Gene Delivery," *Mol. Ther.*, vol. 2, no. 3, pp. 178–187, 2000.

[58] D. Luo and W. M. Saltzman, "Synthetic DNA delivery systems," *Nat. Biotechnol.*, vol. 8, no. 1, pp. 33–37, 2000.

[59] S. R, "Reversible electrical breakdown of the excitable membrane of a Ranvier node," *Ann Acad Brazil Ciens*, vol. 30, no. 1, pp. 57–63, 1958.

[60] A. Sale and W. Hamilton, "Effects of high electric fields on microorganisms I. Killing of bacteria and yeasts," *Biochim. Biophys. Acta - Gen. Subj.*, vol. 148, no. 3, pp. 781–788, 1967.

[61] E. Neumann and K. Rosenheck, "Permeability changes induced by electric impulses in

vesicular membranes," *J. Membr. Biol.*, vol. 10, no. 1, pp. 279–290, 1972.

[62] J. M. Crowley, "Electrical Breakdown of Bimolecular Lipid Membranes as an Electromechanical Instability," *Biophys. J.*, vol. 13, no. 7, pp. 711–724, 1973.

[63] H. Akaike, "Information theory and an extensión of the maximum likelihood principle," *Int. Symp. Inf. theory*, no. 1973, pp. 267–281, 1973.

[64] B. Gauger and F. W. Bentrup, "A study of dielectric membrane breakdown in the Fucus egg.," *J. Membr. Biol.*, vol. 48, no. 3, pp. 249–64, 1979.

[65] R. Benz and U. Zimmermann, "The resealing process of lipid bilayers after reversible electrical breakdown," *BBA - Biomembr.*, vol. 640, no. 1, pp. 169–178, 1981.

[66] R. Benz, F. Beckers, and U. Zimmermann, "Reversible electrical breakdown of lipid bilayer membranes: A charge-pulse relaxation study," *J. Membr. Biol.*, vol. 48, no. 2, pp. 181–204, 1979.

[67] I. G. Abidor, V. B. Arakelyan, L. V. Chernomordik, Y. A. Chizmadzhev, V. F. Pastushenko, and M. P. Tarasevich, "Electric breakdown of bilayer lipid membranes. I. The main experimental facts and their qualitative discussion," *J. Electroanal. Chem.*, vol. 104, no. C, pp. 37–52, 1979.

[68] K. Kinosita Jr and T. Y. Tsong, "Formation and resealing of pores of controlled sizes in human erythrocyte membrane," *Nature*, vol. 268, no. 2, pp. 438–441, 1977.

[69] M. Tarek, "Membrane electroporation: a molecular dynamics simulation.," *Biophys. J.*, vol. 88, no. 6, pp. 4045–53, 2005.

[70] J. C. Weaver and Y. A. Chizmadzhev, "Theory of electroporation: A review," *Bioelectrochemistry Bioenerg.*, vol. 41, no. 2, pp. 135–160, 1996.

[71] J. C. Weaver, "Electroporation: a general phenomenon for manipulating cells and tissues.," *J. Cell. Biochem.*, vol. 51, no. 4, pp. 426–35, 1993.

[72] U. Zimmermann, J. Vienken, and G. Pilwat, "Development of drug carrier systems: Electrical

field induced effects in cell membranes," *J. Electroanal. Chem.*, vol. 116, no. C, pp. 553–574, 1980.

[73] E. Neumann, M. Schaefer-Ridder, Y. Wang, and P. H. Hofschneider, "Gene transfer into mouse lyoma cells by electroporation in high electric fields.," *EMBO J.*, vol. 1, no. 7, pp. 841–5, 1982.

[74] H. Okino, M., Marumoto, M., Kanesada, H., Kuga, K. and Mohri, "Electrical impulse chemotherapy for rat solid tumors," *Proc. Jpn. Cancer Congr.*, vol. 46, no. 1, p. 420, 1987.

[75] S. B. Dev, D. P. Rabussay, G. Widera, and G. A. Hofmann, "Medical applications of electroporation," *IEEE Trans. Plasma Sci.*, vol. 28, no. 1, pp. 206–223, 2000.

[76] F. Feuerbach and R. Crystal, "Progress in human gene therapy," *Kidney Int.*, vol. 49, no. 6, pp. 1791–4, 1996.

[77] C. Jiang, R. V Davalos, and J. C. Bischof, "A Review of Basic to Clinical Studies of Irreversible Electroporation Therapy," vol. 62, no. 1, pp. 4–20, 2015.

[78] M. L. Edelstein, M. R. Abedi, and J. Wixon, "Gene therapy clinical trials worldwide to 2007--an update.," *The journal of gene medicine*, vol. 9, no. 10. pp. 833–842, 2007.

[79] M. Hibino, M. Shigemori, H. Itoh, K. Nagayama, and K. Kinosita, "Membrane conductance of an electroporated cell analyzed by submicrosecond imaging of transmembrane potential.," *Biophys. J.*, vol. 59, no. 1, pp. 209–220, 1991.

[80] E. Neumann, S. Kakorin, and K. Tœnsing, "Fundamentals of electroporative delivery of drugs and genes," *Bioelectrochemistry Bioenerg.*, vol. 48, no. 1, pp. 3–16, 1999.

[81] R. Shirakashi, V. L. Sukhorukov, I. Tanasawa, and U. Zimmermann, "Measurement of the permeability and resealing time constant of the electroporated mammalian cell membranes," *Int. J. Heat Mass Transf.*, vol. 47, no. 21, pp. 4517–4524, 2004.

[82] H. Leontiadou, A. E. Mark, and S. J. Marrink, "Molecular dynamics simulations of hydrophilic

pores in lipid bilayers.," *Biophys. J.*, vol. 86, no. 4, pp. 2156–2164, 2004.

[83] J. Teissie, M. Golzio, and M. P. Rols, "Mechanisms of cell membrane electropermeabilization: A minireview of our present (lack of ?) knowledge," *Biochim. Biophys. Acta - Gen. Subj.*, vol. 1724, no. 3, pp. 270–280, 2005.

[84] M. R. Prausnitz, J. D. Corbett, Q. J. A. Gimm, D. E. Golan, R. Langer, and J. C. Weaverl, "Millisecond Measurement of Transport During and After an Electroporation Pulse," *Biophys. J.*, vol. 68, no. May, pp. 1864–1870, 1995.

[85] B. Gabriel and J. Teissié, "Direct observation in the millisecond time range of fluorescent molecule asymmetrical interaction with the electropermeabilized cell membrane," *Biophys. J.*, vol. 73, no. 5, pp. 2630–2637, 1997.

[86] B. Gabriel and J. Teissié, "Time Courses of Mammalian Cell Electropermeabilization Observed by Millisecond Imaging of Membrane Property Changes during the Pulse," *Biophys. J.*, vol. 76, no. 4, pp. 2158–2165, 1999.

[87] M. Puc, T. Kotnik, L. M. Mir, and D. Miklavčič, "Quantitative model of small molecules uptake after in vitro cell electropermeabilization," *Bioelectrochemistry*, vol. 60, no. 1–2, pp. 1–10, 2003.

[88] S. I. Sukharev, V. A. Klenchin, S. M. Serov, L. V Chernomordik, and C. YuA, "Electroporation and electrophoretic DNA transfer into cells. The effect of DNA interaction with electropores," *Biophys. J.*, vol. 63, no. 5, pp. 1320–1327, 1992.

[89] Maša Kandušer and Damijan Miklavčič, "Electroporation in Biological Cell and Tissue: An Overview," in *Electrotechnologies for Extraction from Food Plants and Biomaterials*, 2009, pp. 1–37.

[90] T. Y. Y. Tsong, "Electroporation of cell membranes.," *Biophys. J.*, vol. 60, no. 2, pp. 297–306, 1991.

[91] U. Zimmermann, "Electric field-mediated fusion and related electrical phenomena," *BBA - Rev. Biomembr.*, vol. 694, no. 3, pp. 227–277, 1982.

[92] M. P. Rols and J. Teissié, "Electropermeabilization of mammalian cells. Quantitative analysis of the phenomenon.," *Biophys. J.*, vol. 58, no. 5, pp. 1089–98, 1990.

[93] H. Wolf, M. P. Rols, E. Boldt, E. Neumann, and J. Teissié, "Control by pulse parameters of electric field-mediated gene transfer in mammalian cells.," *Biophys. J.*, vol. 66, no. 2 Pt 1, pp. 524–31, 1994.

[94] B. Gabriel and J. Teissie, "Spatial compartmentation and time resolution of photooxidation of a cell membrane probe in electropermeabilized Chinese hamster ovary cells," *Eur. J. Biochem.*, vol. 228, no. 3, pp. 710–718, 1995.

[95] M. C. Vernhes, P. A. Cabanes, and J. Teissie, "Chinese hamster ovary cells sensitivity to localized electrical stresses," *Bioelectrochemistry Bioenerg.*, vol. 48, no. 1, pp. 17–25, 1999.

[96] A. M. Lebar, N. A. Kopitar, K. Ihan, G. Sersa, and D. Miklavcic, "Significance of treatment energy in cell electropermeabilization," *Electro- and Magnetobiology*, vol. 17, no. 2, pp. 255–262, 1998.

[97] A. Macek-Lebar and D. Miklavcic, "Cell electropermeabilization to small molecules in vitro: control by pulse parameters," *Radiol. Oncol.*, vol. 35, pp. 193–202, 2001.

[98] M.-P. Rols and J. Teissié, "Electropermeabilization of Mammalian Cells to Macromolecules: Control by Pulse Duration," *Biophys. J.*, vol. 75, no. 3, pp. 1415–1423, 1998.

[99] A. O. Bilska, K. A. Debruin, and W. Krassowska, "Theoretical modeling of the effects of shock duration, frequency, and strength on the degree of electroporation," *Bioelectrochemistry Bioenerg.*, vol. 51, no. 2, pp. 133–143, 2000.

[100] P. J. Canatella, J. F. Karr, J. A. Petros, and M. R. Prausnitz, "Quantitative Study of Electroporation-Mediated Molecular Uptake and Cell Viability," *Biophys. J.*, vol. 80, no. 2, pp. 755–764, 2001.

[101] H. A. Saeed and J. W. Lee, "Experimental Demonstration of Localized Excess Protons at a

WaterMembrane Interface," *Bioenerg. Open Access*, vol. 04, no. 02, pp. 1–7, 2015.

[102] J. W. Lee, "Proton-Electrostatic Localization: Explaining the Bioenergetic Conundrum in Alkalophilic Bacteria," *Bioenergetics*, vol. 4, no. 121, pp. 1–8, 2015.

[103] D. Miklavcic, D. Semrov, H. Mekid, and L. M. Mir, "A validated model of in vivo electric field distribution in tissues for electrochemotherapy and for DNA electrotransfer for gene therapy," *Biochim. Biophys. Acta (BBA)-General Subj.*, vol. 1523, no. 1, pp. 73–83, 2000.

[104] M. Marty *et al.*, "Electrochemotherapy - An easy, highly effective and safe treatment of cutaneous and subcutaneous metastases: Results of ESOPE (European Standard Operating Procedures of Electrochemotherapy) study," *Eur. J. Cancer, Suppl.*, vol. 4, no. 11, pp. 3–13, 2006.

[105] B. Rubinsky, G. Onik, and P. Mikus, "Irreversible electroporation: A new ablation modality - Clinical implications," *Technol. Cancer Res. Treat.*, vol. 6, no. 1, pp. 37–48, 2007.

[106] B. Al-Sakere *et al.*, "Tumor ablation with irreversible electroporation," *PLoS One*, vol. 2, no. 11, pp. 1–8, 2007.

[107] L. Miller, J. Leor, and B. Rubinsky, "Cancer cells ablation with irreversible electroporation.," *Technol. Cancer Res. Treat.*, vol. 4, no. 6, pp. 699–705, 2005.

[108] T. Mars *et al.*, "Electrotransfection and Lipofection Show Comparable Efficiency for In Vitro Gene Delivery of Primary Human Myoblasts," *J. Membr. Biol.*, vol. 248, no. 2, pp. 273–283, 2015.

[109] I. Spanggaard *et al.*, "Gene electrotransfer of plasmid antiangiogenic metargidin peptide (AMEP) in disseminated melanoma: safety and efficacy results of a phase I first-in-man study.," *Hum. Gene Ther. Clin. Dev.*, vol. 24, no. 3, pp. 99–107, 2013.

[110] Y. Terada, S. Hanada, A. Nakao, M. Kuwahara, S. Sasaki, and F. Marumo, "Gene transfer of Smad7 using electroporation of adenovirus prevents renal fibrosis in post-obstructed kidney.," *Kidney Int.*, vol. 61, pp. S94–S98, 2002.

[111] A. Gothelf, L. M. Mir, and J. Gehl, "Electrochemotherapy: results of cancer treatment using enhanced delivery of bleomycin by electroporation," *Cancer Treat. Rev.*, vol. 29, no. 5, pp. 371–387, 2003.

[112] R. V Davalos, L. M. Mir, and B. Rubinsky, "Tissue ablation with irreversible electroporation," *Ann. Biomed. Eng.*, vol. 33, no. 2, p. 223, 2005.

[113] A. Golberg, B. G. Bruinsma, B. E. Uygun, and M. L. Yarmush, "Tissue heterogeneity in structure and conductivity contribute to cell survival during irreversible electroporation ablation by 'electric field sinks,'" *Sci. Rep.*, vol. 5, pp. 1–7, 2014.

[114] E. Neumann, "Membrane electroporation and direct gene transfer," *J. Electroanal. Chem.*, vol. 343, no. 1–2, pp. 247–267, 1992.

[115] T. Kotnik, G. Pucihar, M. Reberšek, D. Miklavčič, and L. M. Mir, "Role of pulse shape in cell membrane electropermeabilization," *Biochim. Biophys. Acta - Biomembr.*, vol. 1614, no. 2, pp. 193–200, 2003.

[116] D. Miklavcic and L. Towhidi, "Numerical study of the electroporation pulse shape effect on molecular uptake of biological cells," *Radiol. Oncol.*, vol. 44, no. 1, pp. 34–41, 2010.

[117] E. Ben-David *et al.*, "Irreversible electroporation: treatment effect is susceptible to local environment and tissue properties.," *Radiology*, vol. 269, no. 3, pp. 738–47, 2013.

[118] J. J. Wendler *et al.*, "A prospective Phase 2a pilot study investigating focal percutaneous irreversible electroporation (IRE) ablation by NanoKnife in patients with localised renal cell carcinoma (RCC) with delayed interval tumour resection (IRENE trial)," *Contemp. Clin. Trials*, vol. 43, pp. 10–19, 2015.

[119] E. Tekle, R. D. Astumian, and P. B. Chock, "Electroporation by using bipolar oscillating electric field: an improved method for DNA transfection of NIH 3T3 cells.," *Proc. Natl. Acad. Sci. U. S. A.*, vol. 88, no. 10, pp. 4230–4234, 1991.

[120] T. Suzuki, B. C. Shin, K. Fujikura, T. Matsuzaki, and K. Takata, "Direct gene transfer into rat liver cells by in vivo electroporation," *FEBS Lett*, vol. 425, no. 3, pp. 436–440, 1998.

[121] M. P. Rols, "Electropermeabilization, a physical method for the delivery of therapeutic molecules into cells," *Biochim. Biophys. Acta - Biomembr.*, vol. 1758, no. 3, pp. 423–428, 2006.

[122] R. Heller *et al.*, "In vivo gene electroinjection and expression in rat liver.," *FEBS Lett.*, vol. 389, no. 3, pp. 225–228, 1996.

[123] B. Gabriel and J. Teissié, "Control by electrical parameters of short- and long-term cell death resulting from electropermeabilization of Chinese hamster ovary cells," *Biochim. Biophys. Acta - Mol. Cell Res.*, vol. 1266, no. 2, pp. 171–178, 1995.

[124] D. Needham and R. M. Hochmuth, "Electro-mechanical permeabilization of lipid vesicles. Role of membrane tension and compressibility," *Biophys. J.*, vol. 55, no. 5, pp. 1001–1009, 1989.

[125] M. Pavlin, T. Kotnik, D. Miklavčič, P. Kramar, and A. M. Lebar, "Electroporation of planar lipid bilayers and membranes," *Adv. planar lipid bilayers liposomes*, vol. 6, pp. 165–226, 2008.

[126] E. Tekle, R. D. Astumian, and P. B. Chock, "Electro-permeabilization of cell membranes: Effect of the resting membrane potential," *Biochem. Biophys. Res. Commun.*, vol. 172, no. 1, pp. 282–287, 1990.

[127] S. J. Beebe, P. M. Fox, L. J. Rec, E. L. K. Willis, and K. H. Schoenbach, "Nanosecond, high-intensity pulsed electric fields induce apoptosis in human cells.," *FASEB J.*, vol. 17, no. 11, pp. 1493–1495, 2003.

[128] J. Piñero, M. López-Baena, T. Ortiz, and F. Cortés, "Apoptotic and necrotic cell death are both induced by electroporation in HL60 human promyeloid leukaemia cells.," *Apoptosis*, vol. 2, no. 3, pp. 330–336, 1997.

[129] J. A. Verheugen, H. P. Vijverberg, M. Oortgiesen, and M. D. Cahalan, "Voltage-gated and Ca (2+)-activated K+ channels in intact human T lymphocytes. Noninvasive measurements of

membrane currents, membrane potential, and intracellular calcium.," *J. Gen. Physiol.*, vol. 105, no. 6, pp. 765–794, 1995.

[130] L. H. Brent, B. Rubenstein, Q. H. Gong, and S. J. Wieland, "Transmembrane Potential Responses During HL-60 Promyelocyte Differentiation," vol. 168, no. 1, pp. 155–165, 1996.

[131] S. Misra, "Human gene therapy: a brief overview of the genetic revolution.," *J. Assoc. Physicians India*, vol. 61, no. 2, pp. 127–133, 2013.

[132] L. Walters, "Gene therapy: overview," *Encycl. Ethical, Leg. Policy Issues Biotechnol.*, 2000.

[133] M. J. Jaroszeski, R. Gilbert, C. Nicolau, and R. Heller, "In vivo gene delivery by electroporation," *Adv. Drug Deliv. Rev.*, vol. 35, no. 1, pp. 131–137, 1999.

[134] L. Fouillard, "Physical method for gene transfer : an alternative to viruses," *Hum. Gene Ther.*, pp. 214–216, 1996.

[135] Z. Wu, A. Asokan, and R. J. Samulski, "Adeno-associated Virus Serotypes: Vector Toolkit for Human Gene Therapy," *Mol. Ther.*, vol. 14, no. 3, pp. 316–327, 2006.

[136] A. D. Miller, "Retroviral vectors: from cancer viruses to therapeutic tools," *Hum. Gene Ther.*, vol. 25, no. 12, pp. 989–994, 2014.

[137] W. Walter and U. Stein, "Viral vectors for gene transfer a review of their use in the treatment of human disease," *Drugs*, vol. 60, pp. 249–271, 2000.

[138] A. C. Nathwani *et al.*, "Adenovirus-Associated Virus Vector–Mediated Gene Transfer in Hemophilia B," *N. Engl. J. Med.*, vol. 365, no. 25, pp. 2357–2365, 2011.

[139] C. S. Manno *et al.*, "Successful transduction of liver in hemophilia by AAV-Factor IX and limitations imposed by the host immune response," *Nat. Med.*, vol. 12, no. 3, pp. 342–347, 2006.

[140] A. Regalado, "Gene Therapy Is Curing Hemophilia," *MIT Technol. Rev.*, vol. 119, no. 5, pp. 13–16, 2016.

[141] M. A. Kay *et al.*, "In Vivo Gene Therapy of Hemophilia B : Sustained Partial Correction in Factor IX-Deficient Dogs," *Am. Assoc. Adv. Sci.*, vol. 262, pp. 117–119, 1993.

[142] F. Liu *et al.*, "Sine-wave current for efficient and safe in vivo gene transfer," *Mol. Ther.*, vol. 15, no. 10, pp. 1842–1847, 2007.

[143] J. J. P. Kastelein, C. J. D. Ross, and M. R. Hayden, "From Mutation Identification to Therapy: Discovery and Origins of the First Approved Gene Therapy in the Western World," *Hum. Gene Ther.*, vol. 24, no. 5, pp. 472–478, 2013.

[144] C. Mueller and T. R. Flotte, "Clinical gene therapy using recombinant adeno-associated virus vectors," *Gene Ther.*, vol. 15, no. 11, pp. 858–863, 2008.

[145] E. Marshall, "Gene Therapy Death Prompts Review of Adenovirus Vector," *Science (80-.).*, vol. 286, no. 5448, pp. 2244–2245, 1999.

[146] A. I. Daud *et al.*, "Phase I trial of interleukin-12 plasmid electroporation in patients with metastatic melanoma," *J. Clin. Oncol.*, vol. 26, no. 36, pp. 5896–5903, 2008.

[147] L. M. Mir *et al.*, "High-efficiency gene transfer into skeletal muscle mediated by electric pulses.," *Proc. Natl. Acad. Sci. U. S. A.*, vol. 96, no. 8, pp. 4262–7, 1999.

[148] M. F. Bureau, J. Gehl, V. Deleuze, L. M. Mir, and D. Scherman, "Importance of association between permeabilization and electrophoretic forces for intramuscular DNA electrotransfer," *Biochim. Biophys. Acta - Gen. Subj.*, vol. 1474, no. 3, pp. 353–359, 2000.

[149] L. Chang *et al.*, "Magnetic tweezers-based 3D microchannel electroporation for high-throughput gene transfection in living cells," *Small*, vol. 11, no. 15, pp. 1818–1828, 2015.

[150] F. Liu, "A Syringe Electrode Device for Simultaneous Injection of DNA and Electrotransfer," *Mol. Ther.*, vol. 5, no. 3, pp. 323–328, 2002.

[151] J. C. Knutson and D. Yee, "Electroporation: parameters affecting transfer of DNA into mammalian cells.," *Anal. Biochem.*, vol. 164, no. 1, pp. 44–52, 1987.

[152] S. C. Nicolson, C. Li, M. L. Hirsch, V. Setola, and R. J. Samulski, "Identification and Validation of Small Molecules That Enhance Recombinant Adeno-associated Virus Transduction following High-Throughput Screens," *J. Virol.*, vol. 90, no. 16, pp. 7019–7031, 2016.

[153] D. Demarais and H. Gifford, "Methods for treating heart arrhythmia." Google Patents, 2007.

[154] E. W. Lee, S. Thai, and S. T. Kee, "Irreversible electroporation: a novel image-guided cancer therapy," *Gut Liver*, vol. 4, no. Suppl 1, p. S99, 2010.

[155] C. L. Size, C. Monolayers, and P. A. O. M. Easy, "Circulation: Arrhythmia and Electrophysiology," 2017.

[156] N. Jourabchi, K. Beroukhim, B. A. Tafti, S. T. Kee, and E. W. Lee, "Irreversible electroporation (NanoKnife) in cancer treatment," *Gastrointest. Interv.*, vol. 3, no. 1, pp. 8–18, 2014.

[157] K. P. Charpentier, "Irreversible electroporation for the ablation of liver tumors: are we there yet?," *Arch. Surg.*, vol. 147, no. 11, pp. 1053–61, 2012.

[158] B. Rubinsky, "Irreversible Electroporation in Medicine," *Technol. Cancer Res. Treat.*, vol. 6, no. 4, pp. 255–259, 2007.

[159] P. Sánchez-Velázquez *et al.*, "Irreversible electroporation of the liver: Is there a safe limit to the ablation volume?," *Sci. Rep.*, vol. 6, no. November 2015, pp. 1–7, 2016.

[160] K. R. Thomson *et al.*, "Investigation of the safety of irreversible electroporation in humans," *J. Vasc. Interv. Radiol.*, vol. 22, no. 5, pp. 611–621, 2011.

[161] I. Sorokin, A. H. Lay, N. K. Reddy, N. E. Canvasser, M. Chamarthy, and J. A. Cadeddu, "Pain After Percutaneous Irreversible Electroporation of Renal Tumors Is Not Dependent on Tumor Location," *J. Endourol.*, vol. 31, no. 8, pp. 751–755, 2017.

[162] W. Denk, J. H. Strickler, and W. W. Webb, "Two-photon laser scanning fluorescence microscopy.," *Science (80-.).*, vol. 248, no. 4951, pp. 73–6, 1990.

[163] R. Wayne, "Bright-Field Microscopy," in *Light and Video Microscopy*, 2014, pp. 79–96.

[164] C. C. Reyes-Aldasoro, "Bright Field Microscopy," *Biomed. Image Anal. Recipes MATLAB® Life Sci. Eng.*, pp. 215–289, 2015.

[165] J. Hickson, "In vivo optical imaging: preclinical applications and considerations.," *Urol. Oncol.*, vol. 27, no. 3, pp. 295–7, 2009.

[166] R. A. Bunce *et al.*, "Camera luminometer for use with luminescent assays," *Analyst*, vol. 110, no. 6, pp. 657–663, 1985.

[167] J. R. De Wet, K. V Wood, M. DeLuca, D. R. Helinski, and S. Subramani, "Firefly luciferase gene: structure and expression in mammalian cells.," *Mol. Cell. Biol.*, vol. 7, no. 2, pp. 725–737, 1987.

[168] "ECM 830 Square Wave Electroporation System." .

[169] R. M. Bernard, "Electrodes and electrode arrays for generating electroporation inducing electrical fields." Google Patents, 1999.

[170] G. A. Hofmann, R. A. Gilbert, Y. Hayakawa, R. Heller, and M. J. Jaroszeski, "Needle electrodes for mediated delivery of drugs and genes." Google Patents, 1997.

[171] J. Gehl *et al.*, "In vivo electroporation of skeletal muscle: threshold, efficacy and relation to electric field distribution," *Biochim. Biophys. Acta (BBA)-General Subj.*, vol. 1428, no. 2–3, pp. 233–240, 1999.

[172] G. A. Hofmann, S. B. Dev, S. C. Dimmer, J. I. Levatter, and G. S. Nanda, "Method of programming an array of needle electrodes for electroporation therapy of tissue." Google Patents, 2001.

[173] M. B. Sano, M. R. DeWitt, S. Teeter, and L. Xing, "Optimization of a single insertion electrode array for the creation of clinically relevant ablations using high-frequency irreversible electroporation," *Comput. Biol. Med.*, 2018.

[174] P. F. Forde *et al.*, "Preclinical evaluation of an endoscopic electroporation system," *Endoscopy*,

vol. 48, no. 05, pp. 477–483, 2016.

[175] K. Neven, V. Van Driel, H. Van Wessel, R. Van Es, P. A. Doevendans, and F. Wittkampf, "Myocardial Lesion Size After Epicardial Electroporation Catheter Ablation After Subxiphoid Puncture," *Circ. Arrhythmia Electrophysiol.*, vol. 7, no. 4, pp. 728–733, 2014.

[176] G. Srimathveeravalli *et al.*, "Normal Porcine Ureter Retains Lumen Wall Integrity but Not Patency Following Catheter-Directed Irreversible Electroporation: Imaging and Histologic Assessment over 28 Days," *J. Vasc. Interv. Radiol.*, vol. 28, no. 6, p. 913–919.e1, 2017.

[177] G. Narayanan and M. H. Doshi, "Irreversible Electroporation (IRE) in Renal Tumors," *Curr. Urol. Rep.*, vol. 17, no. 2, p. 15, 2016.

[178] Student, "The Probable Error of a Mean," *Biometrika*, vol. 6, no. 1, pp. 1–25, 1908.

[179] N. R. Draper and H. Smith, *Applied Regression Analysis*, vol. 47, no. 3. John Wiley & Sons, Inc., 1998.

[180] S. Durrleman and R. Simon, "Flexible regression models with cubic splines," *Stat. Med.*, vol. 8, no. 5, pp. 551–561, 1989.

[181] D. B. Suits, A. Mason, and L. Chan, "Spline Functions Fitted by Standard Regression Methods," *Rev. Econ. Stat.*, vol. 60, no. 1, pp. 132–139, 1978.

[182] S. E. Aggrey, "Comparison of three nonlinear and spline regression models for describing chicken growth curves," *Poult. Sci.*, vol. 81, no. 12, pp. 1782–1788, 2002.

[183] J. H. Friedman and C. B. Roosen, "An introduction to multivariate adaptive regression splines," *Stat. Methods Med. Res.*, vol. 4, no. 1, pp. 197–217, 1995.

[184] D. Bates, M. Mächler, B. M. Bolker, and S. C. Walker, "Fitting linear mixed-effects models using lme4," *J. Stat. Softw.*, vol. 67, no. 1, pp. 1–48, 2015.

[185] A. A. Neath and J. E. Cavanaugh, "The Bayesian information criterion: Background, derivation, and applications," *Wiley Interdiscip. Rev. Comput. Stat.*, vol. 4, no. 2, pp. 199–203, 2012.

[186] H. Bhat and N. Kumar, "On the derivation of the Bayesian Information Criterion," *Sch. Nat. Sci. Univ.* …, no. August, pp. 1–4, 2010.

[187] "Worldwide trends in diabetes since 1980: a pooled analysis of 751 population-based studies with 4.4 million participants," *Lancet (London, England)*, vol. 387, no. 10027, pp. 1513–1530, 2016.

[188] G. Albrektsen, I. Heuch, S. Hansen, and G. Kvåle, "Breast cancer risk by age at birth, time since birth and time intervals between births: Exploring interaction effects," *Br. J. Cancer*, vol. 92, no. 1, pp. 167–175, 2005.

[189] S. R. Okubo, A. Kanawati, M. W. Richards, and S. Childressd, "Evaluation of visual and instrument shade matching," *J. Prosthet. Dent.*, vol. 80, no. 6, pp. 642–648, 1998.

[190] M. L. Yarmush, A. Golberg, G. Serša, T. Kotnik, and D. Miklavčič, "Electroporation-Based Technologies for Medicine: Principles, Applications, and Challenges.," *Annu. Rev. Biomed. Eng.*, vol. 16, pp. 295–320, 2014.

[191] J. C. Weaver, "Electroporation of cells and tissues," *IEEE Trans. Plasma Sci.*, vol. 28, no. 1, pp. 24–33, 2000.

[192] D. S. K. Lu, S. S. Raman, D. J. Vodopich, M. Wang, J. Sayre, and C. Lassman, "Effect of vessel size on creation of hepatic radiofrequency lesions in pigs: Assessment of the 'heat sink' effect," *Am. J. Roentgenol.*, vol. 178, no. 1, pp. 47–51, 2002.

[193] M. D. Rosenberg *et al.*, "Percutaneous cryoablation of renal lesions with radiographic ice ball involvement of the renal sinus: Analysis of hemorrhagic and collecting system complications," *Am. J. Roentgenol.*, vol. 196, no. 4, pp. 935–939, 2011.

[194] C. B. Arena, C. S. Szot, P. A. Garcia, M. N. Rylander, and R. V. Davalos, "A three-dimensional in vitro tumor platform for modeling therapeutic irreversible electroporation," *Biophys. J.*, vol. 103, no. 9, pp. 2033–2042, 2012.

[195] S. F. Badylak, "Xenogeneic extracellular matrix as a scaffold for tissue reconstruction," *Transplant Immunology*, vol. 12, no. 3–4. pp. 367–377, 2004.

[196] M. Konishi, K. Kawamoto, M. Izumikawa, H. Kuriyama, and T. Yamashita, "Gene transfer into guinea pig cochlea using adeno-associated virus vectors," *J. Gene Med.*, vol. 10, no. January, pp. 610–618, 2008.

[197] H. Yin, R. L. Kanasty, A. a Eltoukhy, A. J. Vegas, J. R. Dorkin, and D. G. Anderson, "Non-viral vectors for gene-based therapy.," *Nat. Rev. Genet.*, vol. 15, no. 8, pp. 541–555, 2014.

[198] S. sa Haberl *et al.*, "Effect of different parameters used for in vitro gene electrotransfer on gene expression efficiency, cell viability and visualization of plasmid DNA at the membrane level," *J. Gene Med.*, vol. 15, pp. 169–181, 2013.

[199] T. Steinbrunn, M. Chatterjee, R. C. Bargou, and T. Stühmer, "Efficient transient transfection of human multiple myeloma cells by electroporation - An appraisal," *PLoS One*, vol. 9, no. 6, p. e97443, 2014.

[200] U. Zimmermann, G. Pilwat, F. Beckers, and F. Riemann, "Effects of external electrical fields on cell membranes," *Bioelectrochemistry Bioenerg.*, vol. 3, no. 1, pp. 58–83, 1976.

[201] L. H. Wegner, W. Frey, and A. Silve, "Electroporation of DC-3F cells is a dual process," *Biophys. J.*, vol. 108, no. 7, pp. 1660–1671, 2015.

[202] J. T. Stock and M. V. Ora, *Electrochemistry, Past and Present*. Washington, DC: American Chemical Society, 1989.

[203] K. P. Charpentier, F. Wolf, L. Noble, B. Winn, M. Resnick, and D. E. Dupuy, "Irreversible electroporation of the liver and liver hilum in swine," *Hpb*, vol. 13, no. 3, pp. 168–173, 2011.

[204] R. C. G. Martin, "Irreversible electroporation: A novel option for treatment of hepatic metastases," *Curr. Colorectal Cancer Rep.*, vol. 9, no. 2, pp. 191–197, 2013.

[205] D. Pittet, F. Di Virgilio, T. Pozzan, A. Monod, and D. P. Lew, "Correlation between plasma

membrane potential and second messenger generation in the promyelocytic cell line HL-60," *J. Biol. Chem.*, vol. 265, no. 24, pp. 14256–14263, 1990.

[206] R Core Team, "R Core Team," *R A Lang. Environ. Stat. Comput. R Found. Stat. Comput. Vienna, Austria.*, p. ISBN 3-900051-07-0, URL http://www.R-project.org/., 2013.

[207] S. Talele and P. Gaynor, "Non-linear time domain model of electropermeabilization: Effect of extracellular conductivity and applied electric field parameters," *J. Electrostat.*, vol. 66, no. 5–6, pp. 328–334, 2008.

[208] R. P. Joshi and K. H. Schoenbach, "Mechanism for membrane electroporation irreversibility under high-intensity, ultrashort electrical pulse conditions," *Phys. Rev. E - Stat. Physics, Plasmas, Fluids, Relat. Interdiscip. Top.*, vol. 66, no. 5, p. 4, 2002.

[209] T. R. Gowrishankar, A. T. Esser, K. C. Smith, S. K. Burns, and J. C. Weaver, "In silico estimates of cell electroporation by electrical incapacitation waveforms," *Eng. Med. Biol. Soc.*, pp. 6505–6508, 2009.

[210] Z. Ji, S. M. Kennedy, J. H. Booske, and S. C. Hagness, "Experimental studies of persistent poration dynamics of cell membranes induced by electric pulses," *IEEE Trans. Plasma Sci.*, vol. 34, no. 4 II, pp. 1416–1424, 2006.

[211] F. Mingozzi and K. A. High, "Therapeutic in vivo gene transfer for genetic disease using AAV: Progress and challenges," *Nat. Rev. Genet.*, vol. 12, no. 5, pp. 341–355, 2011.

[212] T. Alam, P. Wai, D. Held, S. T. T. Vakili, E. Forsberg, and H. Sollinger, "Correction of Diabetic Hyperglycemia and Amelioration of Metabolic Anomalies by Minicircle DNA Mediated Glucose-Dependent Hepatic Insulin Production," *PLoS One*, vol. 8, no. 6, 2013.

[213] U.S. Food and Drug Administration, "FDA approval brings first gene therapy to the United States," *U.S. Department of Health and Human Services*, 2017. [Online]. Available: https://www.fda.gov/NewsEvents/Newsroom/PressAnnouncements/ucm574058.htm.

[Accessed: 25-Sep-2017].

[214] Y. Otani, S. Kawakami, H. Mukai, Y. Fuchigami, F. Yamashita, and M. Hashida, "Long-term in vivo gene expression in mouse kidney using φC31 integrase and electroporation.," *J. Drug Target.*, vol. 23, no. 5, pp. 427–435, 2015.

[215] J. M. Wilson, "Lessons learned from the gene therapy trial for ornithine transcarbamylase deficiency," *Mol. Genet. Metab.*, vol. 96, no. 4, pp. 151–157, 2009.

[216] D. Cukjati, D. Batiuskaite, F. André, D. Miklavčič, and L. M. Mir, "Real time electroporation control for accurate and safe in vivo non-viral gene therapy," *Bioelectrochemistry*, vol. 70, no. 2, pp. 501–507, 2007.

[217] N. Somia and I. M. Verma, "Gene therapy: trials and tribulations," *Nat. Rev. Genet.*, vol. 1, no. 2, pp. 91–99, 2000.

[218] M. S. Al-Dosari and X. Gao, "Nonviral gene delivery: principle, limitations, and recent progress.," *AAPS J.*, vol. 11, no. 4, pp. 671–681, 2009.

[219] L. Jaroff, "Fixing the genes," *Time*, vol. 153, no. 1, p. 68—70, 73, Jan. 1999.

[220] T. K. Kim and J. H. Eberwine, "Mammalian cell transfection: The present and the future," *Anal. Bioanal. Chem.*, vol. 397, no. 8, pp. 3173–3178, 2010.

[221] R. Daniel, R. A. Katz, G. Merkel, J. C. Hittle, T. J. Yen, and A. M. Skalka, "Wortmannin Potentiates Integrase-Mediated Killing of Lymphocytes and Reduces the Efficiency of Stable Transduction by Retroviruses," *Mol. Cell. Biol.*, vol. 21, no. 4, pp. 1164–1172, 2001.

[222] A. M. Handorf, H. W. Sollinger, and T. Alam, *Insulin Gene Therapy for Type 1 Diabetes Mellitus : Unique Challenges Require Innovative Solutions*. 2016.

[223] "Detecting a Cell Using Image Segmentation," *MathWorks Documentation*, 2015. [Online]. Available: https://www.mathworks.com/help/images/examples/detecting-a-cell-using-image-segmentation.html. [Accessed: 12-Mar-2015].

[224] Elad, "Circles overlap remover," *MathWorks File Exchange*, 2013. [Online]. Available: https://www.mathworks.com/matlabcentral/fileexchange/42370-circles-overlap-remover?focused=3793851&tab=function. [Accessed: 12-Mar-2015].

[225] Nicholas, "Snip.m Snip elements out of vectors/matrices," *MathWorks File Exchange*, 2013. [Online]. Available: https://www.mathworks.com/matlabcentral/fileexchange/41941-snip-m-snip-elements-out-of-vectors-matrices.

[226] A. M. Ansari *et al.*, "Cellular GFP Toxicity and Immunogenicity: Potential Confounders in in Vivo Cell Tracking Experiments," *Stem Cell Rev. Reports*, vol. 12, no. 5, pp. 553–559, 2016.

[227] M. Karimi, L. C. Goldie, M. N. Cruickshank, E. K. Moses, and L. J. Abraham, "A critical assessment of the factors affecting reporter gene assays for promoter SNP function: A reassessment of -308 TNF polymorphism function using a novel integrated reporter system," *Eur. J. Hum. Genet.*, vol. 17, no. 11, pp. 1454–1462, 2009.

[228] K. Franke, T. Baden, P. Berens, M. Rezac, M. Bethge, and T. Euler, "What the mouse eye tells the mouse brain: Fingerprinting the retinal ganglion cell types of the mouse retina," in *11th Göttingen Meeting of the German Neuroscience Society, 35th Göttingen Neurobiology Conference*, 2015.

[229] M. A. Wild, K. Kumor, M. J. Nolan, H. Lockman, and K. S. Bowdish, "A human antibody against anthrax protective antigen protects rabbits from lethal infection with aerosolized spores," *Hum Antibodies*, vol. 16, no. 3–4, pp. 99–105, 2007.

[230] R. M. Atkins *et al.*, "Impedance spectroscopy as an indicator for successful in vivo electric field mediated gene delivery in a murine model," *Bioelectrochemistry*, vol. 115, pp. 33–40, 2017.

[231] S. E. McCandless, J. W. Brunger, and S. B. Cassidy, "The Burden of Genetic Disease on Inpatient Care in a Children's Hospital," *Am. J. Hum. Genet.*, vol. 74, no. 1, pp. 121–127, 2004.

[232] W. F. Anderson, "Gene therapy for genetic diseases," *Hum. Gene Ther.*, vol. 5, no. 3, pp. 281–282, 1994.

[233] R. N. Aravalli and C. J. Steer, "Gene editing technology as an approach to the treatment of liver diseases," *Expert Opin. Biol. Ther.*, vol. 16, no. 5, pp. 595–608, 2016.

[234] I. M. Verma and N. Somia, "Gene therapy - Promises, problems and prospects," *Nature*, vol. 389, no. 6648, pp. 239–242, 1997.

[235] D. J. Wells, "Gene therapy progress and prospects: Electroporation and other physical methods," *Gene Ther.*, vol. 11, no. 18, pp. 1363–1369, 2004.

[236] F. Liu and L. Huang, "Electric gene transfer to the liver following systemic administration of plasmid DNA," *Gene Ther.*, vol. 9, no. 16, pp. 1116–1119, 2002.

[237] F. Liu and P. Tyagi, "Naked DNA for Liver Gene Transfer," *Advances in Genetics*, vol. 54. pp. 43–64, 2005.

[238] D. Ino and M. Iino, "In Vivo Gene Transfer to Schwann Cells in the Rodent Sciatic Nerve by Electroporation," *J. Vis. Exp.*, no. 115, pp. 1–6, 2016.

[239] S. Bugeon *et al.*, "Direct and efficient transfection of mouse neural stem cells and mature neurons by *in vivo* mRNA electroporation," *Development*, p. dev.151381, 2017.

[240] J. Szczurkowska, A. W. Cwetsch, M. Dal Maschio, D. Ghezzi, G. M. Ratto, and L. Cancedda, "Targeted in vivo genetic manipulation of the mouse or rat brain by in utero electroporation with a triple-electrode probe," *Nat. Protoc.*, vol. 11, no. 3, pp. 399–412, 2016.

[241] S. Satkauskas *et al.*, "Mechanisms of in vivo DNA electrotransfer: Respective contribution of cell electropermeabilization and DNA electrophoresis," *Mol. Ther.*, vol. 5, no. 2, pp. 133–140, 2002.

[242] "CST Studio Suite." CST Computer Simulation Technology AG, Framingham, MA, 2016.

[243] H. Li *et al.*, "Liver lobe volumes and the ratios of liver lobe volumes to spleen volume on magnetic resonance imaging for staging liver fibrosis in a minipig model," *PLoS One*, vol. 8, no. 11, pp. 1–9, 2013.

[244] S. Niehues, J. Unger, M. Malinowski, J. Neymeyer, B. Hamm, and M. Stockmann, "Liver volume measurement: reason of the difference between in vivo CT-volumetry and intraoperative ex vivo determination and how to cope it," *Eur. J. Med. Res.*, vol. 15, no. 8, p. 345, 2010.

[245] T. Hausken *et al.*, "Estimation of the human liver volume and configuration using three-dimensional ultrasonography: effect of a high-caloric liquid meal," *Ultrasound Med. Biol.*, vol. 24, no. 9, pp. 1357–1367, 1998.

[246] M. K. Kan and G. B. Hopkins, "Measurement of Liver Volume by Emission Computed Tomography," vol. 20, pp. 514–520, 1979.